

博士論文

A Study on Heat Transfer inside Fukushima
Daiichi Unit-1 Primary Containment Vessel
Considering Evaporation and Condensation

(蒸発凝縮を考慮した福島第一原子力発電所
内部の熱輸送に関する研究)

エルダル オズデミル

Table of Contents

I. Summary	XII
Chapter 1 Introduction	1
1.1 Background.....	2
1.2 Fukushima Daiichi Accident and Decommissioning Activities	3
1.2.1 Overview of the Fukushima Daiichi Nuclear Power Stations	3
1.2.2 Overview of the Accident.....	4
1.2.3 Decommissioning Activities	7
1.3 Heat Removal from Debris	9
1.3.1 Introduction	9
1.3.2 Radiative Heat Transfer.....	9
1.3.3 Conduction Heat Transfer	10
1.3.4 Natural Convection.....	11
1.3.5 Wall Condensation	12
1.4 Objective.....	14
Chapter 2 Simulations of Gas Flow Inside Fukushima Daiichi Unit-1 Primary Containment Vessel.....	17
2.1 Introduction.....	18
2.2 Computational Fluid Dynamics	18
2.2.1 Finite Volume Method	19
2.2.2 STAR-CCM+	21
2.2.3 CFD as a Tool for Containment Analysis	22
2.3 Fukushima Unit-1 Measurement Data Post-Processing	23
2.4 Geometry	32
2.5 Analysis Setup	33
2.5.1 Model Description	33
2.6 Mesh Sensitivity Analysis	39
2.7 Simulation Results & Discussion	44
2.7.1 Heat Source as a Parameter	44
2.7.2 Simulations for Safety Valve Temperature Asymmetry	51
2.7.3 Spreading of Debris as a Parameter.....	52

2.8	Summary and Conclusion	54
Chapter 3	Wall Condensation Modelling.....	56
3.1	Introduction.....	57
3.2	Literature Review	57
3.3	Diffusion Layer Model	63
3.4	Validation with COPAIN Experiments	70
3.4.1	Introduction	71
3.4.2	Analysis Setup	73
3.4.3	Mesh Sensitivity Analysis	77
3.4.4	Simulation Results & Discussion	79
3.5	Application of Wall Condensation Model to 1F1 PCV	99
3.6	Summary and Conclusion	101
Chapter 4	Nitrogen Injection Effect on Debris Cooling	102
4.1	Introduction.....	103
4.2	Fukushima Unit-1 Measurement Data Post-Processing During Nitrogen Injection	103
4.3	Simulation of Wall Condensation with Consideration of Nitrogen Injection	109
4.3.1	Simulation Results and Discussion	109
Chapter 5	Conclusion and Future Work.....	113
5.1	Conclusion	114
5.2	Future Work.....	115
References	116

LIST OF FIGURES

Figure 1-1 Droplet and Film Condensation [11]	13
Figure 1-2 Outline of the Study	15
Figure 2-1 1D Finite Volume Representation	20
Figure 2-2 Temperature and Pressure Distribution from March 20 th to April 9 th	24
Figure 2-3 Temperature distribution inside PCV on March 21 st 03:00	25
Figure 2-4 Pressure Response	26
Figure 2-5 Pressure Response during Rapid Cooldown	27
Figure 2-6 Temperature distribution inside PCV on March 24 th 01:00	28
Figure 2-7 Temperature distribution inside PCV on March 27 th 09:00	28
Figure 2-8 Condensation within PCV	29
Figure 2-9 Temperature distribution inside PCV on April 1 st 01:00	30
Figure 2-10 Temperature and Pressure Distribution from April 4 th to April 7 th	31
Figure 2-11 Temperature distribution inside PCV on April 6 th 00:00	32
Figure 2-12 3D Cad Model of Mark-1 Containment	33
Figure 2-13 Estimation of Debris Condition from Lumped Parameter Codes [21]	35
Figure 2-14 Representation of debris as heat source	36
Figure 2-15 Different mesh sizes for mesh sensitivity	40
Figure 2-16 Mesh Size Sensitivity	41
Figure 2-17 Computational Mesh	42
Figure 2-18 Mesh Metric : Volume Change	43
Figure 2-19 Mesh Metric : Cell Quality	43
Figure 2-20 Mesh Metric : Skewness Angle	44
Figure 2-21 Estimated Temperature Field for Different Heat Sources	45
Figure 2-22 Estimated Velocity Field for Different Heat Sources	46
Figure 2-23 Heightwise Temperature Measurements and Thermocouple Locations	48
Figure 2-24 Heightwise Temperature Comparison	49
Figure 2-25 Safety Valve Temperature Measurements and Thermocouple Locations ..	50
Figure 2-26 Safety Valve Temperature Comparison	50
Figure 2-27 Heat source to represent local heating on safety valves	51
Figure 2-28 Estimation of Safety Valve Temperature Values for Different Heat Sources	52
Figure 2-29 Schematic for heat source spreading effect	53
Figure 2-30 Heightwise Temperature Comparison for Debris Spreading Analysis	54
Figure 3-1 TOSQUAN Facility [33]	61
Figure 3-2 PANDA Facility [18]	63
Figure 3-3 Simplified Fluid Film Representation during Condensation	64
Figure 3-4 Droplet Formation due to Condensation	69
Figure 3-5 DABACO Project Overview [54]	71
Figure 3-6 Schematic of COPAIN Facility [54][56]	73
Figure 3-7 3D CAD Model of COPAIN Facility	74

Figure 3-8 Schematic of Grids for Mesh Sensitivity Top: Outline, Bottom: Near Wall	78
Figure 3-9 Steam Mass Fraction along Z Direction in the P0444 COPAIN Test	79
Figure 3-10 Steam Mass Fraction along Z Direction in the P0344 COPAIN Test	80
Figure 3-11 Steam Mass Fraction along Z Direction in the P0443 COPAIN Test	80
Figure 3-12 Steam Mass Fraction along Z Direction in the P0441 COPAIN Test	81
Figure 3-13 Steam Mass Fraction along Z Direction in the P0461 COPAIN Test	81
Figure 3-14 Air Mass Fraction along Z Direction in the P0444 COPAIN Test.....	82
Figure 3-15 Air Mass Fraction along Z Direction in the P0344 COPAIN Test.....	82
Figure 3-16 Air Mass Fraction along Z Direction in the P0443 COPAIN Test.....	83
Figure 3-17 Air Mass Fraction along Z Direction in the P0441 COPAIN Test.....	83
Figure 3-18 Air Mass Fraction along Z Direction in the P0461 COPAIN Test.....	84
Figure 3-19 Helium Mass Fraction along Z Direction in the P0461 COPAIN Test	84
Figure 3-20 Mass fraction of steam (on left), mass fraction of air (on right) on the condensing wall in the P0444 COPAIN test	85
Figure 3-21 Estimated Mass Transfer Coefficient of Flow Domain in the P0444 COPAIN Test	86
Figure 3-22 Estimated Mass Transfer Coefficient of Flow Domain in the P0344 COPAIN Test	87
Figure 3-23 Estimated Mass Transfer Coefficient of Flow Domain in the P0443 COPAIN Test	88
Figure 3-24 Estimated Mass Transfer Coefficient of Flow Domain in the P0441 COPAIN Test	89
Figure 3-25 Estimated Mass Transfer Coefficient of Flow Domain in the P0461 COPAIN Test	90
Figure 3-26 Velocity field in the P0444 COPAIN Test	93
Figure 3-27 Velocity field in the P0344 COPAIN Test	93
Figure 3-28 Velocity field in the P0443 COPAIN Test	94
Figure 3-29 Velocity field in the P0441 COPAIN Test	94
Figure 3-30 Velocity field in the P0461 COPAIN Test	95
Figure 3-31 Axial Evaluation of Condensation Flux in the P0444 COPAIN Test.....	96
Figure 3-32 Axial Evaluation of Condensation Flux in the P0344 COPAIN Test.....	96
Figure 3-33 Axial Evaluation of Condensation Flux in the P0443 COPAIN Test.....	97
Figure 3-34 Axial Evaluation of Condensation Flux in the P0441 COPAIN Test.....	97
Figure 3-35 Axial Evaluation of Condensation Flux in the P0461 COPAIN Test.....	98
Figure 3-36 Selected Regions for Heat and Mass Sources.....	99
Figure 3-37 Comparison of Estimated Temperature Field without Wall Condensation Model (on left) and with Wall Condensation Model (on right)	100
Figure 3-38 Heightwise Temperature Comparison with and without Wall Condensation Model.....	101
Figure 4-1 Pressure Response during Nitrogen Injection.....	105
Figure 4-2 Water Injection Mass Flow Rate during Nitrogen Injection.....	105
Figure 4-3 Temperature and Pressure Distribution from April 4 th to April 12 th @	106
Figure 4-4 Temperature distribution inside PCV on April 9 th 06:00.....	107
Figure 4-5 Pressure Measurement from April 6 th to April 26 th	107

Figure 4-6 Increase in water injection on April 26 th	108
Figure 4-7 Temperature distribution inside PCV on April 26 th 06:00.....	108
Figure 4-8 Location of Condensation.....	110
Figure 4-9 Partial Pressure of Steam for Case-3	110
Figure 4-10 Heightwise Temperature Comparison for Cases with Different Nitrogen Amount	111
Figure 4-11 Estimated Mass Fraction of Nitrogen and Partial Pressure of Steam for case with 15wt.% Nitrogen Content.....	112

LIST OF TABLES

Table 2.1 Estimation of decay heat with different volatility models.....	34
Table 2.2 Simulation Settings.....	38
Table 3.1 Common Dimensionless Numbers to Characterize Heat and Mass Transfer	67
Table 3.2 Common Correlations for Heat and Mass Transfer Analogy.....	67
Table 3.3 Selected tests from COPAIN experiment for comparison[56]–[58]	74
Table 3.4 Settings for Simulation of COPAIN Experiments.....	75
Table 3.5 Influence of Grid Resolution on Heat Transfer Coefficient.....	78
Table 3.6 Comparison between Estimated and Overall Mass Transfer Coefficients.....	91
Table 3.7 Modified Ranz-Marshall Coefficients	92
Table 3.8 Estimated Condensation Heat Flux for COPAIN Experiments	98
Table 4.1 Coefficients for Decay Heat Calculation.....	104
Table 4.2 Estimated Condensate Amount for Different Non-condensable Amount....	110
Table 4.3 Estimated Decay Heat Dissipation as Condensation.....	111

LIST OF SYMBOLS

Symbol		Units
<hr/>		
Latin Letters		
A	Area	m^2
B	Bird suction parameter	[-]
c	Speed of light	m / s
c_p	Specific Heat	$J.kg^{-1}.K^{-1}$
D	Diffusion coefficient	$m^2.s^{-1}$
g	Gravitational acceleration	$m.s^{-2}$
h	Heat transfer coefficient	$W.m^{-2}.K^{-1}$
h_D	Mass transfer coefficient	$m.s^{-1}$
H	Enthalpy	$J.kg^{-1}$
J	Diffusion Flux	$mol.s^{-1}.m^{-2}$
k	Thermal conductivity	$W.m^{-1}.K^{-1}$
L	Characteristic length	m
q	Heat transfer	W
T	Temperature	K
w	Mass fraction	[-]
w_{sat}	Mass fraction at saturation temperature	[-]

y^+	Nondimensional distance	[-]
t_s	Time after reactor shutdown	s

Greek Letters

β	Thermal expansion coefficient	K^{-1}
δ	Film thickness	m
ν	Kinematic viscosity	$m^2.s^{-1}$
μ	Dynamic viscosity	$kg.m^{-1}s^{-1}$
φ	Concentration	[-]
ρ	Density	$kg.m^{-3}$
σ	Stefan Boltzmann constant	$W.m^{-2}.K^{-4}$
θ_B	Suction correction factor	[-]

Subscripts

∞	Refer to bulk property
c	Refer to cell
g	Refer to gas
i	Refer to i-th species
l	Refer to liquid
s	Refer to steam
w	Refer to wall
Y	Refer to species

Dimensionless Numbers

Gr	Grashof number
Ra	Rayleigh number
Pr	Prandtl number
Nu	Nusselt number
Sc	Schmidt number
Sh	Sherwood number

Abbreviations

1F1	Fukushima Daiichi Unit-1
BWR	Boiling Water Reactor
CCS	Containment Cooling System
CFD	Computational Fluid Dynamics
D/W	Drywell
ECCS	Emergency Core Cooling System
FVM	Finite Volume Method
HPCI	High Pressure Coolant Injection System
HMTA	Heat and Mass Transfer Analogy
HMTD	Heat and Mass Transfer Diffusion Method
IC	Isolation Condenser
ISP	International Standard Problem
NRG	Nuclear Research and Consultancy Group
PANDA	Passive Decay Heat Removal and Depressurization Test Facility

PCV	Primary Containment Vessel
PDEs	Partial Differential Equations
RCIC	Reactor Core Isolation Cooling
RHR	Residual Heat Removal System
RPV	Reactor Pressure Vessel
S/C	Suppression Chamber
SRV	Safety Relief Valve
VOF	Volume of Fluid Method

ACKNOWLEDGEMENTS

I would like to thank Prof. Koji Okamoto for his support, guidance and advices for this research.

I would also like to thank Dr. Masahiro Kondo and Dr. Nejdert Erkan for their support and guidance. This work could not be possible without the discussions and advices I had from them.

I am also glad to had discussion regarding to measurement data of Fukushima Daiichi Unit-1 and condensation modelling with Dr. Ikken Sato from JAEA and Dr. Rinichi Asano from Hitachi.

I also would like to thank Ms. Komatsu, Ms. Inoue and Ms. Nabeshima for their help to ease my life about the procedures regarding University life and life in Japan.

The financial support of Ministry of Education, Culture, Sports, Science and Technology of Japan is also acknowledged.

I would also like to thanks to member of Okamoto Laboratory for their friendship and guidance. It was very enjoyable to attend laboratory meetings and trips.

Lastly, I would like to thank my family for their encouragement and lifelong support.

I. Summary

Among the issues related to decommissioning of Fukushima Daiichi Power Plants fuel debris retrieval has priority to be solved. In order to conduct fuel retrieval activities safely, information about debris location and its characteristics carry crucial importance.

The present work focused on retrieving more information about debris location and its characteristics to contribute the decommissioning activities in Fukushima Daiichi Unit-1 (1F1) Power Plant.

Despite several attempts, information collected up to now is insufficient to locate debris inside the containment. Such information can be extracted by evaluating gas flow inside primary containment vessel (PCV) considering the measurements taken after the accident. In this study a commercial software STAR-CCM+, was used to conduct simulations and particular attention is given to model gas flow and related heat transfer phenomena inside the PCV.

After post processing the available measurement data published by TEPCO, steady cooling period of debris selected as an analysis date considering availability and stability of data. Steady state CFD analysis are conducted assuming that during this period, decay heat plays a role as a heat source and PCV walls are the ultimate heat sink. Results of the simulations estimated the amount of decay heat dissipated to superheat gas and address the temperature asymmetry on safety valves by introducing additional heat source to represent local heating. Moreover, possibility to predict debris spreading through the opening of the pedestal is also evaluated by altering heat source amount inside pedestal and on the drywell floor.

Noting that the simulations conduct with only convective heat transfer show excessive cooling on top head region of PCV, a condensation model is developed to simulate wall condensation in 1F1 PCV. Condensation model validated based on COPAIN tests implementing model via user defined functions into STAR-CCM+, later applied to 1F1 PCV to evaluate the effect of wall condensation. Furthermore, simulations conducted to estimate the effect of nitrogen injection on debris cooling.

In last chapter, concluding remarks are drawn and future activities are suggested.

Chapter 1 Introduction

1.1 Background

In order to carry out decommissioning activities safely in Fukushima Daiichi Unit-1 (1F1), information about debris location and its characteristics are important. After the accident, several attempts such as muon imaging [1], investigations using robots [2] and analysis with severe accident codes [3] are conducted. However, information gathered up to now is not sufficient to understand debris location and its characteristics. Computer simulations conducted with severe accident codes such as SAMPSON, MAAP, ASTEC, ATHLET-CD/COCOSYS, MELCOR and THALES [3-5] to estimate debris condition are inherently carry some limitations due to lumped parameter approach and simplified physics to represent certain number of phenomena such as flow mixing and natural circulation. Also it is not possible to represent detailed fluid field information for flow patterns such as downward flow near wall or thermal stratification which will effect heat transfer evaluation. Moreover, limitations on estimating physical condition of debris such as shape, volume and spreading also decrease the reliability of the predictions.

On the other hand, detailed analysis of containment thermal hydraulics based on the measurements taken after the accident may reveal more information about debris location and its characteristics in 1F1. Such information can be acknowledged by conducting simulations for gas flow inside primary containment vessel (PCV). Recent studies [6–8] show, computational fluid dynamics (CFD) can be used to analyse gas flow inside containment in detail. Therefore, this study aims to investigate more information about debris location and its characteristics considering measurements taken after the accident by conducting three-dimensional CFD analysis inside 1F1 PCV using commercial software STAR-CCM+.

Focus of the simulations are on the thermal hydraulics behaviour of containment on April 6th where the cooling assumed to be steady. At this phase, natural circulation plays important role regarding energy transfer from debris. Gas inside the PCV heated up by decay heat and carry the energy to structures and PCV walls. In this condition, PCV walls are the ultimate heat sink where the energy from debris will be transferred to the environment. To evaluate such condition debris is represented by defining heat source.

On the other hand, heat sink is defined on PCV walls by using thermal resistance concept. Estimated temperature results compared with the measurements to predict dissipation of decay heat to superheat gas inside PCV. Also, temperature asymmetry related to safety valves addressed by introducing additional heat source at this location and amount of local heating effect is estimated. Moreover, spreading effect of debris is also addressed by changing the distribution of heat source inside the pedestal and on drywell floor. However, due to the limited amount of temperature data and mixing inside containment, information gained was not sufficient. Simulations considering only convective heat transfer through containment walls shows excessive cooling around top head region which indicates the necessity of the condensation modelling. Moreover, total heat transfer is underestimated considering only convection. The structure of the thesis is as follows: in chapter 2 simulations of gas flow inside 1F1 is introduced, in chapter 3 wall condensation modelling is explained, in chapter 4 CFD analysis with wall condensation is explained and in section 5 conclusion and discussion are stated.

1.2 Fukushima Daiichi Accident and Decommissioning Activities

1.2.1 Overview of the Fukushima Daiichi Nuclear Power Stations

On March 11, 2011 the accident at Fukushima Daiichi Nuclear Power Stations occurred by the Great East Japan Earthquake induced the worst case scenario of releasing a massive amount of radioactive materials. Fukushima Daiichi Power Plant Station hold six boiling water reactors. Unit 1-4 are located in Okuma town, Futaba district and Unit 5 and 6 are located in Futaba town, Futaba district. Total installed power generation capacity is of the Fukushima Daiichi Nuclear Power site is 4.696 million kW. Fukushima Daiichi Unit-1 is a BWR-3, units 2-5 are BWR-4, and Unit-6 is BWR-5.

Safety equipment shows differences for each unit. In case of Unit-1(BWR-3) most important safety system is the emergency core cooling (ECCS) system. In the event of

any accident involving loss of coolant, ECCS urgently injects cooling water into the power plant. ECCS consists of two core spray systems, one high pressure coolant injection system and an automatic depressurization system. In case of postulated and severe accident removal of decay heat is the key issue. In BWR-3 systems, decay heat is transferred to suppression pool and two containment cooling systems (CCS) are installed to eliminate heat from suppression chamber and cool the containment vessel. Moreover, two core isolation condensers function to dissipate the heat from the reactor when it is isolated from the turbine system.

For Units 2-5(BWR-4), most important difference compared to Unit-1 is the residual heat removal system (RHR). This system covers the functions of CCS and shutdown cooling system as well as the low pressure coolant injection system. The ECCS in Units 2-5 consists of two core spray systems, one high pressure coolant injection system, one low pressure coolant injection system and an automatic depressurization system. Installed reactor core isolation system as change from isolation condenser of BWR-3 for cooling injection in a reactor isolation event.

In case of Unit-6 (BWR-5), biggest change is the improved efficiency of jet pumps which can obtain larger core flows with a primary circulation pump with a smaller capacity. ECCS in BWR-5, consists of one high pressure core spray system, one low pressure core sprays system, three low pressure coolant injection system and an automatic depressurization system.

1.2.2 Overview of the Accident

On March 11, 2011 the fourth largest earthquake in recorded world history (M9.0) is occurred. Following the earthquake automatic shutdown initiated in Fukushima Daiichi Reactors. Later, 12 emergency diesel generators except that at Unit-4 under inspection, automatically started up to secure the power supply for all units. At this stage, plant parameters do not indicate any damage to the pressure boundary of reactor coolant. In addition, the results of walk down inspections within the extent visually confirmable

showed damage to a tiny portion of equipment with low earthquake resistance, which did not influence safety of nuclear power plants [9].

In case of Unit-1, all the external power supplies were lost and two emergency diesel generators automatically started. Moreover, the main steam isolation valves are also closed and reactor pressure rose. Following this, the isolation condensers (ICs) started up and the reactor water level was maintained. Due to the operation of ICs reactor pressure and temperature are lowered. Later on, an operator operated the IC to avoid a drastic drop in temperature. Even though the external power supplies were lost, safety function were secured as designed and the power plant kept safe until the tsunami hit the station. Following the tsunami, diesel generators lost their function and except the emergency lighting in main control room, all the power in the station was lost. Loss of DC power triggered the IC isolation interlock and led to the closure of isolation valves. So that, IC cooling function was lost due to fail safe design for confinement function. Consecutively, the reactor pressure rose and SRV operate. Steam is channelled the suppression chamber (S/C) and condensed. Based on analytical results, reactor water level estimated to fell below top of active fuel around 18:00 March 11 and core damage progressed. On the other hand, the reactor pressure reported as 7.0 MPa by the on-site indicator which indicates that pressure boundary if the reactor coolant was sound and that the pressure boundary of reactor coolant was sound by the SRV safety valve function. On March 12, measurements showed that drywell (D/W) pressure was 0.6 MPa which is higher than that of operating pressure (0.531 MPa). Such pressure increase in D/W without any operator action indicates that the pressure boundary of the reactor has already been damaged. At around 4:00, alternative water-injection line is established to inject water with fire engines. Initially, fresh water was used but as it is soon depleted, sea water continued to be injected. Such activity took ample amount of time due to difficulties in finding the nozzle to be connected to fire engine hoses and rubble that was scattered in the site. Based on analytical results, water injection was not effective to prevent core damage cool the molten fuel in the pedestal area. As the molten fuel reached the pedestal area, the molten core concrete interaction also expected which eroded the pedestal floor. Following the core damage, hydrogen was generated through a reaction between zirconium and water and accumulated in the containment vessel and leaked through the

unknown paths to the reactor building. As the hydrogen concentration exceeds certain concentration there was an explosion occurred at 15:36 on March 12 at the reactor building.

In case of Unit-2, the earthquake stopped the reactor and the all external power supplies were lost. The emergency diesel generators automatically started up and main steam isolation valves closed and reactor pressure was controlled by the safety relief valves (SRV). Later on, an operator start the reactor core isolation cooling system in order the keep the reactor water level at desired point. After the tsunami hit the power plant, almost all power panels were disabled. Furthermore operators become unable to determine the operational state of the RCIC. As they cannot determine the reactor water level either, they prepared for an alternative water injection path. Around 22:00, it was reported that the water level exceed the top of active fuel from the measurement taken by using battery. During this time the SRV did not functioned due to low reactor pressure. On the other hand, it was assumed that the RCIC operational conditions were not sufficient, and the water injection flow was smaller than the rated value. In order to ensure cooling of the core in case of failure of RCIC system, an alternative water-injection line was established in 13th of March. However, the explosion in Unit-3 damaged the prepared fire engines and hoses. On 14th of March, the reactor water level started to decrease possibly to the deterioration in the function of the RCIC. Following that the pressure in the reactor vessel is increased. In order to countermeasure SRV operation and water injection by fire engines were prioritized and after 18:00 the depressurization is reported to be successful. The analytical results by severe accident codes show the reactor water level decreased below the top of active fuel level around 17:00 on the 14th of March. Subsequently, core damage was progressed. However, core damage in Unit-2 is quite different compared the other units due to operation of RCIC and no hydrogen explosion. It is assumed that the gas containing the hydrogen was released from the blowout panel which was opened due to the impact of the explosion in Unit-1.

In case of Unit-3, reactor is automatically stopped due to earthquake and external power supplies were lost. Later on, the emergency diesel generators automatically started up and main steam isolation valve is closed. The reactor pressure was controlled by SRVs and the operators manually started RCIC before the water level declined in the reactor

vessel. After tsunami attacked the power station, many power panel functions were lost but DC power remained available unlike Units 1 and 2. Due to this fact, DC-powered turbine driven equipment, including the device to monitor the reactor water level RCIC, and the high pressure coolant injection system (HPCI system) remained available. At 11:36, on March 12, the RCIC automatically stopped, and the reactor water level declined. Following this the HPCI system is actuated to maintain the water level. As a result of continuous operation of HPCI system, large amount of steam generated by decay heat was continuously discharge to the HPCI turbine, and the reactor pressure was kept at low level. On 13th of March, the measured reactor pressure value decreased below 1MPa, and HPCI system is manually shut down due to concern about damaging the HPCI system. Following this, reactor water level fell below top of active fuel level after 9:00 on 13th of March and core damage estimated to occur at around 10:40. In order to, avoid similar explosion as in Unit-1, several measures were considered such as opening the blowout panel, forming holes in the ceiling of the reactor building etc. However, before performing such actions an explosion occurred at 11:01 on March 14. The explosion observed was more violent compared to Unit-1. This might be due to fact that the reactor building of the Unit-3 was a reinforced concrete rather than a steel like in Unit-1.

1.2.3 Decommissioning Activities

Up to now several important milestones achieved to stabilize the site condition as a part of decommissioning activities such as completion of water removal from the Unit 1-3 condensers, installation of Unit3 fuel removal cover, construction of land side impermeable walls, installation of the Unit-1 windbreak fences, removal of unit 2 reactor building roof protection layer, removal of spent fuel of Unit-4 from the spent fuel pool. Besides those activities, several improvements established for the environment within the site. Those actions targeted to reduce the effect of additional release from the entire power station and radiation from radioactive waste generated after the accident to limit the effective radiation dose to below 1mSv/year at the site boundaries also to prevent contamination expansion in sea. Activities for these purposes includes optimization of

radioactive protective equipment, Installation of dose-rate monitors and installation of sea-side impermeable walls.

Moreover, several countermeasures are taken to store and treat the contaminated water after the accident. Those countermeasures depend on 3 principles eliminating contamination sources, isolating water from contamination and preventing leakage of the contaminated water. In order to eliminate contamination sources, multi nuclide removal equipment installed on the site contaminated water is removed from the trench. In order to isolate the water from contamination, groundwater is pumped up for bypassing, land site impermeable walls are installed and waterproof pavements are installed. To prevent leakage of the contaminated water, sodium silicate is added to soil, sea side impermeable walls are installed and welded joints tanks are increased. Nuclide removal from the contaminated water is conducted with multi-nuclide removal equipment. Such equipment removes radionuclides from the contaminated water in tanks and reduces risks. Treatment of contaminated water is completed in May 2015 via multi-nuclide removal equipment.

Completion of several activities to stabilize the condition at site enable further work to remove debris from the power plants. According to technical strategic plan 2016 for decommissioning of the Fukushima Daiichi Nuclear Power Station of Tokyo Electric Company Holding, Inc. published by Nuclear Damage Compensation and Decommissioning Facilitation Corporation [10] fuel debris retrieval proceed with the following steps:

- Maintaining and management of stable condition of fuel debris retrieval
- Safe retrieval of fuel debris
- Stable storage of retrieved fuel debris after collection and transport.

After aforementioned activities, stable conditions in Fukushima site is achieved. In order to achieve next step which is safe retrieval of fuel debris, understanding the location and characteristics of debris is important. Investigation for the location and characteristics of debris, several activities are ongoing such as estimation by actual unit investigation, estimation by analysis and estimation based on knowledge or experiments. Besides, safety of the retrieval activities also be assured. For this purpose, structural integrity of primary containment vessel has to be ensured, criticality of fuel debris has to be controlled,

cooling function of the debris has to be maintained, and work safety has to be assured. After such considerations, debris retrieval method can be put into work. Such method includes development of equipment or device for fuel debris retrieval, establishment of access route to fuel debris and establishment of system equipment and areas.

1.3 Heat Removal from Debris

1.3.1 Introduction

In this section heat transfer mechanisms that play role in heat removal from discharged debris will be introduced. During the cooling of debris, heat is removed by several heat transfer mechanisms such as radiation, conduction, convection and evaporation-condensation. Radiation and conduction are the dominant mechanisms during early period after discharge as the debris has high temperatures and in touch with the basement of the containment. With the injection of coolant convection and wall condensation play key role in heat removal from debris. After the injection of coolant, decay heat plays role as a heat source and the PCV walls are the ultimate heat sink. Steam generated due to decay heat rises through containment dome, then condenses on the containment walls. Following sections give introductory information about heat removal mechanisms from debris.

1.3.2 Radiative Heat Transfer

After the discharge of debris from RPV, some portion of the decay heat is transferred to the other structures inside the PCV by radiative heat transfer. As the debris is at high temperature and it is open the PCV environment, structures such as pedestal inside the PCV are exposed to intense radiation heating. The radiation of a black body can be expressed with Stefan-Boltzmann law as:

$$q = \sigma T^4 A \quad (1.1)$$

where q is heat transfer per unit time, σ is the Stefan-Boltzman constant, T is absolute temperature in Kelvin and A is the area of the emitting body. As thermal radiation grows with the 4th power of the temperature, radiation heat transfer is important at early phases after the discharge of the debris since it is at high temperature. On the other hand, as debris cooled down by time or with external intervention such as coolant injection, effect of radiative heat transfer becomes less significant. In this study, radiative heat transfer is neglected as the analysis conducted for the phase far after the coolant injection.

1.3.3 Conduction Heat Transfer

After discharge of the debris from RPV, it come into contact with the pedestal and drywell floor. Due to this contact, decay heat is transferred to the concrete structures by conduction. Conduction heat transfer occurs with the movement of particles and electrons within the body or between two or more bodies in contact. It takes place in all phases of matter and can be expressed by Fourier's law:

$$q = -k \nabla T \quad (1.2)$$

where q is heat transfer per unit time, k is thermal conductivity and ∇T is the temperature gradient. As thermal conductivity of concrete is relatively low, it is expected that the heat transfer through the concrete will also be low. However, due to the efficient thermal mass property of the concrete, decay heat will be absorbed and stored on the structures for a long time. This will also increase the overall temperature of the containment environment. In this study, conduction heat transfer is considered for the solid structures inside the PCV such as, top plate, bioshield, pedestal and RPV etc.

1.3.4 Natural Convection

Heat transfer by natural convection is an important phenomena to understand dissipation of decay heat from debris for post severe accident cases. Gas flow by natural circulation distributes the energy from debris to other regions of the containment. Natural convection can be defined as a transport mechanism where no external force acting on the flow and flow motion is due to buoyancy-induced motion resulting from internal body force generated by density gradients. The dimensionless Grashof number is used to characterize natural flow which represents ratio of buoyancy force to viscous force acting on fluid and defined as follows:

$$Gr = \frac{g \beta (T_{surface} - T_{\infty}) L^3}{\nu^2} \quad (1.3)$$

Where g is gravitational acceleration, β is coefficient of volume expansion, T_{∞} is temperature of fluid, L is characteristic length of geometry and ν is kinematic viscosity of fluid. The coefficient of volume expansion at constant pressure is expressed as

$$\beta = -\frac{1}{\rho} \left(\frac{\partial \rho}{\partial T} \right)_p \quad (1.4)$$

For numerical simulations Grashof number determines if the simulations will be steady state or transient. If the Grashof number is greater than 1×10^{10} , flow considered to be transient. Another dimensionless number so called Rayleigh number is used to estimate the strength of buoyancy induced flow. Rayleigh number is defined as:

$$Ra = Gr Pr = \frac{g \beta (T_{surface} - T_{\infty}) L^3}{\nu^2} Pr \quad (1.5)$$

Rayleigh number less than 10^8 indicates a buoyancy induced laminar flow, and the transition to turbulence occurring between $10^8 < Ra < 10^{10}$. When Rayleigh number exceeds 10^{10} flow becomes turbulent. To determine if the case is dominated by natural convection or forced convection, the ratio of the Grashof number over the Reynolds number squared can be examined. In case this ratio exceeds 1.0, it can be assumed that natural convection

does indeed dominate. In case of numerical simulations concerning natural convection following steps are important to achieve convergence:

- For accurate results a low Reynolds number turbulence model has to be used and near wall prism layer has to be adjusted to achieve $y^+=1$.
- Proper equation of state has to be utilized for the working fluid. For atmospheric air the ideal gas law is the best choice but for liquids density variation with temperature has to be accounted.
- If there is pressure boundary in the model that use the piezo metric pressure it is critical that reference pressure is set to working fluid density at these boundaries so that hydrostatic pressure variations are included in the boundary pressure correctly.
- While using a two layer all y^+ wall treatment for turbulence model, proper model that considers buoyancy driven flow should be used since the turbulent quantities and the averaged flow influence each other, it is crucial that the function used inside the near wall layer be accurate. The balance of turbulent production, diffusion, dissipation is quite different between flows where convection is forced, and flows which are dominated by natural convection. Therefore, different formulations of the near wall layer should be used depending on the type of flow simulated.

1.3.5 Wall Condensation

As vapor comes into contact with the cold wall surface at a temperature below the saturation temperature for the corresponding partial pressure of the vapor condensation starts to form on the surface. As vapor condenses on the cooled surface, latent heat released and transferred to wall cooling down the surrounding gas layer while the phase change is occurring.

In case of condensation in nuclear power plant containment, two types of condensation may occur region wise. One is main stream condensation and the other is wall condensation. Considering that gas in the main stream is easily heated to the steam saturation temperature, such condensation can be neglected whereas wall condensation is

the dominant form of containment residual heat removal. Formation of wall condensate may occur as droplets or a film as in Figure 1-1. Dominant factor for the form of the condensate is the surface condition. In case of surfaces with fine finishing film condensation is likely to be occurred. Regardless of the condensation form, condensate acts as a resistance to heat transfer between the vapour and the surface. Dropwise condensation has higher heat transfer rates compared to film wise condensation however it is harder to achieve dropwise condensation in practical applications. Heat and mass transfer rates during condensation mostly depend on the local mixture parameters such as species concentration. Another important point during condensation process is the presence of non-condensable gases. Even small amount of non-condensable gases can deteriorate condensation. If the non-condensable gas is consists of heavy molecules, it tends to accumulate near the liquid-gas interface due to its impermeability. This creates additional resistance to the mass transfer during condensation as condensable gas has to diffuse through non-condensable gas layer accumulated near cold structures.

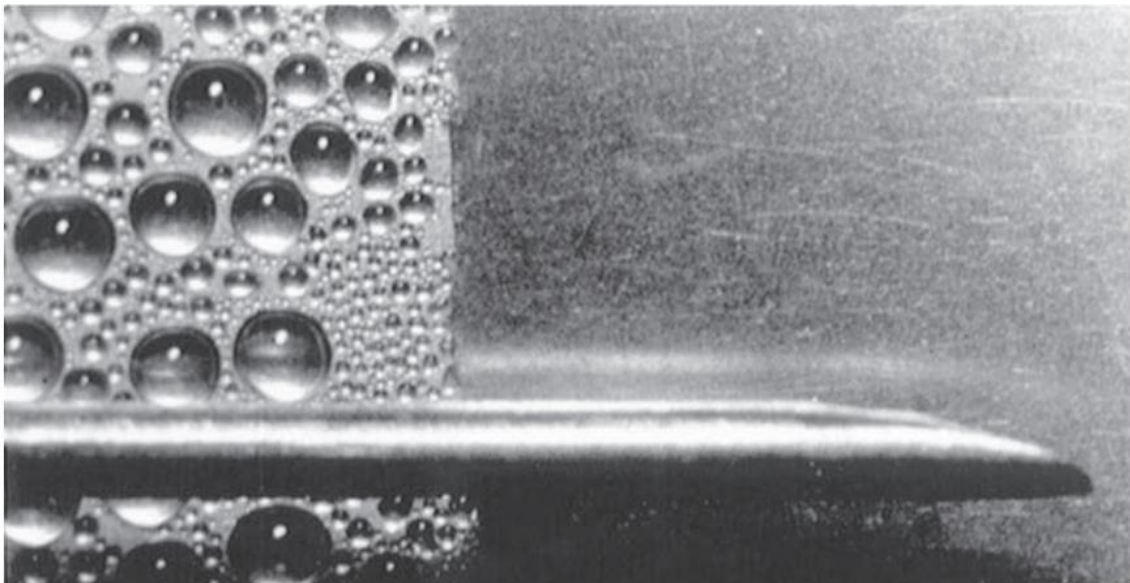


Figure 1-1 Droplet and Film Condensation [11]

Steam condensation on containment walls plays role as a passive energy heat sink. During the late phase of severe accident, condensation on containment wall has important

effect on removing decay heat. Also pressure inside the containment largely effected by the condensation. With increasing condensation rate pressure is decreasing and vice versa. During condensation of steam in presence of non-condensable gases, condensation heat transfer is hindered by accumulation of non-condensable gases near the wall. Due to the accumulation of non-condensable gases, steam partial pressure at the liquid-gas interface becomes smaller than the bulk flow which produce a driving force that forces steam diffuse toward the condensate film. Accumulation of non-condensable gases, greatly reduces the heat transfer through the containment walls.

1.4 Objective

This study aims to contribute decommissioning activities particularly fuel debris retrieval in 1F1 by conducting computer simulations to investigate about debris location and its characteristics.

Outline of the study is as shown in Figure 1-2. With recent investigations using muon imaging techniques and robots, information gathered is insufficient to locate debris in 1F1. On the other hand, detailed analysis of containment thermal hydraulics based on the measurements taken after the accident may reveal more information about debris location and its characteristics. Such information can be acknowledged by conducting simulations for gas flow inside primary containment vessel (PCV). Simulations are conducted by using computational fluid dynamics technique which uses numerical calculations to analyse problems that includes both fluid flow and heat transfer. With the recent advancement in CFD, it becomes possible to conduct detailed gas flow analysis inside large cavities such nuclear power plant containments.

Choice of computer simulation to evaluate the debris condition in 1F1 is cost effective and suitable to consider several possibilities that may reveal information about debris location. Moreover, as CFD can resolve flow field more in detail compared to lumped parameter codes debris condition can be estimated more reliably. As lumped parameter codes do not model details of flow, estimated heat transfer usually do not

represent reality. Moreover, 3 dimensional effects cannot be represented in lumped parameter codes where those effects are being implemented from the expected flow behaviour of the scaled experiments. Despite the fact that high quality CFD analysis is a complex process, recent numerical schemes and matured single phase models make it applicable for analysis of several physical phenomena. Furthermore effect of complex geometry including turbulent flows and phenomena that requires specific modelling such as mixed convection, multiphase flow, phase change and general mixing at experimental conditions of beyond the limits of experimental data can be address by using CFD.

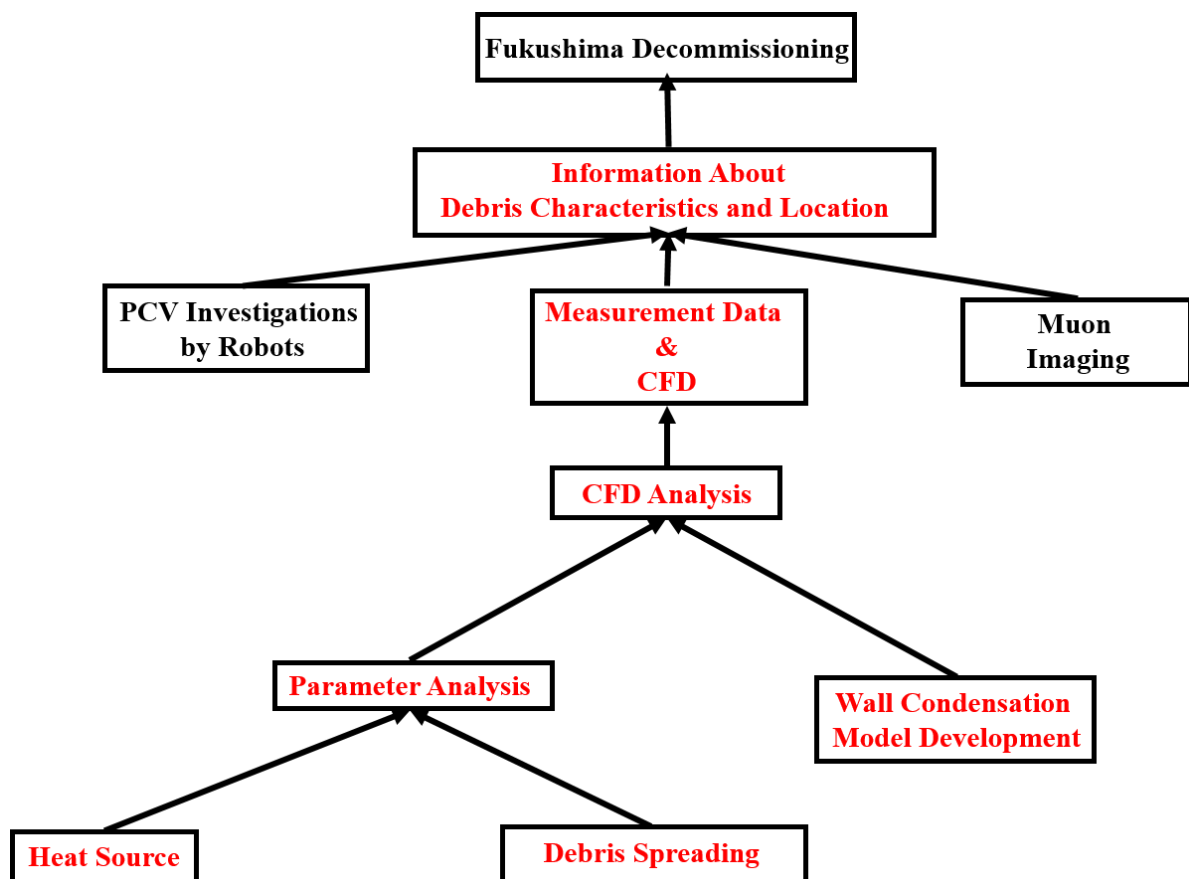


Figure 1-2 Outline of the Study

In this study aim of using CFD is to simulate gas flow and heat transfer inside 1F1`PCV to solve the inverse problem and estimate the condition of fuel debris. Two main activities are realized:

1. Parameter analysis
2. Wall condensation model development

Parameter analysis aimed to estimate amount of decay heat dissipated to superheat the gas inside the PCV and evaluate the effect of debris spreading through the opening of the pedestal. Wall condensation modelling on the other hand aims to come up with a suitable wall condensation model which is applicable to evaluate condensation inside the 1F1 PCV.

**Chapter 2 Simulations of Gas Flow
Inside Fukushima Daiichi Unit-1
Primary Containment Vessel**

2.1 Introduction

In this section CFD analysis for the gas flow inside the 1F1 PCV will be introduced without considering wall condensation. As mentioned in previous section, during long term containment cooling of debris natural circulation plays an important role. Gas at lower elevation is heated up due to the decay heat and dissipate the energy to other regions inside PCV. Simulations will be conducted using a CFD code STAR-CCM+. Firstly, simulation will be conducted to validate the natural convection for a selected case from literature. Later, natural convection inside the PCV will be evaluated by introducing heat source to represent the debris in 1F1 and heat sink on PCV walls.

2.2 Computational Fluid Dynamics

Goal of CFD analysis is to retrieve deeper understanding of the problems including heat transfer and fluid flow. The simulated thermo-physical phenomenon needs proper mathematical model which in turn requires to make valid choice of the appropriate settings in CFD software. CFD study consists of several states. This process starts with problem definition. From the engineering point of view, problem in interest needs to be described in simplest form possible. On the other hand it should still accurately describes the actual real world engineering system. After defining the problem, mathematical model has to be defined properly. Proper mathematical modelling is crucial in order to obtain a valid solution to the simulated problem. Next stage after mathematical modelling is pre-processing and mesh generation. The flow domain must be discretized in order to approximate the model solution numerically. Spatial discretization of the computational

domain so called mesh generation is used to separating flow domain into volumes (cells), using different shapes. CFD analysis usually concern about optimum computational time and number of cells after spatial discretization. As rule of thumb mesh can be further refined if for regions of interest and locations consist of large gradients. Next step after pre-processing and mesh generation is solving the CFD problem. This step is one of the time consuming step in CFD along with pre-processing and mesh generation. Required time depends on the mathematical model, the numerical scheme and computational mesh. During this process analytical model gets replaced by a system of algebraic equations. By using iterative linear solvers, system of algebraic equations are solved to compute field variables such as temperature, pressure etc. After the simulations, user will have large amount of data which has to be discussed. In order to have useful information from data visualization is necessary. This step of visualizing data is called post processing. During post processing variables in interest are selected and presented to drive the right conclusions from the solution.

Main idea behind the CFD is to solve Navier-Stokes equations to describe the motion of fluids. Navier-Stokes equations are based on the application of Isaac Newton's second law to fluid motion with the assumption that the stress in the fluid is total of a diffusing viscous term which is proportional to the gradient of velocity and a pressure term.

2.2.1 Finite Volume Method

Main purpose of the computer simulations is to understand phenomena that we cannot always be measured or observed by experimental methods. With the fact that all physical processes are governed by the conservation laws, computer simulations may predict phenomenon that cannot be measured or too costly to conduct experiment. Therefore key point in computer simulations is how we can accurately solve those conservation equations. In computational fluid dynamics conservation equations are represented by partial differential equations (PDEs) which satisfies conservation equations on a fluid element which is infinitesimally small. Validity of those equations

can only be tested in finite size domain for which there is a leap in fate while assuming conservation equations will be valid for finite size control volume as in infinitesimal control volume. Solution of conservation equations must satisfy conservation laws globally, as well as locally for the numerical method otherwise it is not suitable for solution of physical problem. Finite volume method (FVM) inherently satisfies local and global conservation. Figure 2-1 shows one dimensional representation of finite volume discretization and related terminology. In FVM, computational domain discretized into control volumes called cells. Information is stored at the centroids of each cell which are referred as cell center. Another terminology used FVM for the bounding surfaces of each cell which is called as face.

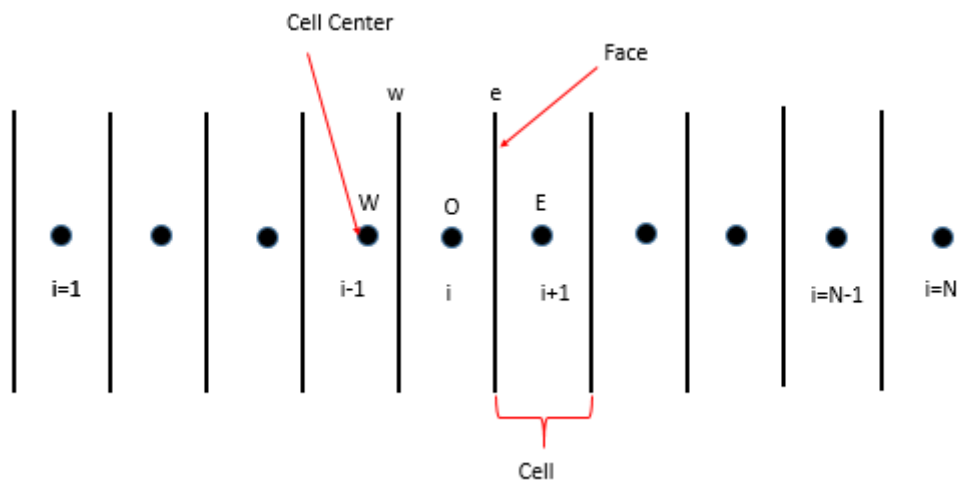


Figure 2-1 1D Finite Volume Representation

In FVM, governing partial differential equation is satisfied over finite-sized control volumes, rather than at points. So in order to represent the conservation of governing equations, the computational domain has to split into a set of control volumes. Generally, shapes that are used to represent the domain are convex polygons for 2D domains and polyhedrons for 3D domains. As those cells are bounded by straight curves, if the boundary surface is curved, it will be approximated by a straight curve. Another aspect of FVM is that conservation property of it, is mesh independent. However error occurs in each individual fluxes compared with analytical solution between two faces which depends on the mesh. So that proper meshing is a key element for the reliable analysis using FVM.

2.2.2 STAR-CCM+

STAR-CCM+ is CFD solver for solving multidisciplinary problems in both fluid and solid continuum mechanics using finite volume method. STAR-CCM+ has capabilities to model variety of flow types such as;

- Inviscid, laminar, or turbulent
- Newtonian and non-newtonian viscosities
- Incompressible and compressible
- Multi-component mixtures
- Multiphase mixtures
- Porous resistance
- Gravitational acceleration

Temporal discretization can be established with both steady and unsteady schemes. Equation of state which relates state variables such as temperature, volume or pressure can be described with constant density, ideal gas law, real gas law, polynomial density or user-defined functions. Software is also capable of simulate all modes of heat transfer in both fluid and solid materials which are conduction, convection and radiation. The solver consists of all the elements of the pre and post processing of CFD problem from generating CAD data to a final flow analysis and visualization. STAR-CCM+ utilizes the latest numerical algorithms, physical models and state of the art software coding which gives advantage to the user to tackle complex multi-disciplinary engineering problems without compromising ease-of-use over accuracy or capability. The governing equations solved in STAR-CCM+ that represents mass, momentum, energy and species conservation are as follows [12]:

Mass conservation:

$$\frac{\partial \rho}{\partial t} + \nabla \cdot (\rho \mathbf{w}) = S_m \quad (2.1)$$

where ρ is density, w is the continuum velocity and S_m is the mass source term.

Momentum conversation:

$$\frac{\partial(\rho \mathbf{w})}{\partial t} + \nabla \cdot (\rho \mathbf{w} \mathbf{w}) = \nabla \cdot \mathbf{P} + \rho f_b + S_{\rho v} \quad (2.2)$$

where f_b the resultant of the body forces, P is the pressure and $S_{\rho v}$ is the source term.

Energy conversation:

$$\frac{\partial(\rho E)}{\partial t} + \nabla \cdot (\rho E \mathbf{v}) = f_b \cdot \mathbf{v} + \nabla \cdot (\mathbf{v} \cdot \boldsymbol{\sigma}) - \nabla \cdot \mathbf{q} + S_E \quad (2.3)$$

where E is the total energy per unit mass, \mathbf{q} is the heat flux, and S_E is the energy source.

Species conversation:

$$\frac{\partial}{\partial t} \left(\int_V \rho Y_i \right) d\tilde{V} + \oint_A \rho Y_i (\mathbf{v} - \mathbf{v}_g) \cdot d\tilde{\mathbf{a}} = \oint_A \left[J_i + \frac{\mu_t}{\sigma_t} \nabla Y_i \right] \cdot d\tilde{\mathbf{a}} + \int_V S_{Y_i} d\tilde{V} \quad (2.4)$$

where ρ is density, Y_i is mass fraction, i is the component index, $d\tilde{V} = \alpha_i \chi dV$, α_i is the volume fraction of phase i and χ is the void fraction, $d\tilde{\mathbf{a}} = \alpha_i \chi d\mathbf{a}$, \mathbf{v} is the velocity. \mathbf{v}_g is the grid velocity, μ_t is the turbulent dynamic viscosity, σ_t is the turbulent Schmidt number, S_{Y_i} is user specified region source term for species i and J_i is the diffusive flux.

2.2.3 CFD as a Tool for Containment Analysis

With the availability of the faster computers for numerical calculations, simulation studies for large cavities such as power plant containments are shifting the approach from analysis with lumped parameter codes to more sophisticated CFD codes. Even though CFD analysis can provide detailed flow properties, there is still need experimentation to validate the mathematical models used to represent physical phenomena that occurs inside containment such as condensation, natural convection, flow mixing, stratification, turbulent diffusion and interaction between them as well. For this purpose several

experimental facilities constructed and experiments conducted. Those facilities mainly fall under two category which are separate effect facilities such as CONAN [13] and COPAIN [14] and large integral test facilities such as ThAI [15], TOSQAN [15-16] and PANDA [18]. Main purpose of both experimental and numerical activities is to achieve better reliability in the prediction of plant response. As the lumped parameter codes used in nuclear industry have their inherent limitation for simulating flow patterns and atmosphere mixing inside the containment, more fundamental and mechanistic approach aimed to be applied to CFD codes which are validated with dedicated experiments.

2.3 Fukushima Unit-1 Measurement Data Post-Processing

Measurements taken after Fukushima is important to understand characteristics of fuel debris. Measurement locations and temperature data used in this study is based on the reliability report and data issued by TEPCO [19]. Figure 2-2 shows both temperature and pressure recordings for period from March 20th to April 7th. Despite there are several thermocouples placed on both PCV and RPV region, number of reliable measurements are limited.

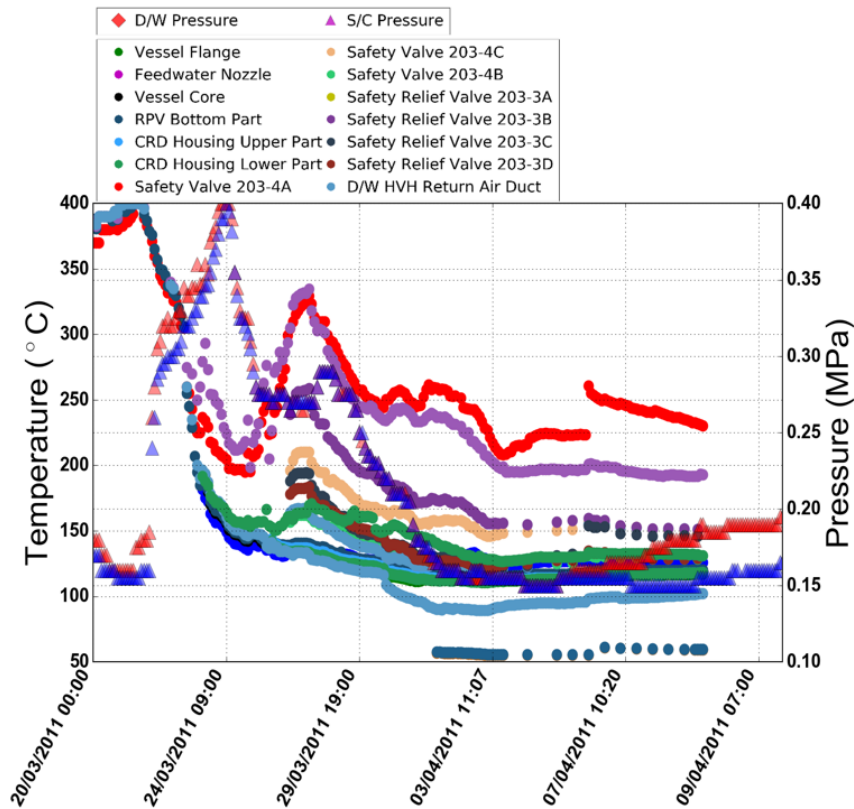


Figure 2-2 Temperature and Pressure Distribution from March 20th to April 9th

Beginning of this period available thermocouple measurements show high values around 400 °C which suggests superheated gas flows inside primary containment vessel tends to equilibrate temperature distribution as seen on Figure 2-3. Before this period no effective water injection can be assumed due to the fact that there is no abrupt pressure change observed before.

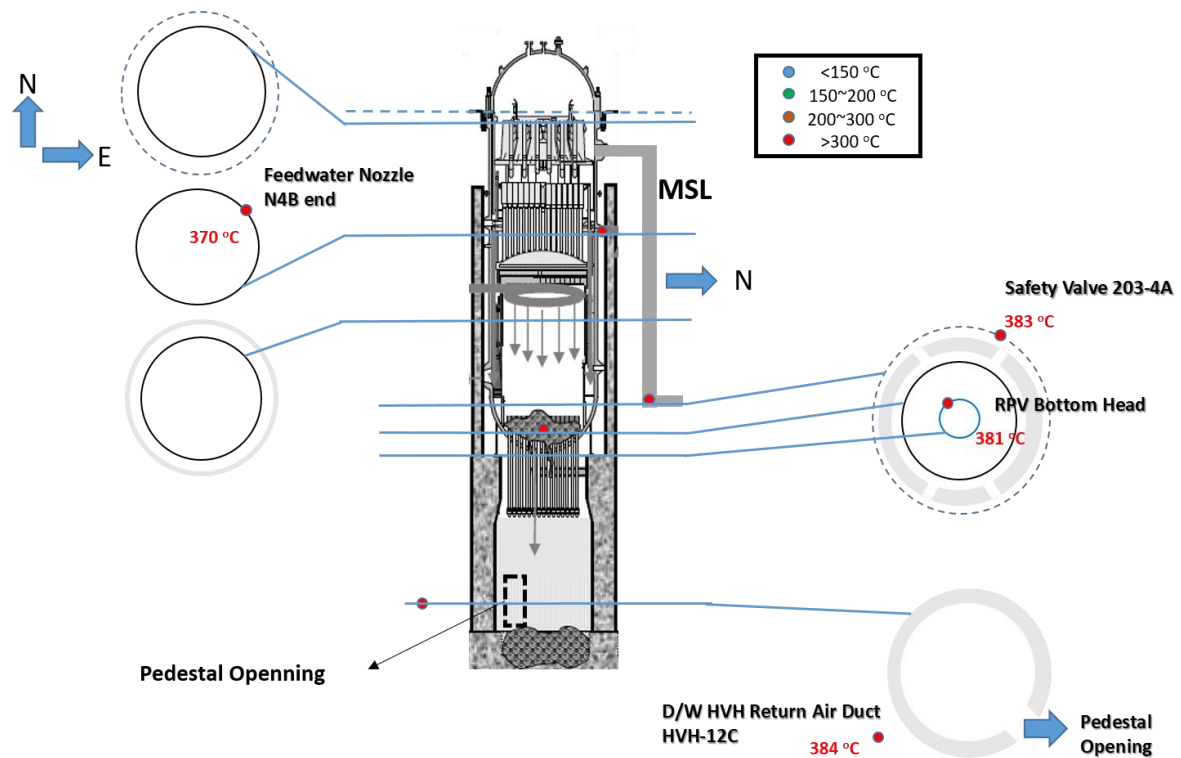


Figure 2-3 Temperature distribution inside PCV on March 21st 03:00

However, on 22nd of March pressure values started to increase due to slight increase in water injection. Increase of pressure becomes significant after water injection increased notably. During this period a pick observed in reactor pressure as in Figure 2-4 which can be interpreted as physical response of the system due to increased water injection.

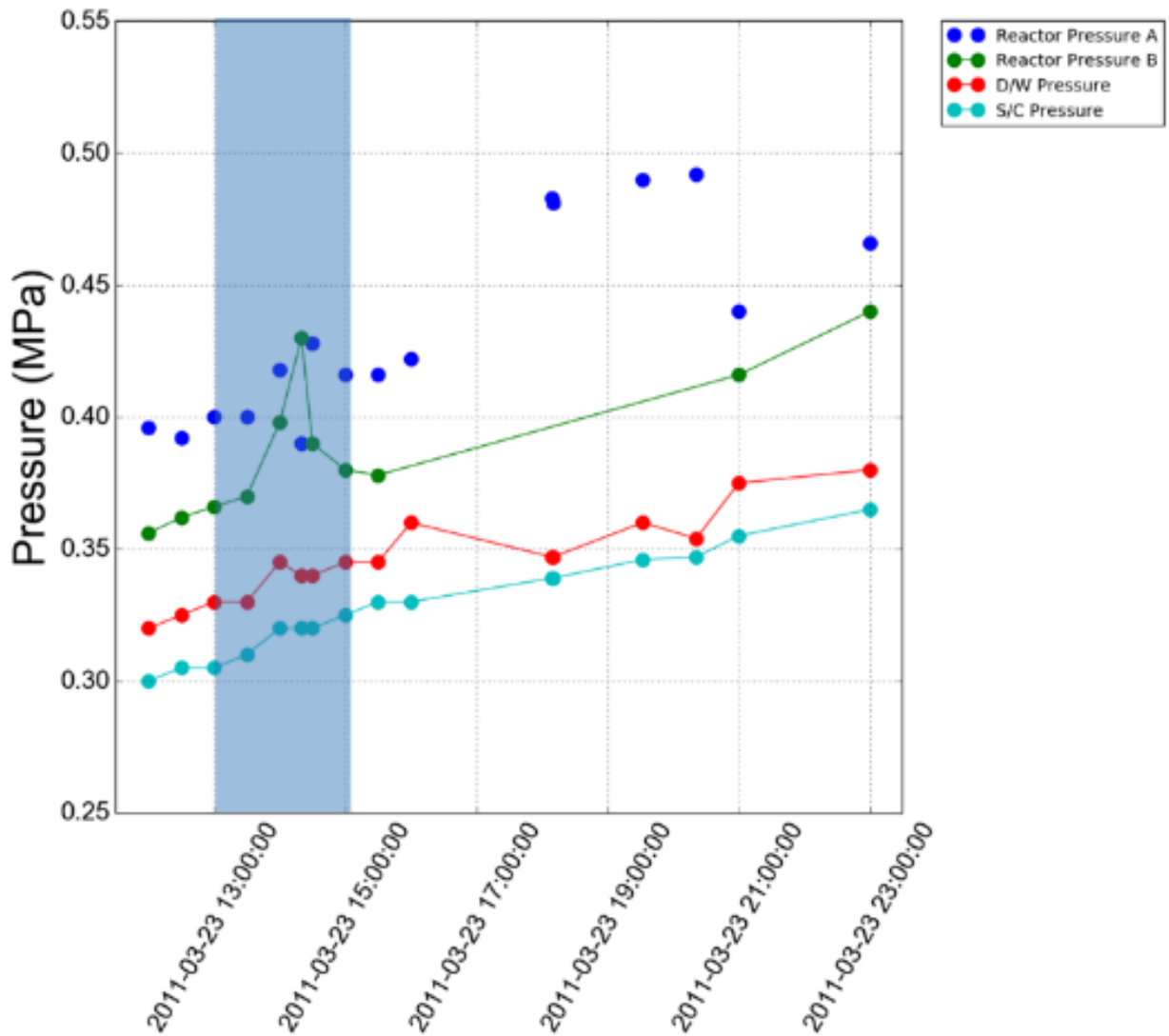


Figure 2-4 Pressure Response

Following the increase of water injection, temperature values started to decrease rapidly. This rapid cooling can be explained by availability of a significant heat sink because injected water can only serve as means to transfer the heat. Due to increased water injection, non-condensable gases that accumulate inside the downcomer of S/C pushed away. With release of such non-concondesable gas layer, vapor inside the D/W rapidly condensed into S/C which plays an important heat sink role. After release of non-condensable gas layer, pressure difference between S/C and D/W oscillates towards balance while pressure was building up both in S/C and D/W as observed in Figure 2-5.

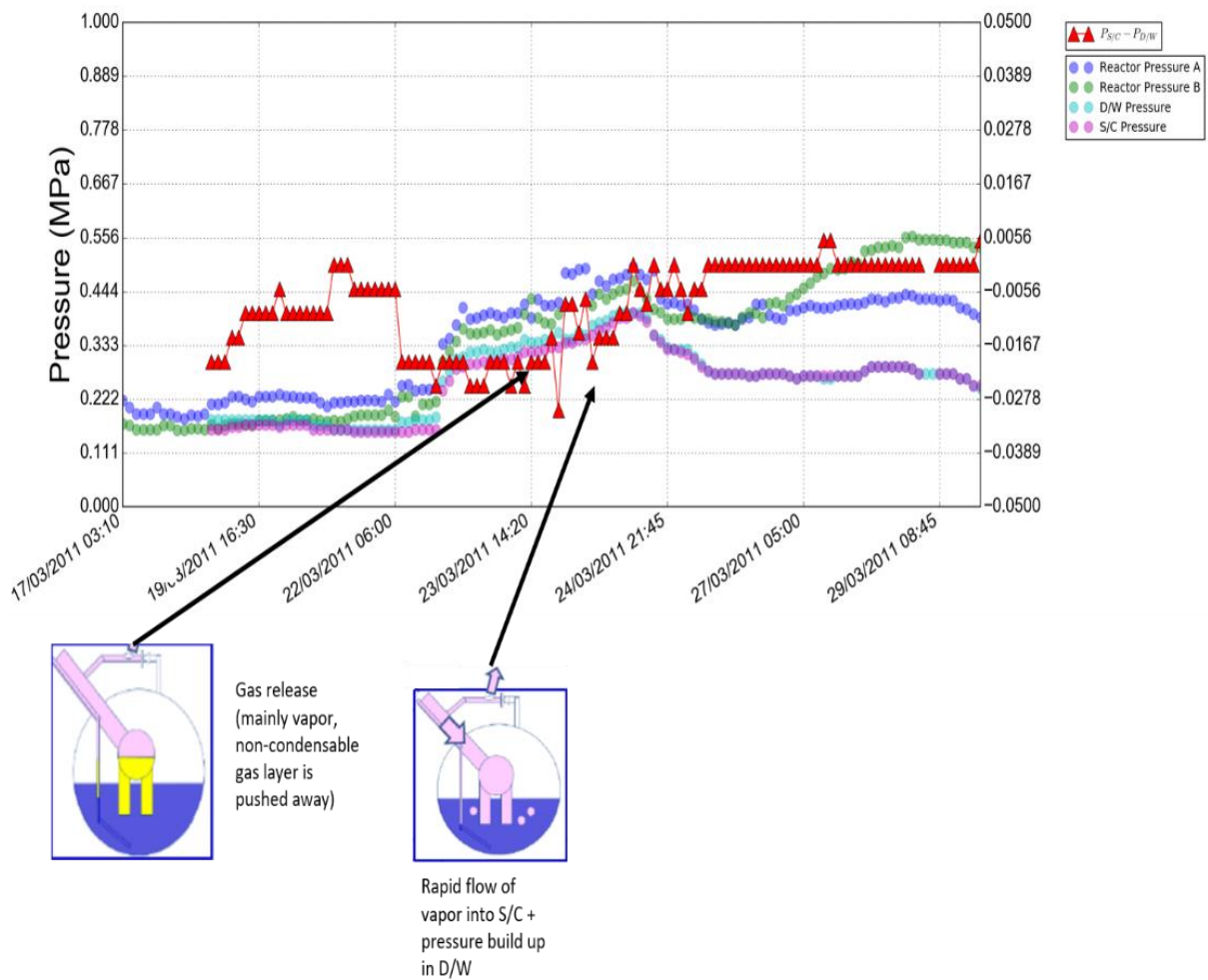


Figure 2-5 Pressure Response during Rapid Cooldown

Around 24th of March rapid cooling slows down and condensation rate in S/C reduce due to reduction of sub-cooling in upper part of S/C. This leads to secondary condensation sites to be revealed within PCV. From this time, the dissipation of decay is mainly depends on the convection inside the containment and related phenomena. Temperature distribution inside PCV on March 24th is shown in Figure 2-6. Temperature values indicates the cooling inside PCV after the increase of water injection.

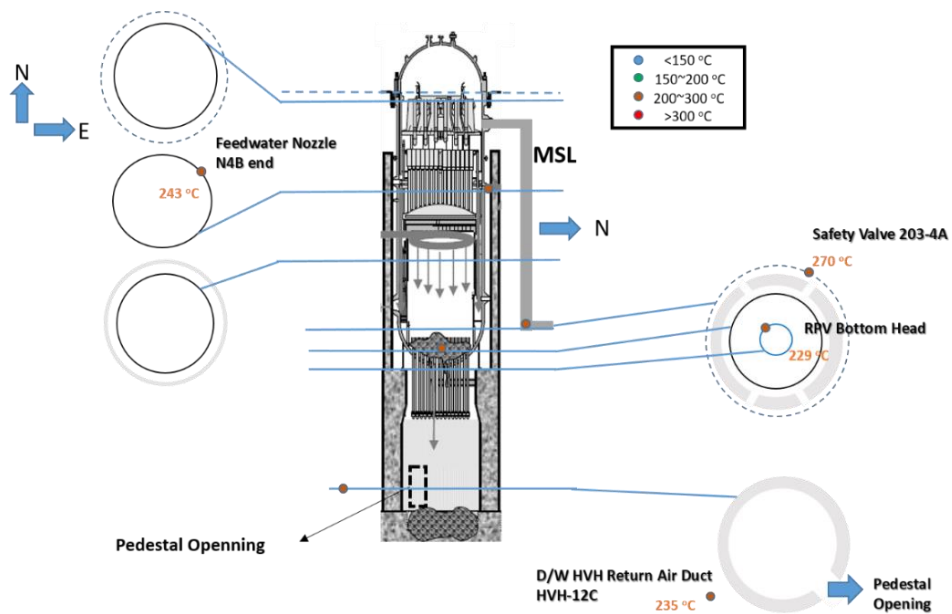


Figure 2-6 Temperature distribution inside PCV on March 24th 01:00

On March 27th, it is more clearly seen that cooling spreads inside the PCV with the increase in the number of available thermocouples. However certain locations still has high temperatures such as feedwater nozzle, and safety valve as seen on Figure 2-7.

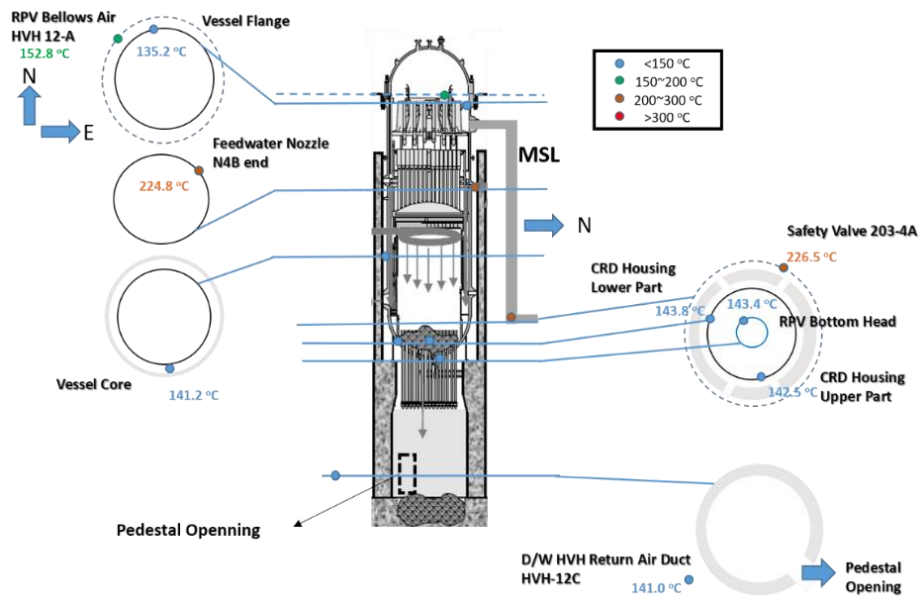


Figure 2-7 Temperature distribution inside PCV on March 27th 09:00

Start of effective debris cooling with condensation around D/W floor region can be observed more clearly in Figure 2-8 which shows temperature measurements vs pressure in S/C. On March 29th around midnight HVH-12C thermocouple value reaches saturation temperature which indicates possible condensation around this region. Availability of vapor inside PCV can also be deduced from Figure 2-8 as temperature are higher than saturation temperatures.

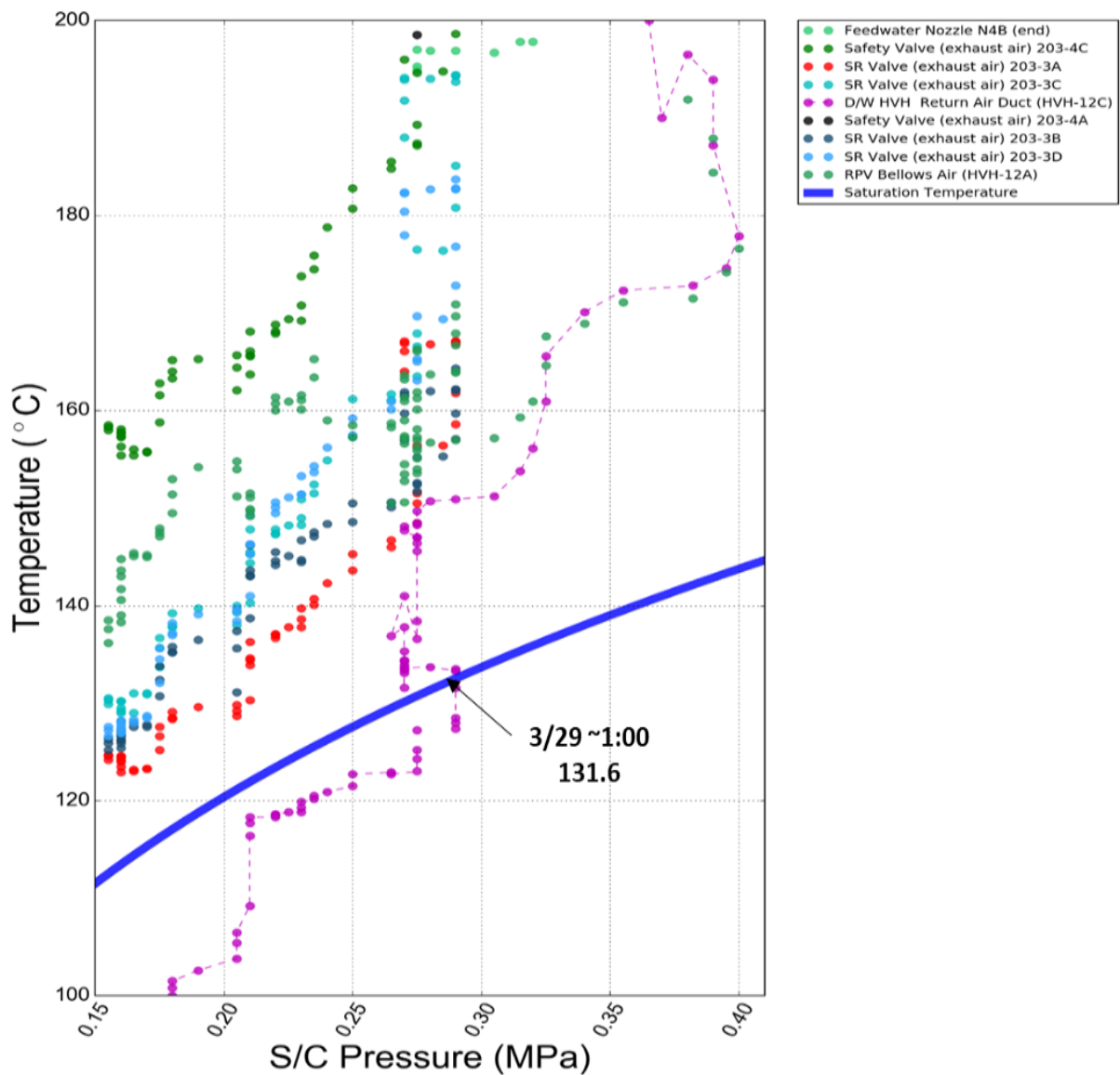


Figure 2-8 Condensation within PCV

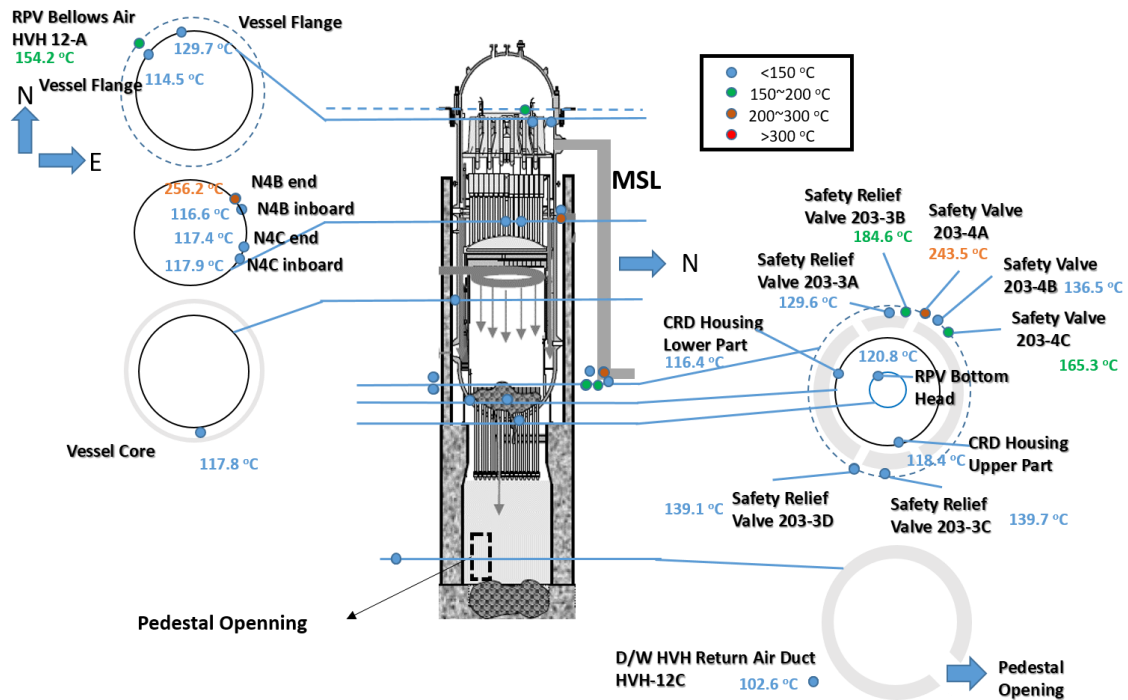


Figure 2-9 Temperature distribution inside PCV on April 1st 01:00

On April 1st 01:00 number of available thermocouples are increased that makes it possible to observe progressing of cooling inside the PCV more clearly. Measurements on the safety valves and feedwater nozzle still show high temperature values whereas the temperatures measured on the RPV is decreased. At this time it becomes clear that not only the safety valve 203-4A has high temperature but thermocouples safety relief valve 203-3B and safety valve 203-4B also shows high temperature values.

From April 4th to April 7th before nitrogen injection, temperature and pressure values show steady values which suggest heat transfer through PCV is in steady state. Such condition makes it possible to conduct steady state analysis to simulate gas flow and heat transfer inside the PCV. In this study April 6th targeted as analysis date for steady state simulations.

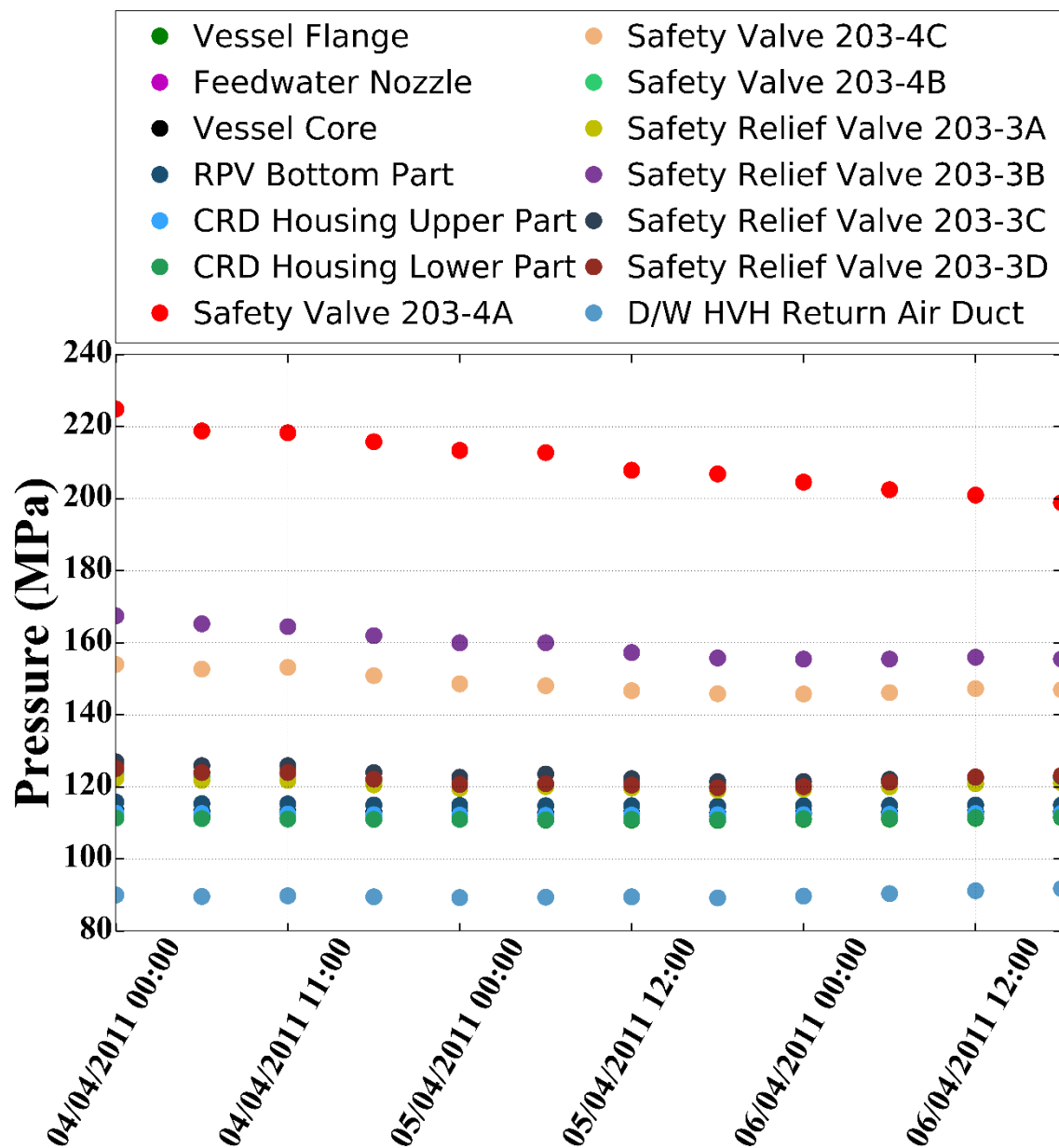


Figure 2-10 Temperature and Pressure Distribution from April 4th to April 7th

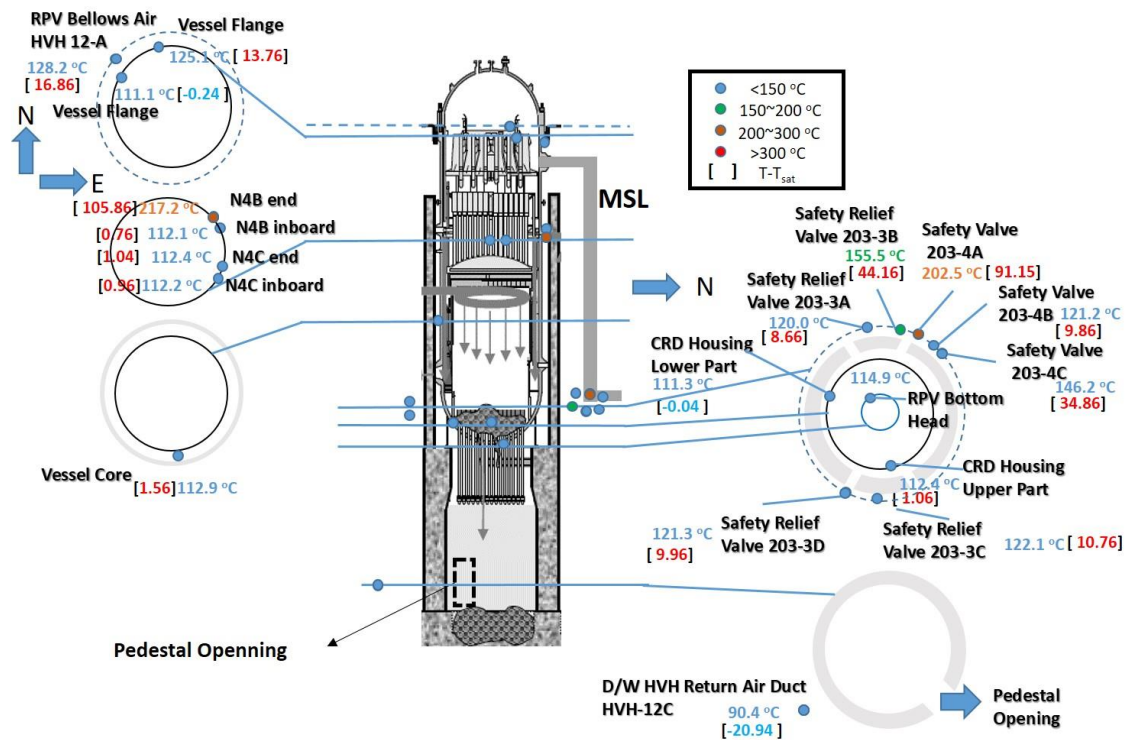


Figure 2-11 Temperature distribution inside PCV on April 6th 00:00

Figure 2-11 shows thermocouple locations and temperature distribution on April 6th. Except thermocouples Safety Relief Valve 203-3B, Safety Relief Valve 203-4A, Safety Valve 203-4B all thermocouples show slightly superheated temperature. On the other hand thermocouple D/W HVH Return Air Duct shows subcooled values which points out an ongoing condensation inside the PCV.

2.4 Geometry

Preliminary CFD analysis conducted to observe flow paths and temperature distribution inside drywell (D/W). Geometry used for the analysis is shown in Figure 2-12. Fukushima Daiichi Unit-1 has a MARK-1 type containment vessel with light bulb shape which has a steel lined pressure vessel backed over most of its surface with reinforced concrete. Starting with spherical wall, continues in cylindrical shape and ends as a hemispherical top head which is designed to contain energy released during a postulated design basis accident. In the current model, piping in the system represented by 2 recirculation pump and 2 feedwater line piping. Model's inner structures are consists of

pedestal, pressure reactor vessel and top plate that separates top head region from main body.

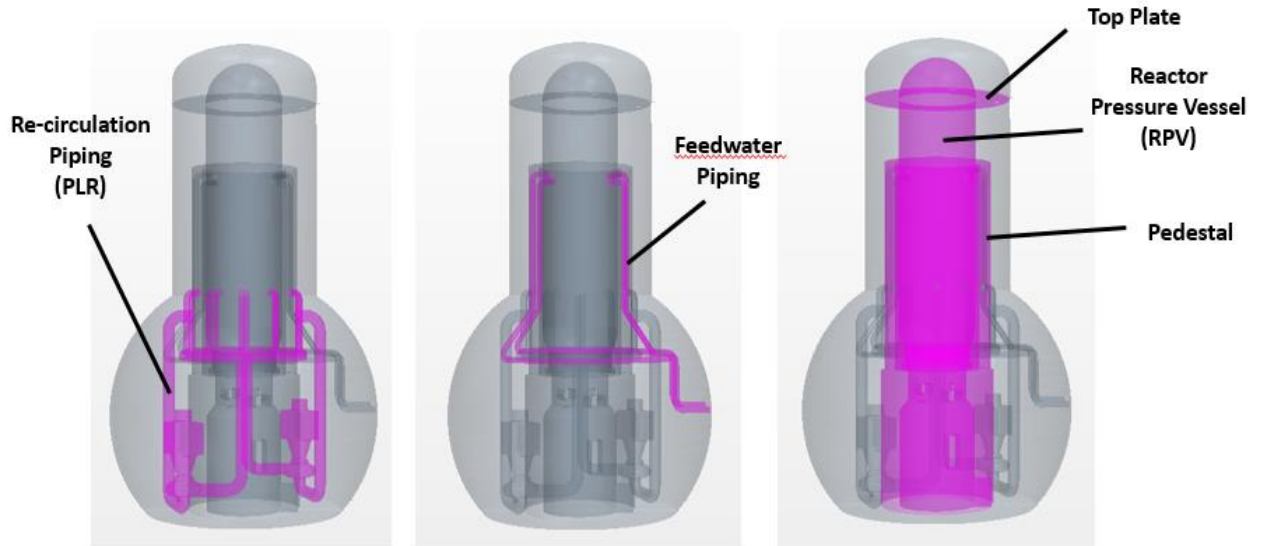


Figure 2-12 3D Cad Model of Mark-1 Containment

2.5 Analysis Setup

In this section model to describe gas flow inside the PCV is introduced. Heat source and heat sink modelling along with simulation settings are discussed. Furthermore, mesh sensitivity result to select suitable mesh for the analysis is explained.

2.5.1 Model Description

In this study, simulations focus on the steady cooling period of debris where the gas flow is dominated by natural circulation. The gas inside 1F1 containment is heated up by decay heat and carries energy to containment walls and other structures inside the containment. Such phenomena can be modelled by introducing heat source representing fuel debris and heat sink on containment walls. Previous studies concerning the condition of 1F1 after the accident suggest that most of the fuel debris discharge from RPV to the

pedestal area and some debris may spread through the opening of the pedestal to drywell floor. Considering such a condition for the debris, a heat source is defined as shown in Fig. 5. Estimated decay heat value is used to determine heat source magnitude. Calculations are done by using SuperBacon code with JENDL-4.0 nuclear data library [20]. 3 different models with a different volatility of radionuclides taken into account. High volatility model assumes 99% release for noble gas elements (Kr,Xe,..) high volatile fission products (Cs,I,Te,Sb) and medium volatile fission products (Ru,Mo,Sr,Ra,Pd,Rh). Low volatility model assumes 90% release for noble gas elements, 60% for high volatile fission products and no release for medium volatile fission products. No release model assumes all nuclides kept inside containment. Estimated decay heat values for all 3 models on April 6th is shown in Table 2.1.

Table 2.1 Estimation of decay heat with different volatility models

	High Volatility	Low Volatility	No Release
Decay Heat	1.11 MW	1.91 MW	1.97 MW

As on April 6th, most of the volatile nuclides already assumed to be escaped out of the system, decay heat value estimated using high volatility model considered as total decay heat. Another assumption is made to roughly estimate the amount of decay heat that superheats the gas inside the primary containment vessel using simple heat balance for decay heat dissipation.

$$Q_{decay} = Q_{sub} + Q_{vap} + Q_{sup} \quad (2.5)$$

$$Q_{decay} = \dot{m}_l c_l (T_{sat} - T_{inj}) + \dot{m}_s L + \dot{m}_s c_s (T_{sup} - T_{sat}) \quad (2.6)$$

In above, Q_{decay} is the decay heat, Q_{sub} is decay heat removal by increasing subcooled water temperature, Q_{vap} is decay heat removal by phase change Q_{sup} is decay heat removal by increasing superheated gas temperature, \dot{m}_l is rate of water injection, c_l is specific heat of water, T_{sat} is the saturation temperature, T_{inj} is the temperature of injected water, \dot{m}_s is

rate of steam generation, L is the latent heat, c_s is specific heat of steam, T_{sup} is maximum temperature of superheated gas. Estimation of debris condition by lumped parameter analysis is shown in Figure 2-13.

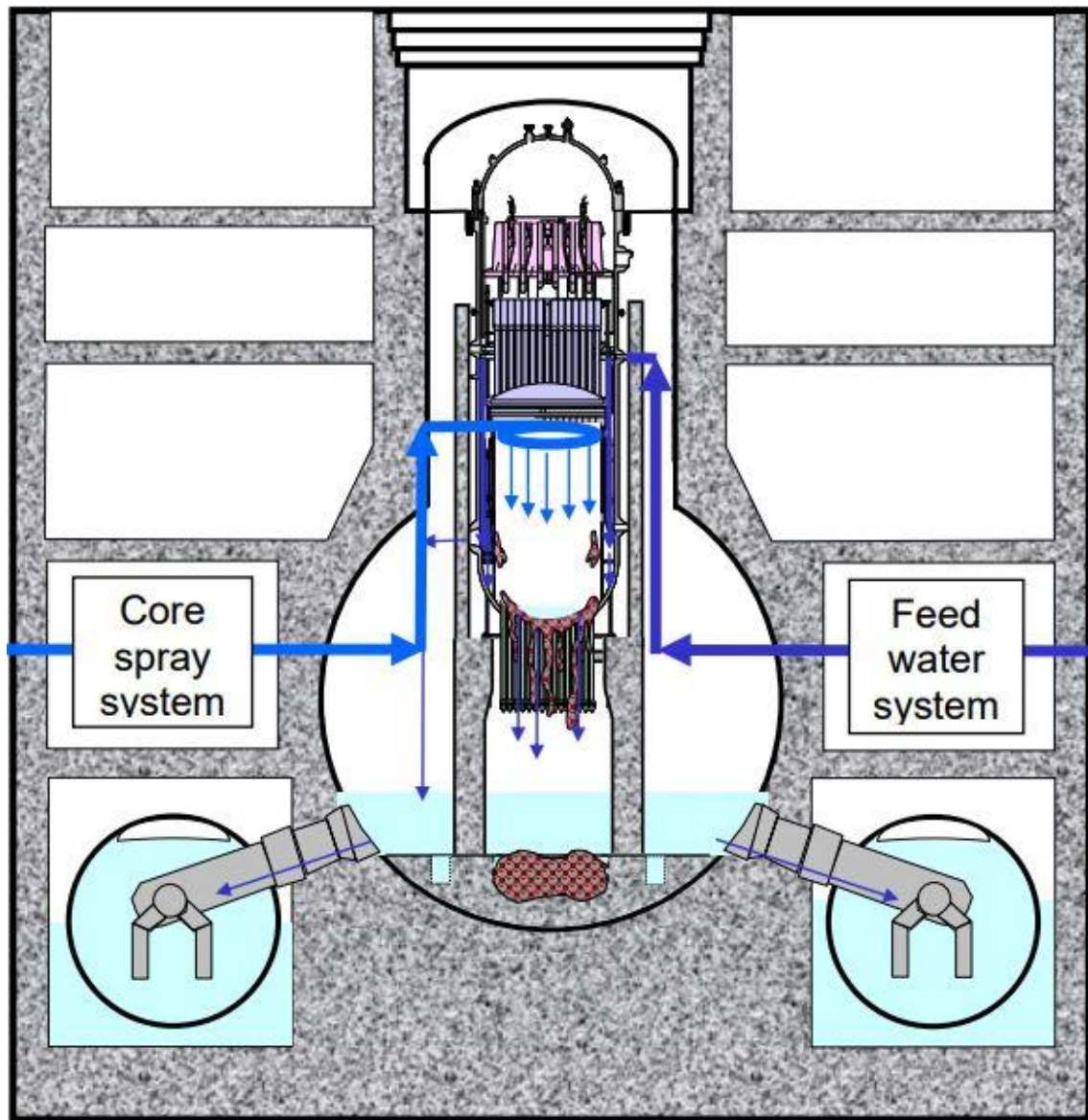


Figure 2-13 Estimation of Debris Condition from Lumped Parameter Codes [21]

According to this estimation there is no or very few fuel left in the Fukushima Unit-1 core. This suggest, most of the fuel drops out of the core to pedestal area through the failure on

the bottom part of RPV. Considering such condition debris is represented as a heat source on pedestal and drywell floor as in Figure 2-14.

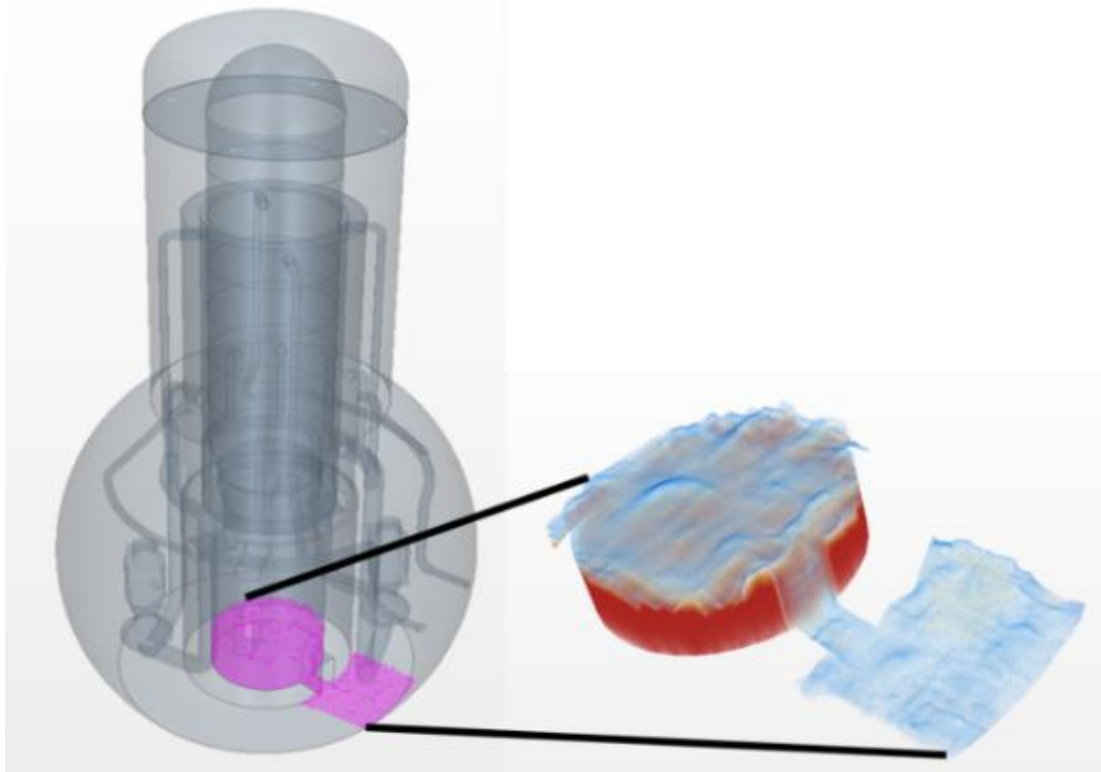


Figure 2-14 Representation of debris as heat source

Heat sink is defined on the PCV walls by applying thermal resistance concept to reflect the effect of different mediums between gas inside PCV and environment on heat transfer. Assuming mediums between environment and gas inside PCV are steel PCV liner, air and concrete for side walls of PCV, total thermal resistance can be estimated as;

$$R_{tot} = \frac{1}{h_{PCV}A} + \frac{L}{k_{wall}A} + \frac{1}{h_{air}A} + \frac{L}{k_{conc}A} + \frac{1}{h_{env}A} \quad (2.7)$$

h_{PCV} represents heat transfer coefficient of gas inside PCV, A is the wall surface area, k_{wall} is conductivity of PCV steel liner, h_{air} is heat transfer coefficient of air, k_{wall} is

conductivity of concrete wall, L is the characteristic length and h_{env} is heat transfer coefficient of surrounding environment which is assumed to be air at 30 °C. In case of PCV wall at the top resistance term for concrete wall is omitted as it is surrounded by air medium. Corresponding heat loss term is defined as;

$$Q_L = \frac{T_{gas} - T_{env}}{R_{tot}} \quad (2.8)$$

In the above, Q_L is estimated heat loss, T_{gas} is the temperature of the gas inside PCV and T_{env} is the temperature of the environment. Heat transfer coefficient for air and environment is estimated by using Churchill and Chu [11] correlation which provides empirical expression for natural convection adjacent to a vertical wall.

$$Nu = 0.68 + \frac{0.67 Ra^{1/4}}{\left[(0.492 / Pr)^{9/19} \right]^{4/9}} = \frac{hL}{k} \quad (2.9)$$

Nu is Nusselt number, Ra is Rayleigh number, Pr is Prandtl number, h is heat transfer coefficient and k is the thermal conductivity. Computational geometry divided into 4 different regions considering different materials including vapour, stainless steel, and carbon steel and concrete. Vapour selected as a material to simulate gas region inside the containment, stainless steel selected as a material for top plate, carbon steel selected as a material for reactor pressure vessel and concrete selected for bioshield and pedestal. Main assumptions for the simulation are as follows;

- D/W is leak tight.
- Debris represented as heat source inside pedestal and D/W floor.
- Working flow defined as ideal gas.
- Radiation heat transfer between solid regions neglected.
- Thermocouples assumed to indicate gas temperature of the surrounding.

Computational geometry is defined as 4 different regions considering different materials

1. Fluid region for gas phase using $H_2O_{(g)}$
2. Solid region for RPV using carbon steel

3. Solid region for top plate using stainless steel
4. Solid region for pedestal and bioshield using concrete

Settings for the simulation summarized for 4 regions in Table 2.2:

Table 2.2 Simulation Settings

Items		Settings	
Calculation	Space	Dimension	3
		Gravity	9.81 m/s ²
Time		Steady State	3000 iteration
Gas	H ₂ O _(g)	Equation of State	Ideal Gas
		Turbulent Model	K-Epsilon
		Dynamic Viscosity	IAPWS-95
		Specific Heat	IAPWS-95
		Thermal Conductivity	IAPWS-95
Top Plate	Stainless Steel	Equation of State	Constant Density
		Density	8055.0 kg/m ³
		Specific Heat	480.0 J/kg-K
		Thermal Conductivity	15.1 W/m-K
RPV Wall	Carbon Steel	Equation of State	Constant Density
		Density	7832.0 kg/m ³
		Specific Heat	434.0 J/kg-K
		Thermal Conductivity	63.9 W/m-K
Pedestal and Bioshield	Concrete	Equation of State	Constant Density

Density	2240.0 kg/m³
Specific Heat	750.0 J/kg-K
Thermal Conductivity	0.53 W/m-K

2.6 Mesh Sensitivity Analysis

Mesh is a discretized representation of the geometry which should present acceptable resolution of geometry and expected flow features. Grids cells has to be arranged in a way to minimize errors and capture flow phenomena in interest. However, number of elements are proportional to storage requirements as well as computing time. Many problems require a compromise between the desired accuracy of the numerical result and number of cells. So that, by conducting mesh sensitivity analysis suitable mesh size can be decided for the simulation. There are several sources of errors and uncertainties for CFD simulations such as numerical errors, modelling errors, user errors, application uncertainties and software errors.

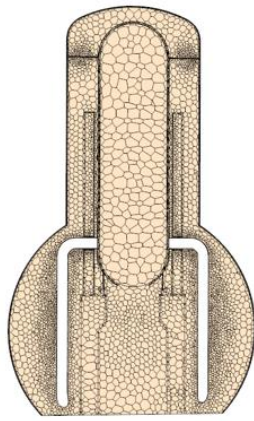
Mesh sensitivity analysis conducted according to best practice guidelines [22] which suggests to employ at least 2 better 3 grids with significantly different mesh sizes. Moreover if this is not feasible, results obtained with different discretization schemes can also be compared. Following the best practice guidelines 4 different grid sizes ranging from total cell number of 300000 - 2000000 considered to assess the effect on heat transfer on PCV walls as in Figure 2-15. Near wall region resolved using 10 prism layers with having first layer thickness of 0.0001m and stretching factor of 2. Total thickness of the prism layer set as 0.1m. For low y^+ wall treatment with low Reynolds number models y^+ value could be assumed approximately 1 or less. This wall treatment assumes that the viscous sublayer is well resolved and wall laws are not needed. In order to achieve y^+ values less or equal to 1 extra attention to prism layer mesh was given. y^+ is defined as a distance normal to the wall normalized with the inner length scale of the flow. Relation to calculate y^+ is given by:

$$y^+ = y \frac{\rho u_\tau}{\mu} \quad (2.10)$$

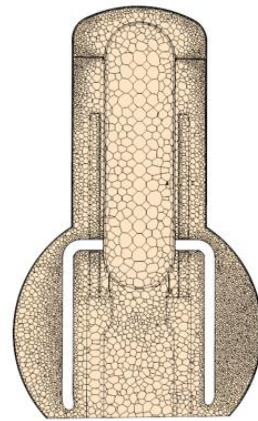
where y is the distance normal to the surface to the first grid point, ρ density, μ is dynamic viscosity and u_τ is called the friction velocity . Friction velocity is calculated as:

$$u_\tau = \sqrt{\frac{\tau_w}{\rho}} \quad (2.11)$$

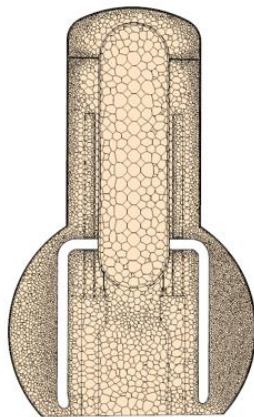
where τ_w is the wall shear stress.



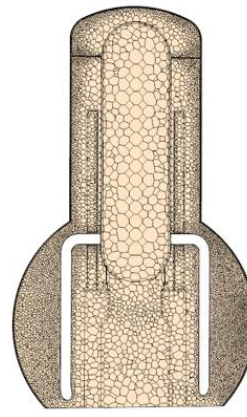
~300000 Cells



~1000000 Cells



~1400000 Cells



~2000000 Cells

Figure 2-15 Different mesh sizes for mesh sensitivity

During the simulations temperatures inside the PCV were monitored for 4 different locations to assess the effect of mesh size. As in Figure 2-16, results suggest that simulations with 1.4 million or larger mesh size change in temperature is negligible.

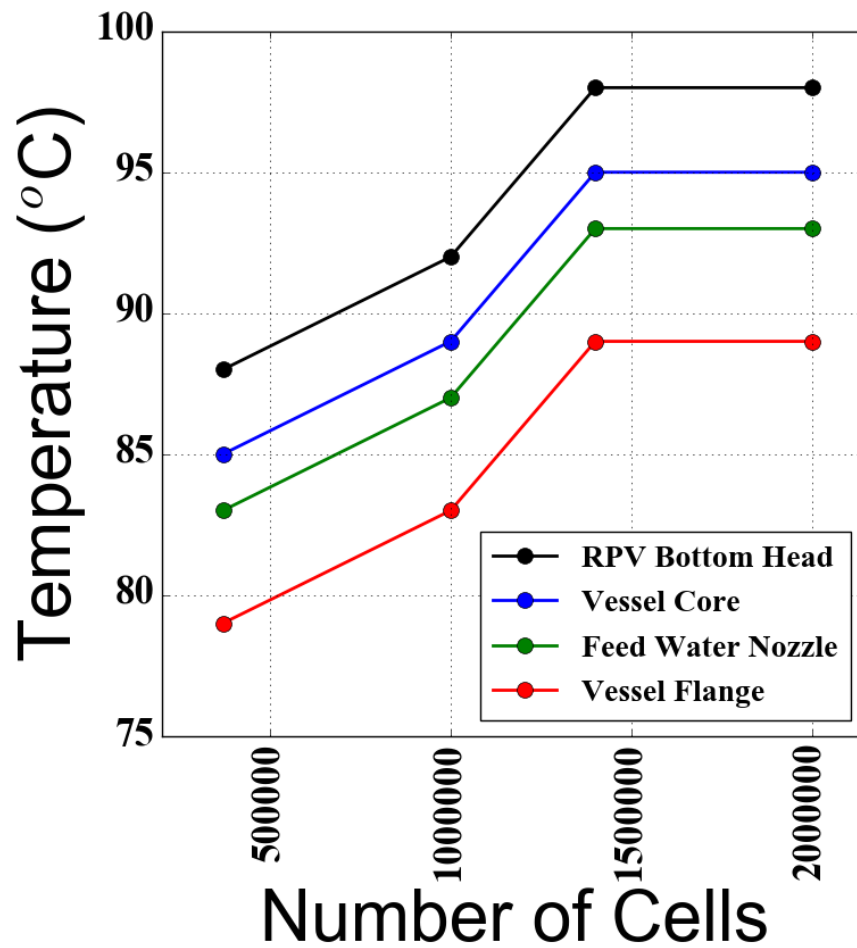


Figure 2-16 Mesh Size Sensitivity

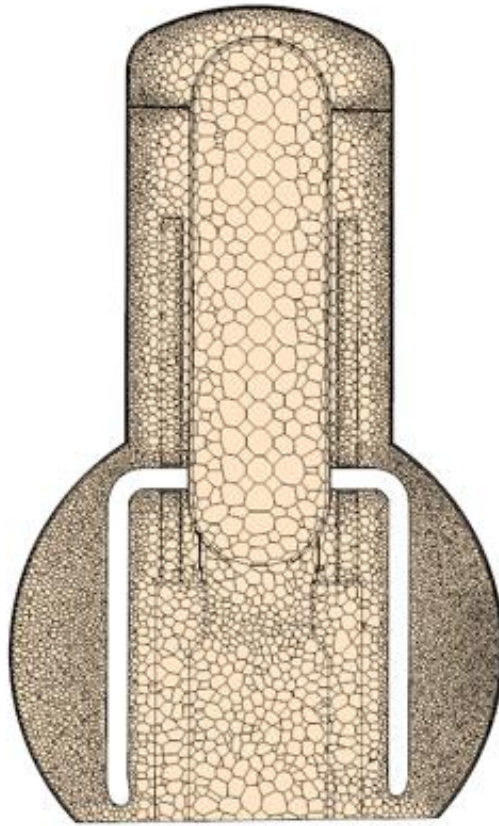


Figure 2-17 Computational Mesh

Thus, mesh with 2 million cells selected for further simulations which is shown in Figure 2-17. Furthermore to assess the quality of mesh, following mesh metrics are checked. One of the important mesh metric is the volume change which describes the ratio of the volume of a cell to that of its largest neighbor. In order to avoid potential inaccuracies and instability in the solver, there shouldn't be a large jump in volume from one cell to another. Threshold value for the volume change is 0.01. Cells with volume change of 0.01 or lower are considered as bad cells.

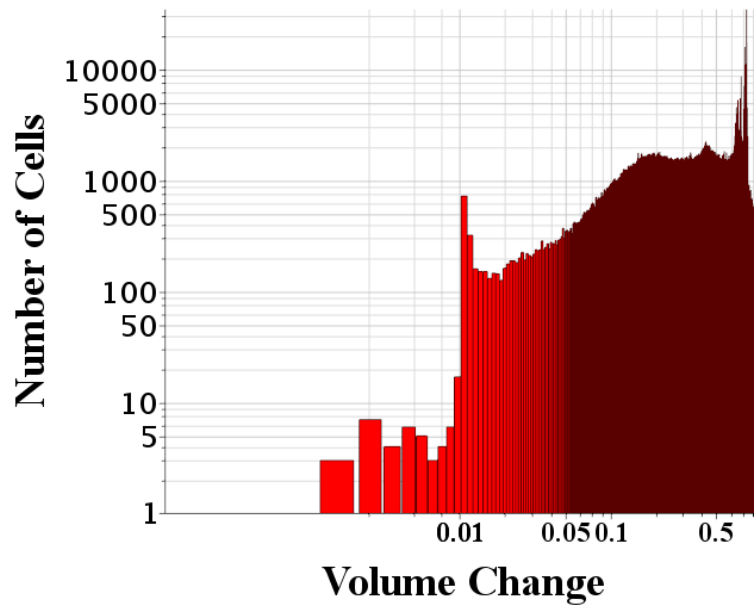


Figure 2-18 Mesh Metric :Volume Change

Cell quality is determined considering orientation of cell faces and relative geometric distribution of the cell centroids of the face neighbor cells. Flat cells with highly non-orthogonal faces have a low cell quality. If the quality of cell is approaching zero, it is considered to be a bad cell whereas cell with a quality of 1 considered as a perfect cell. A cubic cell can be example of such cell however other polyhedral cell shapes can also attain this level of perfection.

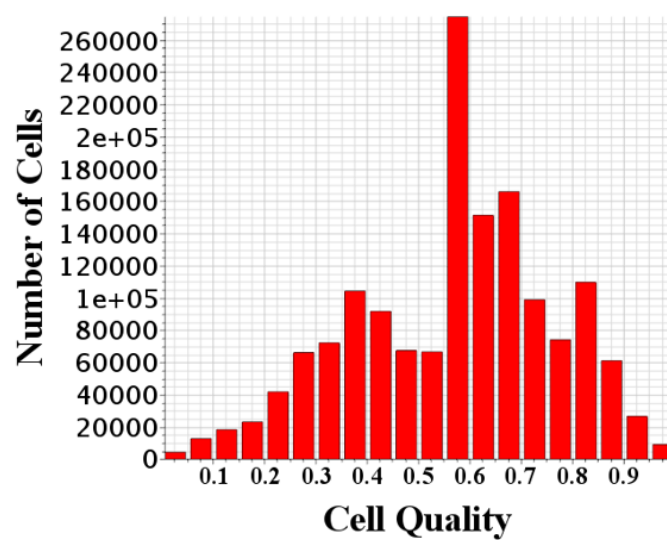


Figure 2-19 Mesh Metric : Cell Quality

The skewness angle θ is defined as the angle between the face area vector a (face normal) and the vector connecting the two cell centroids, ds . Perfect orthogonal mesh can be achieved with θ equals to 0. In order to avoid convergence issues skewness angles should be kept below 90° . Skewness angles of 90° or greater cause occurrence of concave cells where the centroid of both cells lies on the same side of the boundary face.

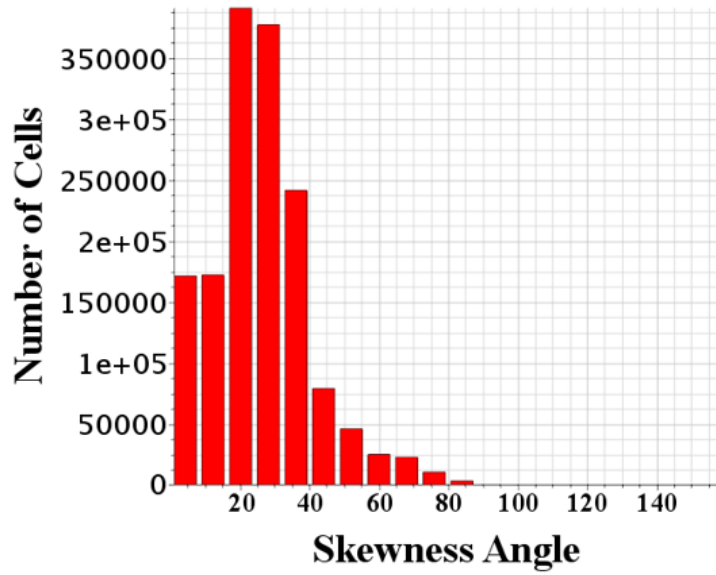


Figure 2-20 Mesh Metric : Skewness Angle

After ensuring topological validity, no negative volume cells, conformal mesh and suitable mesh metrics, analysis setup for physical models and grid refinement analysis are conducted.

2.7 Simulation Results & Discussion

2.7.1 Heat Source as a Parameter

In this chapter, simulations conducted to observe effect of heat source inside D/W will be discussed. Recent study estimated decay heat as around 1.1 MW [20] on April 6th for 1F1. Using Equation 2.5 range of the decay heat consumed to heat up superheated gas

is estimated and parameter analysis conducted between 25kW (%2 of decay heat) to 150kW (%12 of decay heat). Resulting temperature field is shown in Figure 2-21 for selected cross section.

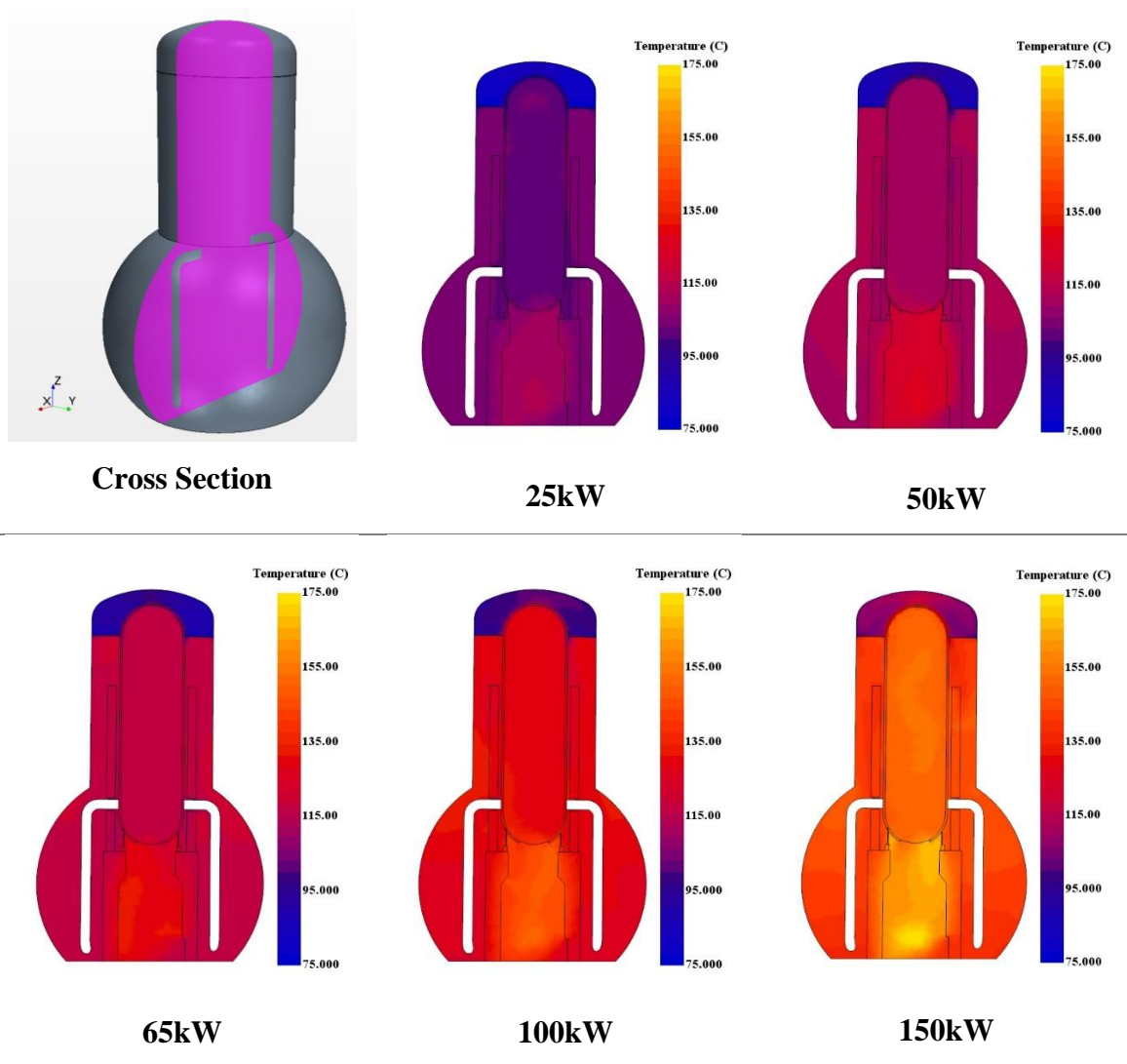


Figure 2-21 Estimated Temperature Field for Different Heat Sources

Results show high temperatures inside pedestal area which is rising through the RPV inside through the RPV bottom opening. Top head region shows lower temperatures to the presence of top plate that separates main body from the top head. For higher heat sources, even though the temperatures inside the pedestal show high values, excessive cooling is observed due to the fact that heat sink on D/W walls defined proportional to

heat source. This shows that better heat sink definition is needed on D/W walls. Also debris inside the RPV can greatly effects temperature distribution inside the D/W due to the fact that RPV is made up of steel which is a good thermal conductor. Nevertheless, as thermocouple measurements on lower part of D/W shows slightly superheated values, more proper heat sink values on D/W walls will be considered later. Velocity fields for the simulations shown in Figure 2-22.

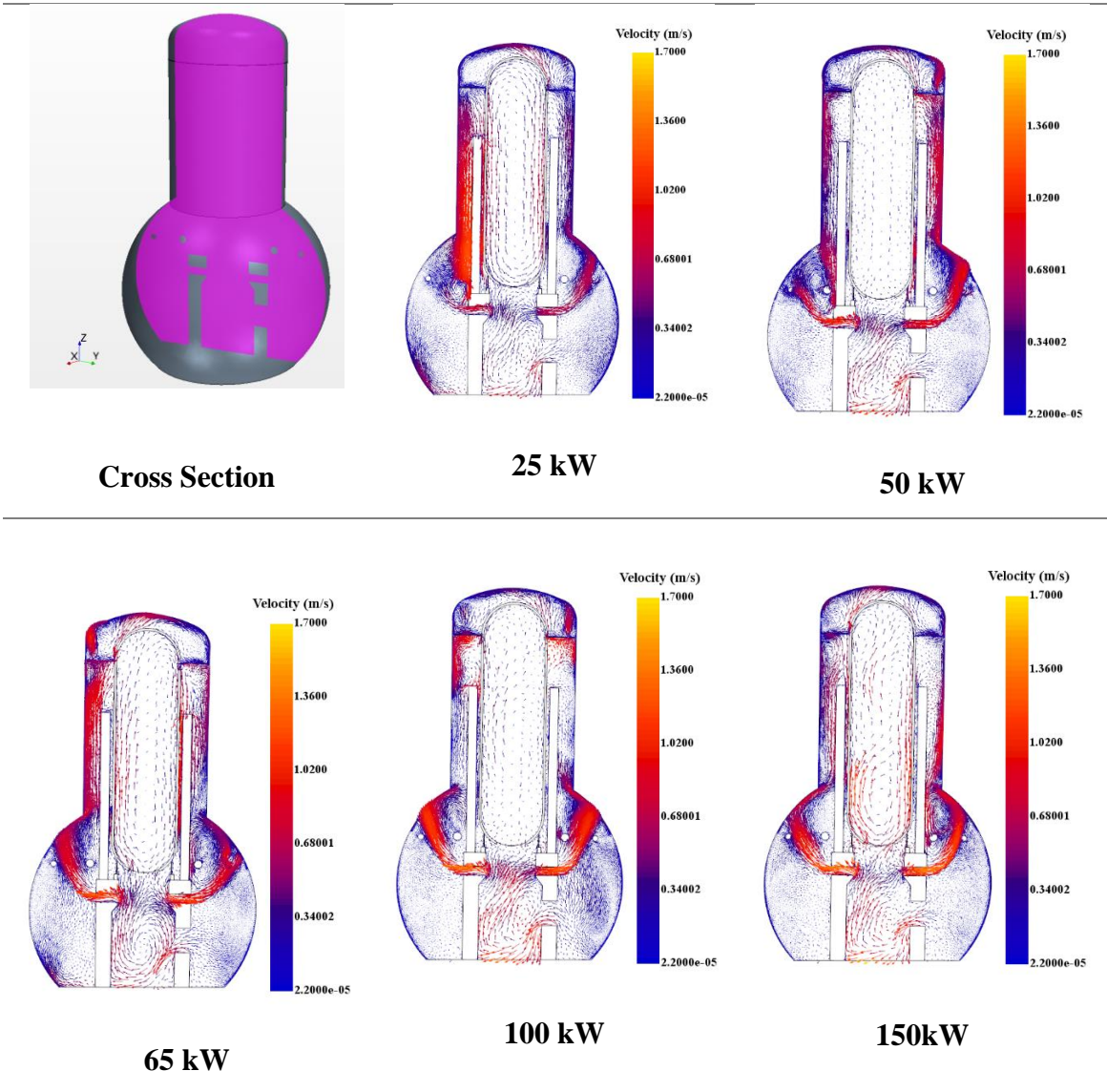


Figure 2-22 Estimated Velocity Field for Different Heat Sources

Results show rising plume at the bottom of the pedestal reaching D/W through control rod drive mechanism openings. This plume later rises to top head region through

the manhole openings of top head. Flow outside pedestal enters pedestal region through the doorway opening of pedestal and rise with the hot plume that either exists pedestal area to the outer region of D/W or further rise inside RPV through the hole at the bottom of RPV. Gas inside the RPV recirculates and transfers energy to RPV walls. Heat transfer through the RPV walls also effect the flow inside top head region. Gas velocity near wall region is nearly stagnant and flow downwards due to the heat transfer through the PCV walls. Available temperature data is compared with simulation results for 11 different thermocouple measurements. Thermocouples located at RPV bottom head, vessel core, feedwater nozzle and vessel flange change heightwise between 14 to 31 meters. Remaining thermocouples on safety valves are located at the same elevation (17.05 meters) ranging in the radial direction between 90 to 270 degrees. Temperature comparison between simulation and measurements for thermocouples changing heightwise and on safety valves shown Figure 2-24 and Figure 2-26 respectively.

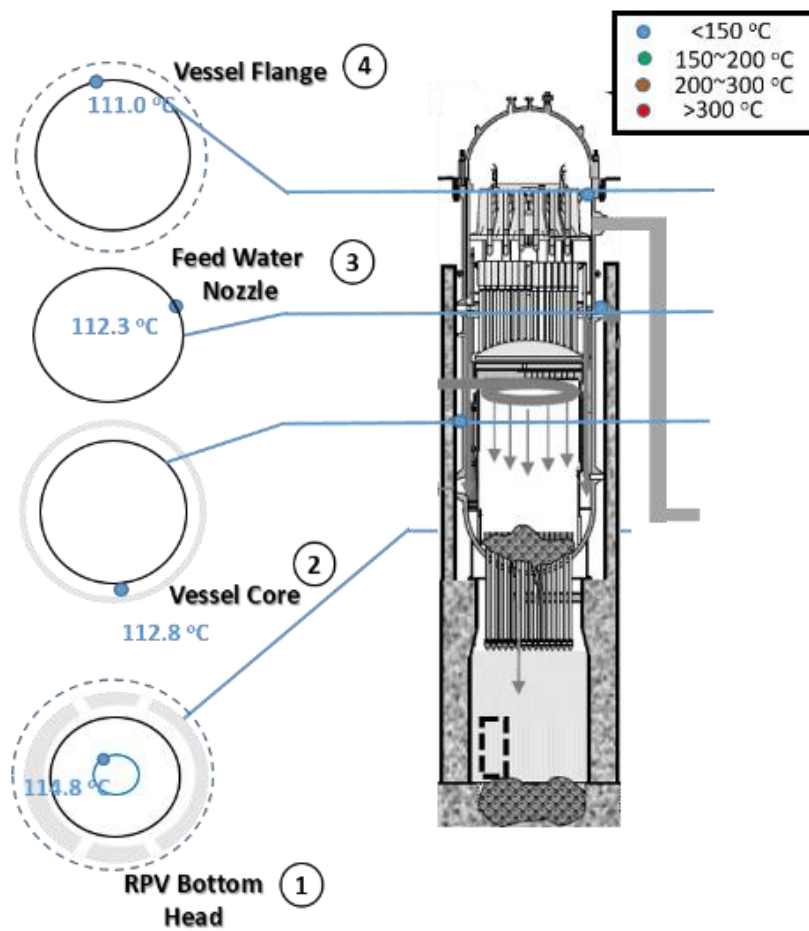


Figure 2-23 Heightwise Temperature Measurements and Thermocouple Locations

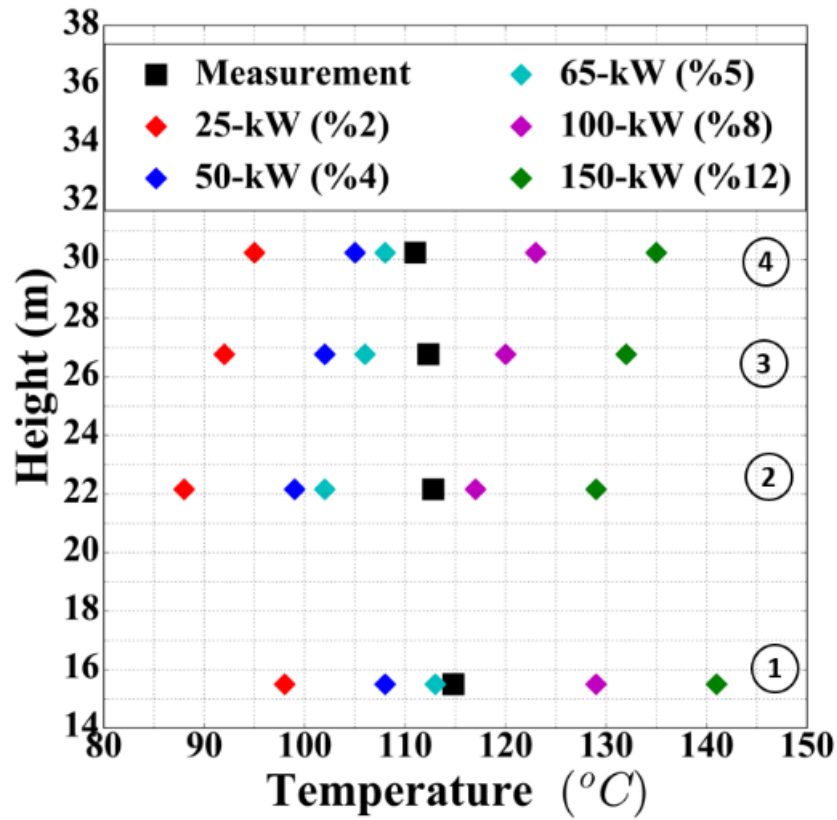


Figure 2-24 Heightwise Temperature Comparison

Results suggest that between 65-kW(%5 of decay heat) to 100kW(%8 of decay heat) is dissipated to superheat gas circulating inside PCV. On the other hand, temperature predictions on safety relief valves could not capture temperature asymmetry due to the high temperature on safety valve 203-4A, safety relief valve 203-3B and safety valve 203-4C as in Figure 2-26.

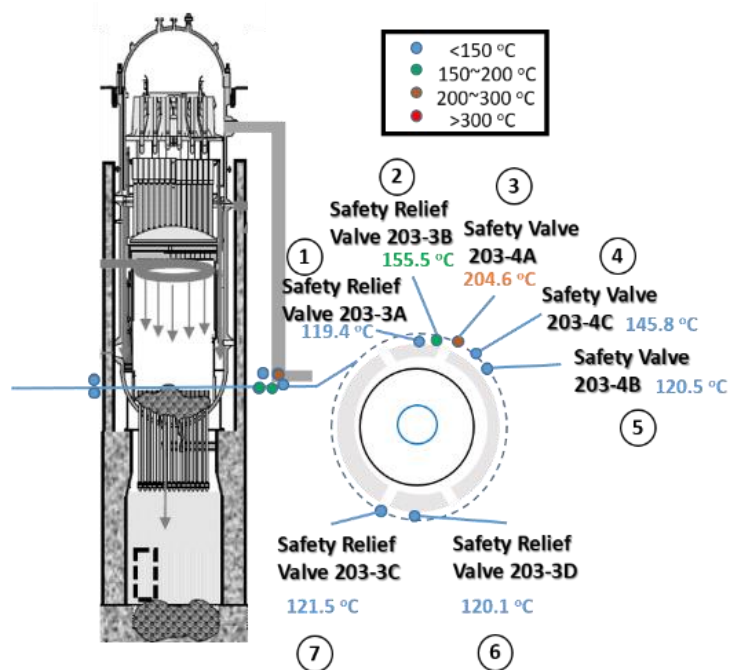


Figure 2-25 Safety Valve Temperature Measurements and Thermocouple Locations

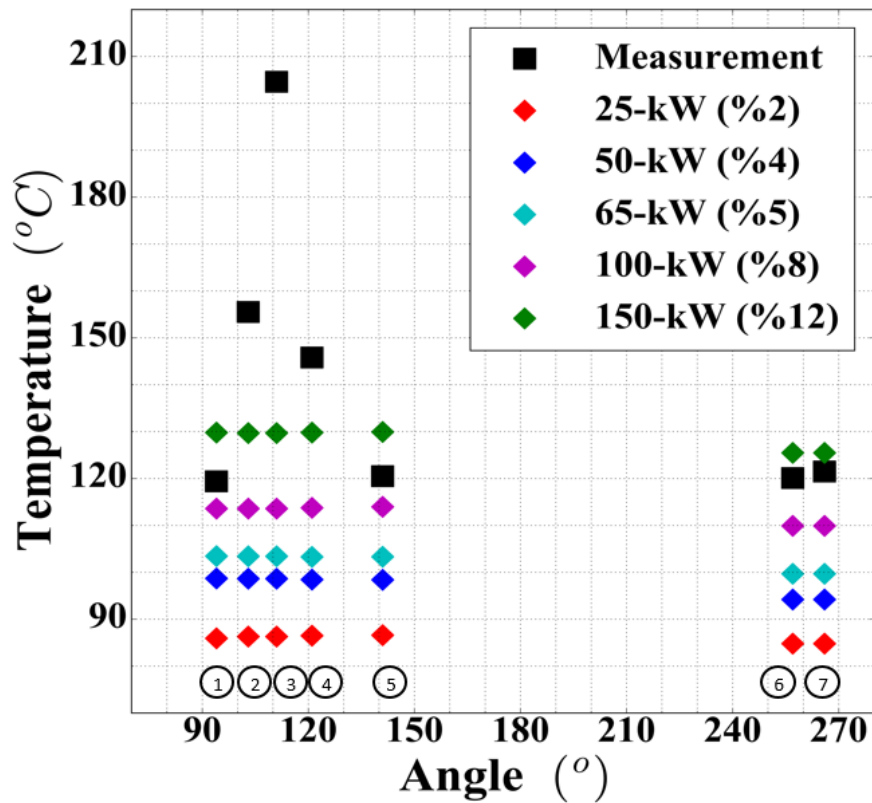


Figure 2-26 Safety Valve Temperature Comparison

2.7.2 Simulations for Safety Valve Temperature Asymmetry

Post-processing of Fukushima Daiichi Unit-1 measurement data shows that for safety valve 203-4A, safety relief valve 203-3B and safety valve 203-4C show high temperatures which suggest local heating effect around this region. Reason for this heating effect could be due to either leaking hot gas or attached radionuclides because of the previous gas leakage. Assuming RPV bottom head is heavily damaged in 1F1, the temperature increase due to the accumulation of fission products is a more likely case due to the fact that there is no driving force for hot gas to discharge from SRVs. Previous simulations considering heat source only on pedestal and drywell floor could not address the temperature asymmetry on safety valves. In order address such condition, local heat source defined on safety valve locations as shown in Figure 2-27.

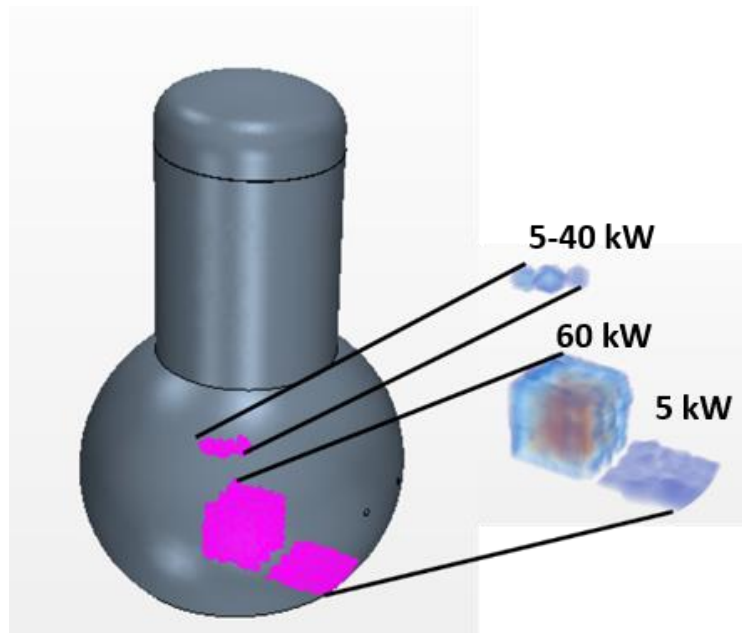


Figure 2-27 Heat source to represent local heating on safety valves

A parameter analysis for 4 different cases by altering heat source on safety valves ranging from 5 to 40 kW is conducted as in Figure 2-27. Results shown in Figure 2-28 suggests that case with 20-kW heat source on safety valve location well estimates

measured temperatures on safety valve 203-4A, safety relief valve 203-3B and safety valve 203-4C.

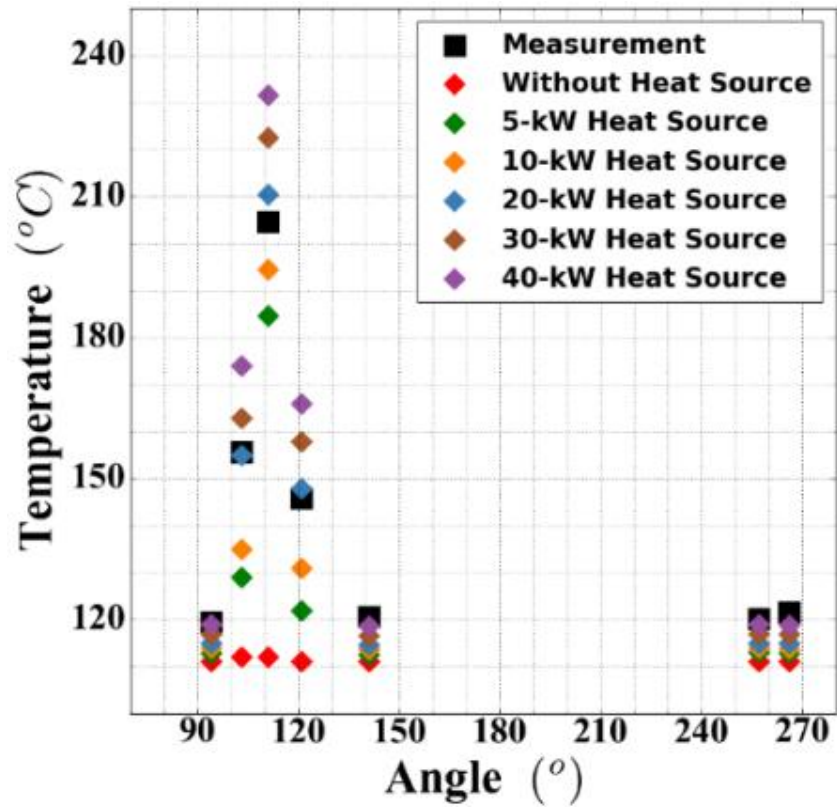


Figure 2-28 Estimation of Safety Valve Temperature Values for Different Heat Sources

2.7.3 Spreading of Debris as a Parameter

Another parameter analysis conducted to assess whether it is possible to estimate effect of debris spreading. 3 different spreading pattern considered as shown in Figure 2-29.

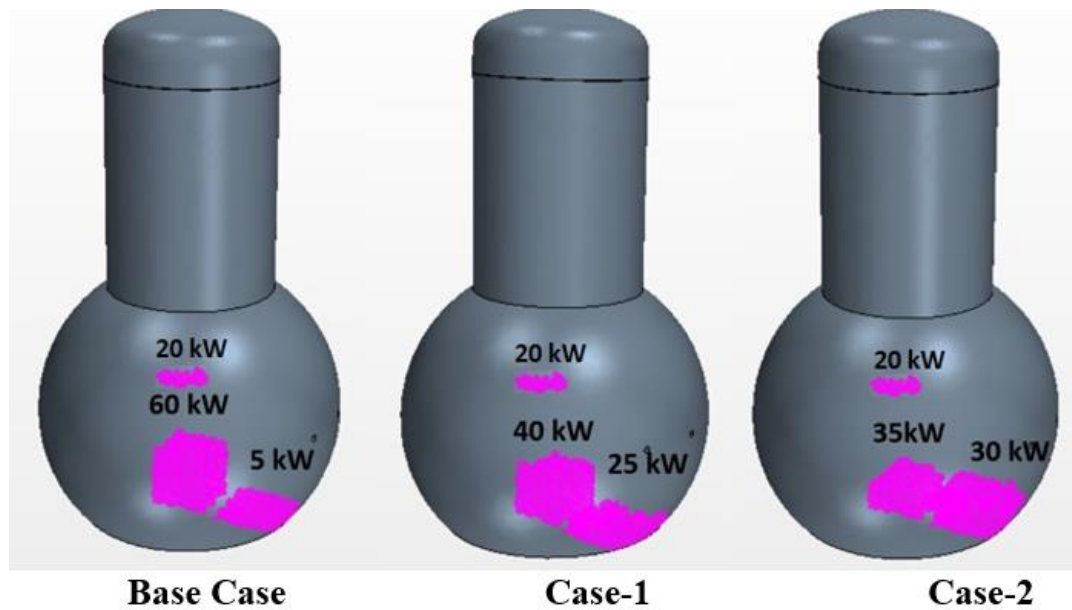


Figure 2-29 Schematic for heat source spreading effect

Heat source values are proportional to volume of heat source. Temperature values between simulation results and measurements of vessel flange, feedwater nozzle, vessel core and RPV bottom head are compared. Due to the mixing inside the PCV and lack of available temperature data, this approach could not evaluate the debris spreading properly. On the other hand, there is a small change for the heightwise temperature estimations. With more measurement data this approach may help to evaluate debris spreading through the opening of pedestal.

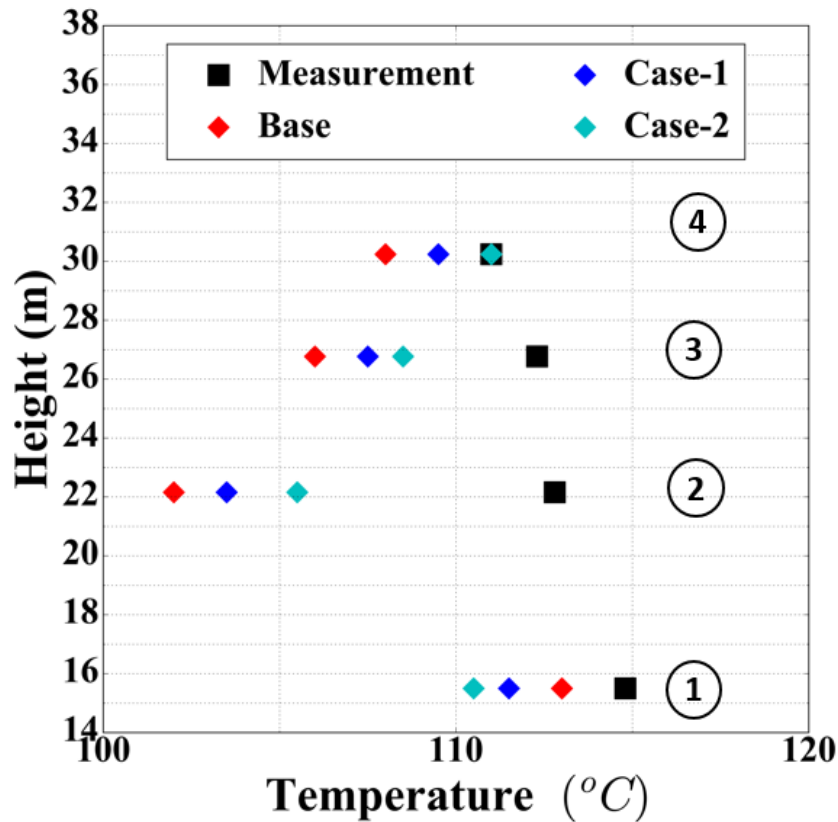


Figure 2-30 Heightwise Temperature Comparison for Debris Spreading Analysis

2.8 Summary and Conclusion

Parameter analysis conducted to estimated amount of decay heat dissipated to superheat the gas inside the PCV. Further parameter analysis conducted to address temperature asymmetry on the safety valves and effect of debris spreading to drywell floor. Parameter analysis conducted by changing heat source on pedestal and drywell floor suggests between 65-kW(5% of decay heat) to 100-kW(8% of decay heat) is dissipated to superheat the gas inside the PCV. Remaining part possibly be removed to increase the temperature of the subcooled water pool and by vaporization. Further analysis to estimate the amount of local heating regarding the temperature asymmetry on the safety valves suggest that around 20-kW heat source can represent the local heating on safety valves. This local heating might be due to the accumulated radioactive material on the valves due to the gas leak through RPV. Estimated result might be useful to predict

amount of accumulated radioactive material on the valves. Furthermore, 3 different simulations conducted to estimate debris spreading through the opening of the pedestal. However, due to the lack of measurement data and mixing inside the PCV, only small changes observed for heightwise temperature measurements which is not sufficient to address the spreading of the debris.

Chapter 3 Wall Condensation Modelling

3.1 Introduction

This chapter introduces previous work regarding wall condensation and approaches to model wall condensation in 1F1. Wall condensation is an important phenomenon in containment thermal hydraulics as it is an effective way of heat transfer. It plays a dominant role in many accident scenarios postulated to occur in the containment. One of the specific examples of the importance of wall condensation is the concern about hydrogen distribution after a severe accident. In order to evaluate the hydrogen distribution inside the containment, condensation phenomena should be represented properly. Another example for the importance of wall condensation can be given in case of evaluation of pressure inside the containment. In case of loss of coolant or main steam line break accidents, large amounts of high-temperature steam are released to the containment, which increase the pressure of the containment. In order to evaluate the safety limits of the containment in a case of such accident, proper estimation of wall condensation is crucial in order to keep the last line of defence between the radioactive materials and the environment. Moreover, since the Fukushima Daiichi accident, more attention has been paid to the safety of the containment. To condense the high-temperature steam and maintain the containment pressure within the security limits, the passive containment cooling system has been designed and applied to third-generation nuclear power plants [23].

In this study, wall condensation modelling is considered for better evaluation of heat transfer in 1F1 containment. The condensing steam on the PCV walls will also affect the convection inside the PCV, which will in turn affect the estimated temperatures. Therefore, in order to increase the reliability of estimated temperature distribution inside the PCV, wall condensation should be implemented into the simulations.

3.2 Literature Review

Research regarding water vapour condensation in the presence of non-condensable gases follows mainly two paths. The first approach aims to represent condensation phenomena with simple models based on experimental observations given in forms of

correlations. For such models most important parameter regarding heat transfer is the heat transfer coefficient which is obtained by heat flux measurements from known boundary conditions. Further extension to this approach is based on correlation development process by including heat and mass transfer analogy for example. Second approach aims to develop numerical models which are based on solving two or three dimensional coupled liquid and mixture conservation equations. This type of research both has industrial importance and it also contributes to the fundamental knowledge regarding multi-component diffusion effects in gaseous mixtures. Recent advances in computing and numerical methods makes it possible to simulate evaporation and condensation simultaneously in presence of non-condensable gases for large cavities such as nuclear power plant containment.

In case of first research path, experimental data usually correlated to come up with empirical relations in forms of average heat transfer coefficients or Nusselt number which are usually functions of Reynolds number, Prandtl number, non-condensable mass fraction etc. Widely known of those correlations which considers condensation with multicomponent non-condensable gas are developed by Uchida, Tagami, Kataoka and Dehbi. Along those correlations Dehbi's correlation considers the effect of pressure also.

Dehbi et al. [24] conducted an experimental and theoretical investigation to determine the extent of steam condensation when non-condensable gases are present. Experiments conducted by using steam-air and steam-air-helium in internally cooled copper cylinder enclosed in a large pressure vessel. Correlations for the condensation heat transfer coefficient were developed based on boundary layer approximations. At low pressure reported correlations give similar results to those reported by Tagami and Uchida.

Siddique et al. [25] conducted an experimental investigation to determine local condensation heat transfer coefficient of steam in presence of air or helium. Experiments conducted in 46 mm id vertical tube. Obtained data correlated in terms of the local mixture Reynolds number, Jacob number, Schmidt number and gas mass fractions. As a conclusion it is reported that if the ratio between air and helium mass fractions is equal to unity, helium has the most dominant influence on the heat transfer degradation. On the

other hand, in case that molar fractions of these gases are equal to one, dominant influence noted to be on the air side.

Anderson et al. [26] investigated steam condensation onto the internal surfaces of the AP600 containment wall using two scaled vessels with similar aspect ratios to actual AP600. Effect of non-condensable gases on heat transfer degradation studied for different mixtures of air and helium. Moreover, effect of bulk temperatures, the mass fraction of non-condensable /steam, the cold wall surface temperature, the pressure, non-condensable composition and inclination of the condensing surface were reported.

Mantley et al [27] conducted study to analyse formation and behaviour of fog during partial condensation of humid air in a vertical tube bundle condenser. It is shown numerically and experimentally that local effects during spontaneous condensation of humid air cannot be neglected for the highly supersaturated mixtures. Also it is concluded that the number concentration of foreign nuclei shows no influence on the amount of fog provided that a certain level of number concentration is exceeded.

Martin et al.[28]conducted analysis by implementing different fluid film models into CFD code and compare with experimental data. Models based on correlation are reported to be more robust and simpler however they perform badly out of experimental conditions. Mechanistic model perform well in numerous conditions however algorithms for such modelling are complicated.

Siow et al [29]conducted analysis with two phase flow model with laminar flow condensation from mixtures of vapour and non-condensable gas in parallel-plate channels. Results indicates increasing angle of declination produces thinner faster moving films and condensation heat transfer mostly effected by film Reynolds number.

Recently, several studies regarding simulation for large cavities such as nuclear power plant containments conducted. One of the most important activity to validate the evaporation and condensation models carried through international standard problem (ISP-47) [30]. In scope of this activity, several large facilities such as MISTRA, TOSQAN, and ThAI is used to obtain experimental data to validate both computational fluid dynamics and lumped parameter codes. A recent study conducted by M. Kondo et al. [31]discuss about prediction of steam concentration in case of no power for cooling of

the spent fuel pool and conditioning of the air in the boiling water reactor (BWR), reactor building. Throughout this study lumped parameter model is introduced which considers evaporation from the pool and condensation to the walls with parametric studies to identify the dominant parameters for the evaporation and condensation. Moreover, comparison with the results of the CFD tool is also presented. As the result of the parametric study, it is noted that coefficient in the evaporation model had large impact on the spent fuel pool evaporation whereas the wall condensation did not have much dependency on the condensation model.

Another study conducted by S. Mimouni et al. [32] discuss about the modelling of wall steam condensation by two phase flow approach using CFD. Throughout the paper COPAIN facility that deals with studying phenomenon of wall condensation in the presence of non-condensable gases and TOSQAN facility which is designed to simulate typical accidental thermal hydraulic flow conditions of the reactor containment were introduced. Vessel is highly instrumented with non-intrusive optical diagnostics aimed to gather data for CFD code validation. Furthermore, by implementing wall condensation model in NEPTUNE CFD atmosphere mixing and stratification in vessel reproduced.

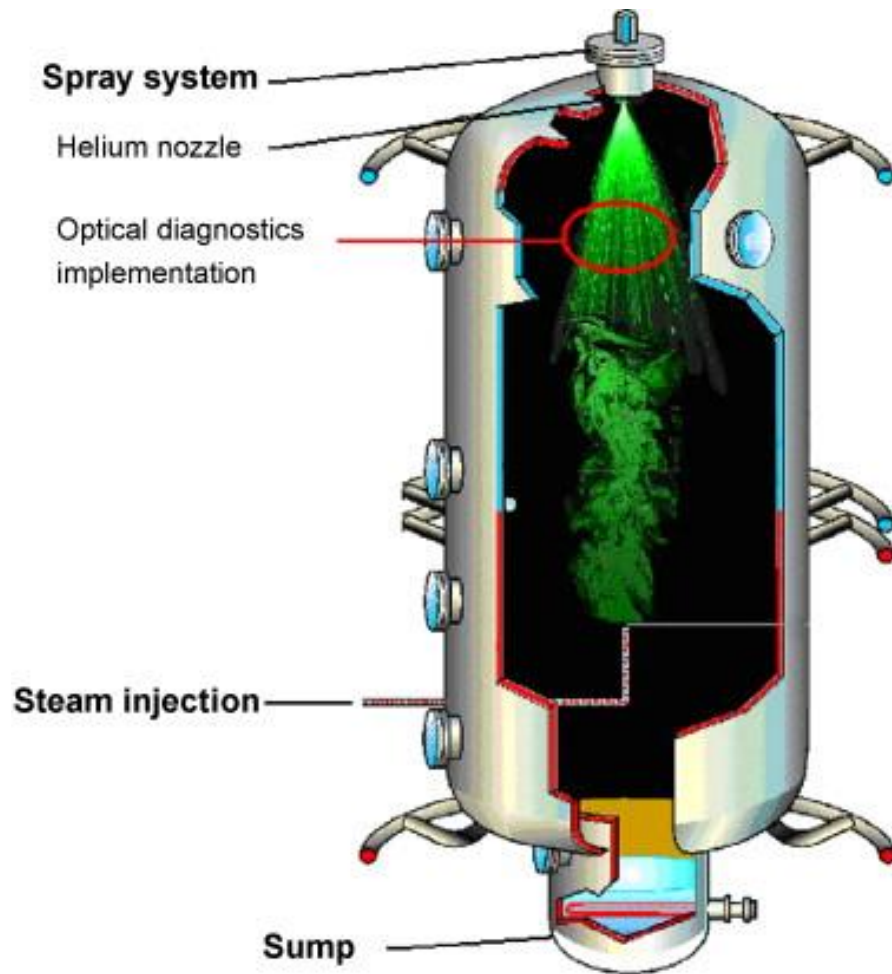


Figure 3-1 TOSQUAN Facility [33]

Study by J. Malet et al. [34] aims to compare the results of numerical study and experimental results on different wall condensation tests in TOSQUAN facility. Study points out that there are three kinds of heat and mass transfer modelling generally found for the description of the wall condensation which are:

- Modelling using degradation coefficients
- Models based on the heat and mass transfer analogy (HMTA)
- Heat and mass transfer diffusion method (HMTD)

In this study, HMTA modelling of the TONUS-CFD code is used. HMTA modelling based on the analogy of the heat, mass and momentum (in forced convection)

transfer in the boundary layer. The results of the code experiment comparison in this study shows rather good agreement for local results inside the vessel however due to turbulence modelling which was chosen simple in order to avoid high computational times put some limitations on the simulations. Another source of the limitation is pointed as boundary layers.

M. Houkema et al. [7] conducted a study about the validation of Nuclear Research and Consultancy Group (NRG) condensation model in CFX4 with the different experiments which addressed thermal hydraulic phenomena such as wall condensation, atmospheric stratification, natural circulation, turbulent diffusion and the interactions between those phenomena. NRG steam condensation model consists of sinks of steam, total mass, enthalpy and turbulent quantities in which the sinks depends on the steam condensation rate. The predictions of numerical analysis with condensation model predicted fairly well for the validation cases with some deviations primarily raised from the wall treatment. Also authors point out that for condensation and stratification phenomena further improvement needed to apply CFD approach for containment thermal-hydraulics.

T. Zitzmann et al. [35] investigate the air flow and heat transfer over a heated vertical plate in differentially heated cavity with conducting parametric studies to inspect the effect of near wall mesh density on air flow and heat transfer for natural convection. Paper also provides guidelines on how to use CFD with unstructured meshes to model buoyancy driven flow. Authors concluded that prism mesh is required in the near wall region to accurately resolve the wall boundary layer. Moreover, for the laminar simulations, predicted results agreed well with published data. In case of turbulent simulations, authors noted that SST and $k-\omega$ models predict the most favourable predictions compared with the experiments. Panda (Passive Decay Heat Removal and Depressurization Test Facility, PANDA) test carried out in PSI to generate high-quality experimental data for the assessment and validation of lumped parameter and computational fluid dynamics codes.

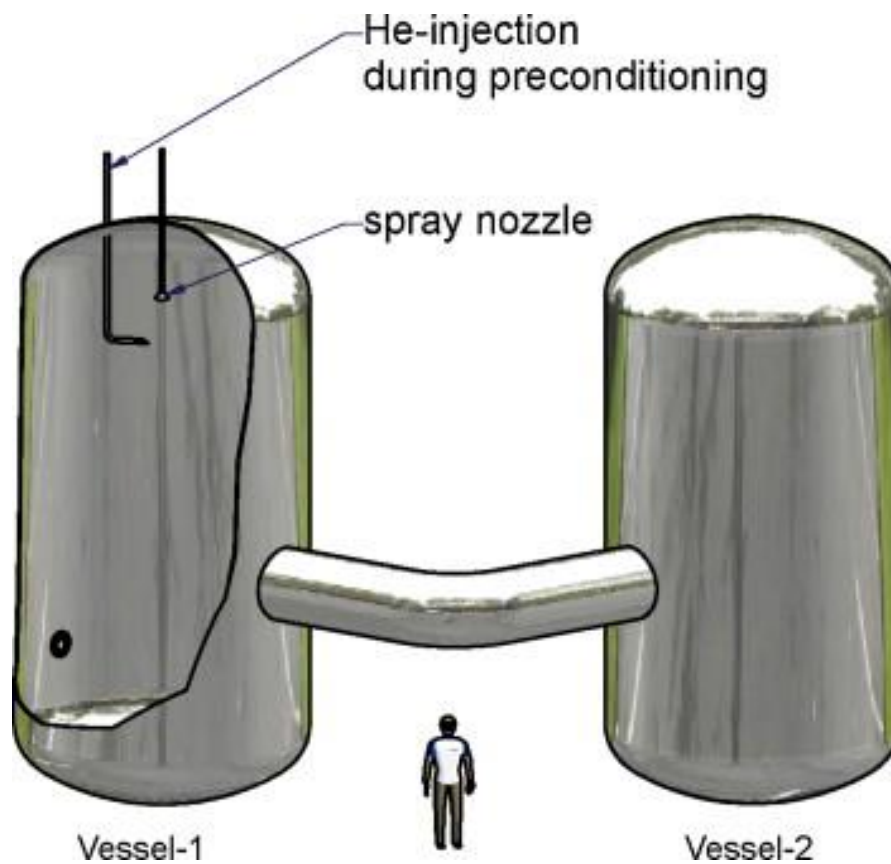


Figure 3-2 PANDA Facility [18]

3.3 Diffusion Layer Model

When steam including non-condensable gases condenses on a wall, the non-condensable gas accumulates near the wall which deteriorates the condensation heat transfer. Furthermore, due to the accumulation of the non-condensable gases the steam partial pressure at the liquid gas interface becomes smaller than the bulk flow which provides the driving force that allows the steam to diffuse toward the condensate film as demonstrated in Figure 3-3. Furthermore, as the gradients in normal direction to the surface during steam condensation in the presence of non-condensable gas, physics of the condensation problem can be addressed through the boundary layer approximation. Presence of boundary layers can be categorized into two as the one that is closer to the

wall is characterized by condensed steam and the accumulated non-condensable gas layer. In this study, only the non-condensable gas layer is considered whereas the layer due to the condensed steam is omitted.

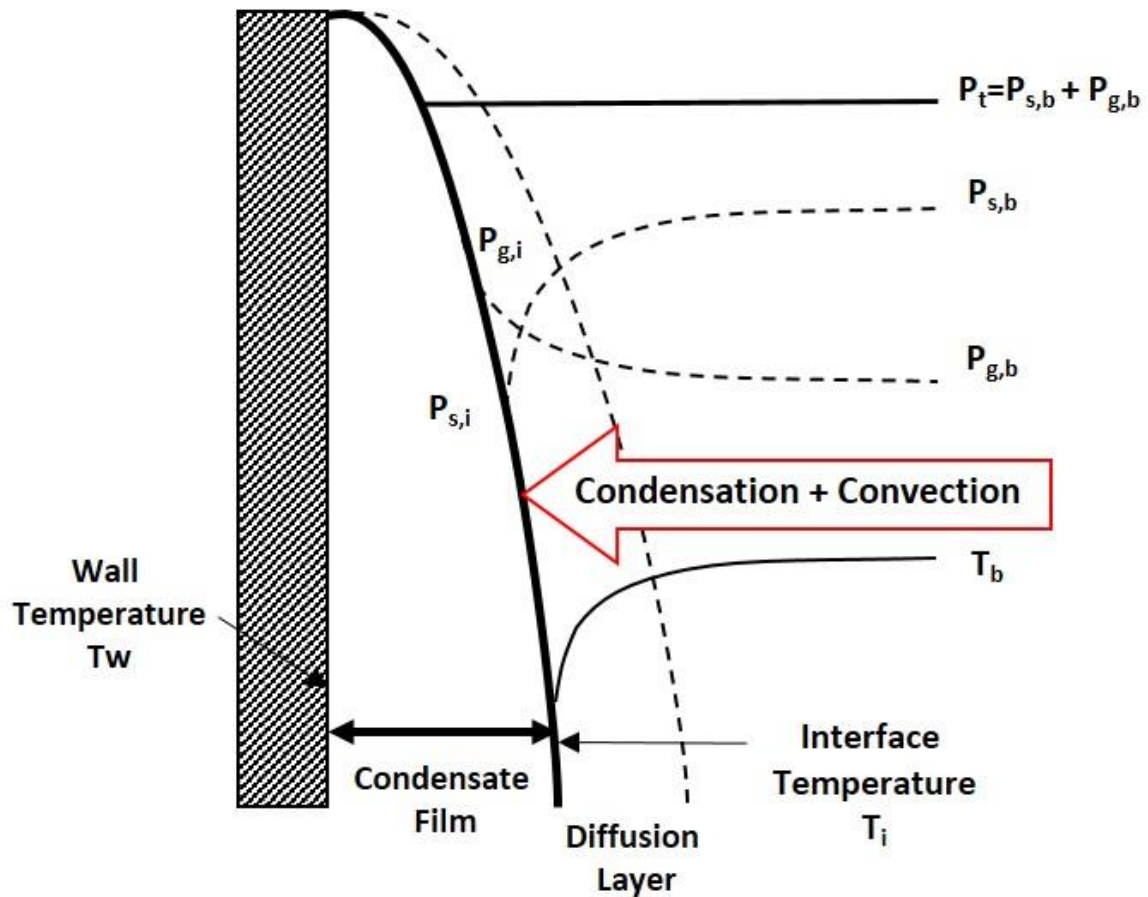


Figure 3-3 Simplified Fluid Film Representation during Condensation

During condensation the local concentration of steam and non-condensable gases changes. The concentration of steam reduces locally and density of the mixture is affected. Thus, steam diffusion and Stefan flow (flow induced by production or removal of species at the interface) from bulk toward structures are promoted.

Diffusion is a process where the particles move from regions of high concentration into regions of lower concentration. There are two approaches to analyse such phenomena which are using Fick's law given by;

$$J = -D \frac{d\varphi}{dx} \quad (3.1)$$

where J is the diffusion flux, D is the diffusion coefficient φ is the concentration and x is the position or applying an engineering approach by using mass transfer coefficient. Analysing diffusion with mass transfer coefficients limited to cases where changes in concentration occurs near the system's boundaries. Absorption of one gas into liquid is one of the example for such a case. Rate of mass transfer can be defined as follows;

$$(\text{rate of mass transferred}) = k (\text{interfacial area}) (\text{concentration difference}) \quad (3.2)$$

Where h_d is called a mass transfer coefficient. Equation (3.38) further be simplified by dividing area which results in

$$N = h_D (c_{li} - c_1) \quad (3.3)$$

Where N is the flux at the interface and c_{li} and c_1 are the concentrations at the interface and in the bulk flow, respectively.

Common approach to analyse the governing equations to describe the thermal-hydraulic behaviour of the multicomponent mixture is proposed by Bird [43] and Taylor and Khristna [44]. Considering a single phase multicomponent mixture which includes N different chemical species, the molar concentration of the mixture C is defined as the number of moles of the mixture per unit volume. Partial molar concentration can be defined considering the fraction of these moles X_i , so called molar fraction that belongs to i -th species as follows

$$C_i = X_i C \quad (3.4)$$

The density of the mixture is defined as the mass of the mixture per unit volume. Some portion of this mass is associated to the i -th species. The contribution of this species is proportional to its molar concentration and its molar weight. Thus the partial species density is given by

$$\rho_i = C_i M_i \quad (3.5)$$

The density ρ of the mixture further be defined as the sum of the n species partial densities

$$\rho = \sum_{i=1}^n \rho_i \quad (3.6)$$

Mass fraction Y_i is defined as the ratio of the species density to the mixture density.

Hence, following properties are applicable for both mass and molar fractions:

$$\sum_{i=1}^n Y_i = 1 \quad (3.7)$$

$$\sum_{i=1}^n X_i = 1 \quad (3.8)$$

Using molar fractions, the mixture average molar weight is defined by

$$M = \frac{\rho}{C} = \frac{\sum_{i=1}^n \rho_i}{C} = \frac{\sum_{i=1}^n M_i C_i}{C} = \sum_{i=1}^n X_i M_i \quad (3.9)$$

or alternatively as a function of mass fractions

$$M = \frac{\rho}{C} = \frac{\rho}{\sum_{i=1}^n C_i} = \frac{\rho}{\sum_{i=1}^n \frac{\rho_i}{M_i}} = \frac{1}{\sum_{i=1}^n \frac{Y_i}{M_i}} \quad (3.10)$$

In case of diffusion layer modelling, condensation acts as a sink of mass and energy. Therefore, the liquid film and the influence of the non-condensable gas layer are reduced to a simple sink term. CFD codes usually do not acquire a model for heat and mass transfer which has to be introduced through user defined functions into the codes. In this model condensation rate per each cell is defined as;

$$\dot{m}_c = h_d (w_{sat} - w) \rho \frac{A_{cell}}{V_{cell}} \quad (3.11)$$

where \dot{m} is condensation rate per volume. h_d is mass transfer coefficient, w_{sat} is saturation mass fraction, w is the mass fraction at cell center, ρ is the density of bulk flow, A_{cell} is the cell surface area and V_{cell} is the cell volume.

Mass transfer coefficient can be approximated by using mass and heat transfer analogy. This analogy arise from the fact that, mass, in essence is an energy and heat is an energy in transfer. Change in between mass and energy is also stated by Einstein with his influential formula $E = mc^2$. Therefore, one can look at mass and heat as two different forms of energy and use this advantage to analysis conditions that includes simultaneous mass and heat transfer such as evaporation and condensation. The important dimensionless numbers regarding heat and mass transfer analogy is summarized in Table 3.1.

Table 3.1 Common Dimensionless Numbers to Characterize Heat and Mass Transfer

Heat Transfer	Mass Transfer
$Pr = \frac{\nu}{\alpha}$	$Sc = \frac{\nu}{D}$
$Nu = \frac{h_h L}{k}$	$Sh = \frac{h_m L}{D}$
$Ra = \frac{g \beta \Delta T H^3}{\alpha \nu}$	$Ra = \frac{g H^3}{D_m \nu} \frac{\Delta \rho}{\rho}$

Mass transfer coefficient can be estimated by using correlations for heat and mass transfer analogy. Some of the well-known correlations are listed in Table 3.2.

Table 3.2 Common Correlations for Heat and Mass Transfer Analogy

Correlations	
Frössling [45]	$Nu = 2 + 0.552 Re^{1/2} Pr^{1/3}$ $Sh = 2 + 0.552 Re^{1/2} Sc^{1/3}$
Ranz Marshall [46]	$Nu = 2 + 0.6 Re^{1/2} Pr^{1/3}$ $Sh = 2 + 0.6 Re^{1/2} Sc^{1/3}$

Clift et al. [47]	$Nu = 1 + (1 + Re Pr)^{1/3} Re^{0.077}$ $Sh = 1 + (1 + Re Sc)^{1/3} Re^{0.077}$
Chuchottaworn et al. [48]	$Nu = 2 + 0.37 Re^{0.61} Pr^{0.51}$ $Sh = 2 + 0.37 Re^{0.61} Sc^{0.51}$

Sherwood number can be used to calculate mass transfer coefficient:

$$h_D = \frac{ShD}{L} \quad (3.12)$$

Where Sh is Sherwood number, L is characteristic length and D is the diffusion coefficient. Sherwood number is estimated by using Ranz-Marshall correlation given in Table 3.2 where Reynolds and Schmidt numbers are given by;

$$Re = \frac{\rho v L}{\mu} \quad (3.13)$$

$$Sc = \frac{\mu}{\rho D} \quad (3.14)$$

where ρ is density, v is velocity and μ is dynamic viscosity. The diffusion coefficient D estimated by considering temperature dependency [49];

$$D(T) = 2.2 \times 10^{-5} \left(\frac{T}{273} \right)^{1.75} \quad (3.15)$$

In case of high condensation rates suction effect will take place, and the boundary layer will experience sharper gradients. As suction effect cannot be directly taken into account by the code a correction factor has to be applied. The most common expression for the correction factor is the logarithmic form derived by Bird et al. [43]:

$$\theta_B = \frac{\ln(1+B)}{B} \quad (3.16)$$

where the bird suction parameter B is defined as[50] :

$$B \equiv \frac{W_{s,i} - W_{s,\infty}}{1 - W_{s,i}} \quad (3.17)$$

where the subscripts i and ∞ are refer to the interface and bulk flow respectively. Bird formulation is valid for cases which assumes the radial fluid velocity towards the wall is zero and only diffusion is exits in that direction. On the other hand, studies conducted both for turbulent forced flows [51] and naturally driven flows [52].

Vapor mole fraction at saturation temperature calculated as;

$$w_{sat}(T) = \frac{P_{sat}(T)}{P_{gas}} \quad (3.18)$$

where saturation pressure is estimated using Tetten's [53] equation;

$$P_{sat}(T) = 611 \times 10^{7.5 \left(\frac{T-273}{T-35.7} \right)} \quad (3.19)$$

As this model only considers gas phase, calculations during simulations accounts for the sensible heat only. Figure 3-4 shows the droplet formation on the wall after the condensation of the vapor molecule where only sensible heat is removed from the gas domain.

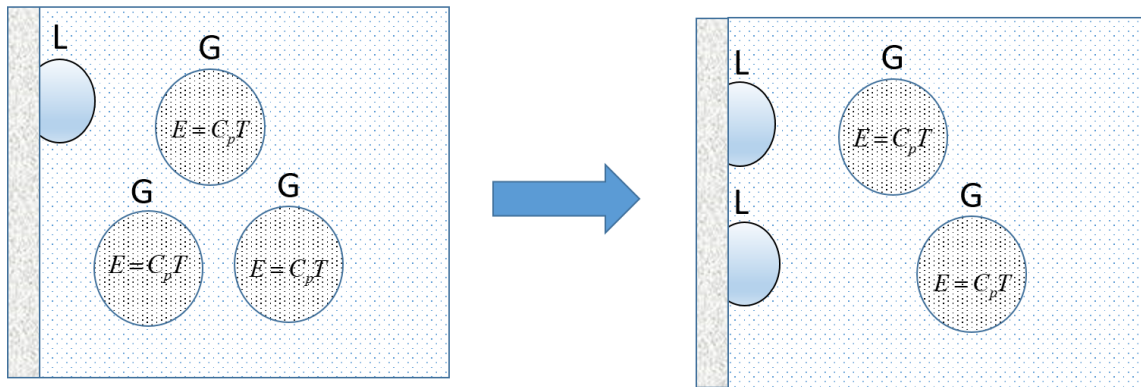


Figure 3-4 Droplet Formation due to Condensation

Thus, in order to estimate corresponding heat transferred to the wall due to condensation following expression can be used;

$$q = \dot{m}_c V_{cell} h_{fg} \quad (3.20)$$

where q released heat per cell and h_{fg} is the latent heat. Total heat released Q_{cond} during condensation can be calculated by summing all heat sink for each cell on diffusion layer;

$$Q_{cond} = \sum_{i=1}^n \dot{q} \quad (3.21)$$

where subscript i is cell number and n is total number of cells. Further the wall heat flux q_w'' is calculated as follows;

$$q_w'' = \frac{Q_{cond}}{A_w} \quad (3.22)$$

where A_w is surface area of wall where condensation occurs.

Main assumptions in this approach are as follows:

- The working fluid is consists of a multi-component gaseous mixture with one condensable and one or more non-condensable component.
- The condensation rate is controlled by the concentration of condensable gas on the boundary layer.
- The partial pressure of the condensable gas at the wall is equal to its saturation pressure evaluated at the wall temperature.
- At the condensation heat transfer interface, the latent heat released by condensation is assumed to be absorbed by the wall.

Diffusion layer model considered to be suitable wall condensation model for this study due to fact that it can be applicable to complex geometry as in 1F1 PCV and can represent wall condensation physically considering diffusion of the species.

3.4 Validation with COPAIN Experiments

3.4.1 Introduction

In order to validate the diffusion layer model in a simple geometry with predominantly 2D flow, COPAIN test cases are selected. Main idea behind selecting simple geometry for validation activity is that to ensure numerical errors are low and deviations from experimental results can be assumed to be originated from the uncertainties in turbulence modelling, modelling assumptions, etc.

COPAIN experimental facility is designed to conduct separate-effect test experiments to investigate condensation heat transfer involving non-condensable gases on a vertical plate under DABASCO [54] project at CEA, Grenoble, FRANCE.

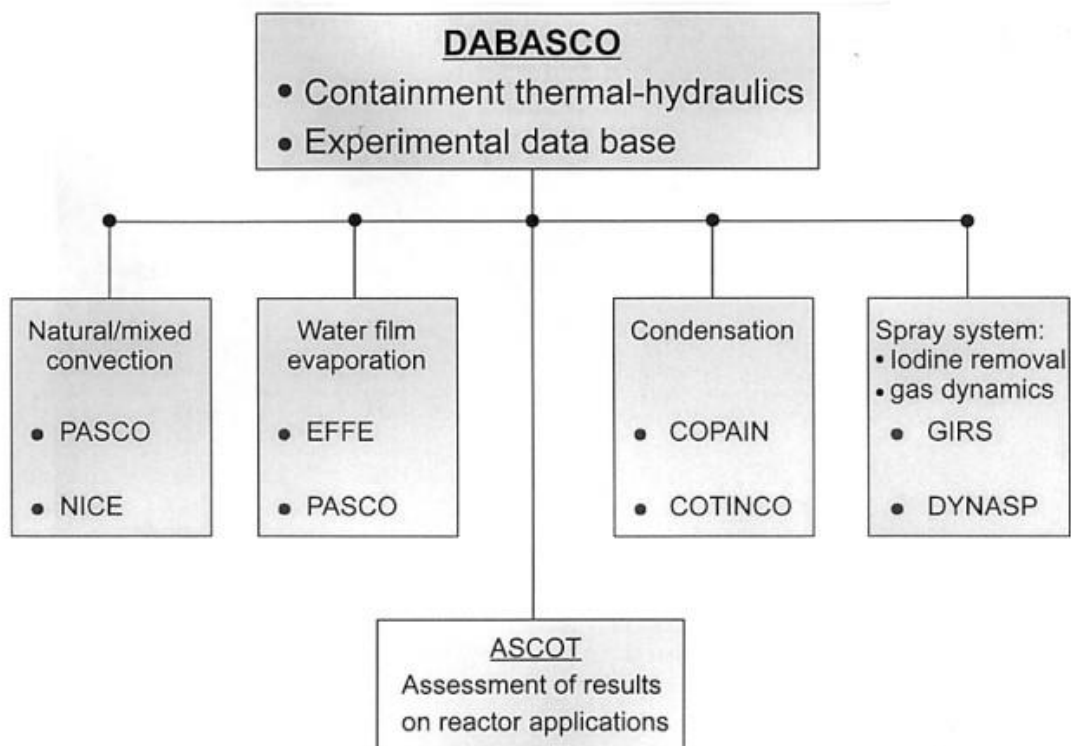


Figure 3-5 DABACO Project Overview [54]

Experimental apparatus consists of a rectangular channel with a width and depth dimension of 0.6m and 0.5 m respectively. Condensing section of facility is a vertical

plate with a height of 2.0 m and a width of 0.6 m. Schematic of the test facility is given in Figure 3-5. Test conditions include inlet velocities between 0.3 to 3.0 m/s, pressures between 1.0 to 7.0 bar with temperature under 165 °C, heat flux exchanged with the plate between 1 and 30 kW/m² flow conditions from natural to forced convection and wide range of the non-condensable gas content [55]. During experiments several local parameters such as pressure, wall temperature and bulk temperature are measured. In case of severe accident considerable amount of gas species released to containment along with the steam. Steam inside containment will condense on the walls and generates convective motion. During condensation wall temperatures will be around saturation temperature and amount of steam will decrease. However, presence of non-condensable gas will affect the condensation rate dramatically. Most important objective of the COPAIN experiments is to investigate effect of non-condensable gases on condensation by studying the effect of various parameters such as pressure, temperature, gas velocity and gas steam mixture composition.

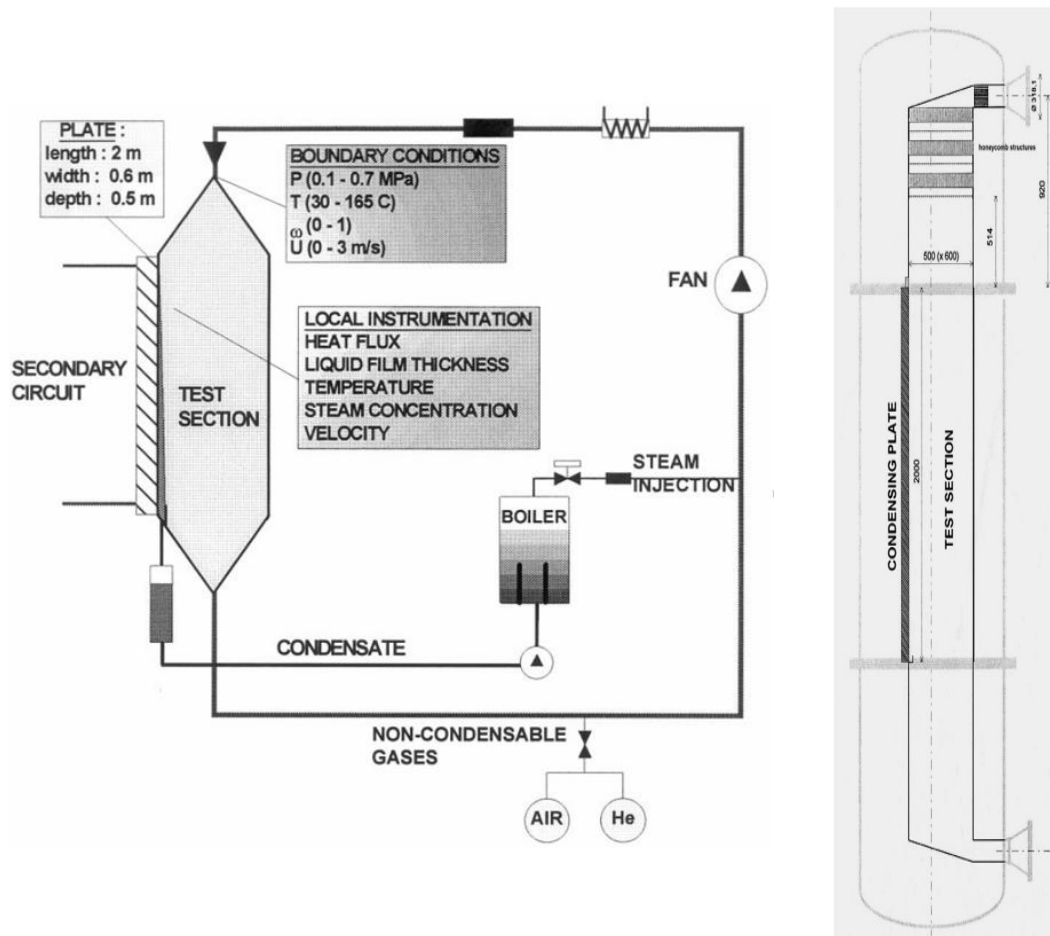


Figure 3-6 Schematic of COPAIN Facility [54][56]

3.4.2 Analysis Setup

Analysis conducted for 5 different COPAIN test cases that includes both natural and forced flow regime with mixture of air, steam and helium at different compositions. Initial and boundary conditions for the each test are given in Table 3.3.

Table 3.3 Selected tests from COPAIN experiment for comparison[56]–[58]

Test No	Convective Heat Transfer	Air Velocity at Inlet (m/s)	Pressure (bar)	Air Temperature Inlet (K)	Wall Temperature (K)	Mass Fraction (Y_{nonc})	Molar Fraction ($X_{\text{He/nonc}}$)
P0441	Forced	3	1.02	353.23	307.4	0.767	0.0
P0443	Natural	1	1.02	352.33	300.06	0.772	0.0
P0444	Natural	0.5	1.02	351.53	299.7	0.773	0.0
P0344	Natural	0.3	1.21	344.03	322	0.864	0.0
P0461	Forced	3	1.22	344.43	329.92	0.803	0.4

3D-Cad model is prepared as shown in Figure 3-7. Velocity inlet boundary and pressure outlet boundary is defined on the top and bottom boundary of the domain. Boundary for condensing wall is defined at constant temperature and remaining walls defined as an adiabatic wall.

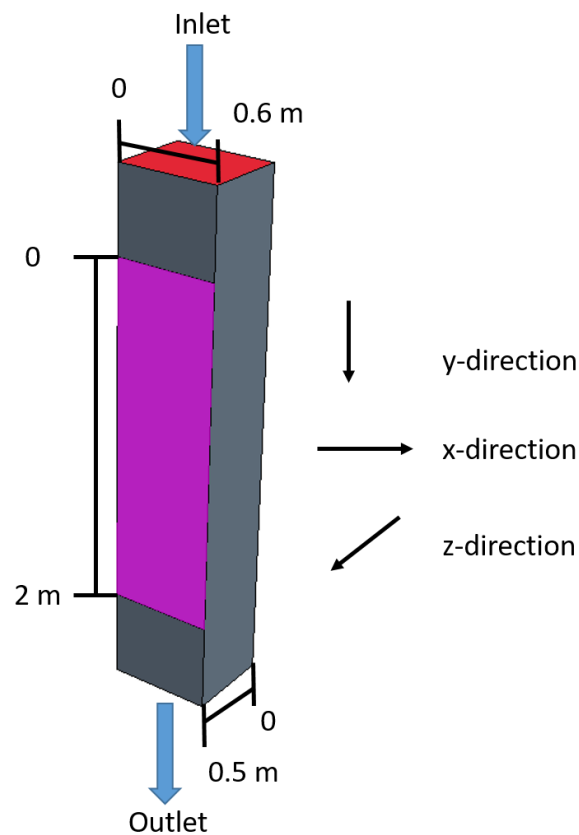


Figure 3-7 3D CAD Model of COPAIN Facility

Working fluid defined as a multicomponent gas mixture with steam, air and helium species. All gas species assumed to behave as an ideal gas. Standard k- ϵ turbulent model is used with two layer all y^+ wall treatment. All y^+ wall treatment in STAR-CCM+ combines turbulence quantities such as dissipation, production, stress tensor, etc. calculated by the high y^+ and low y^+ approach using an exponential weighing function. The high y^+ wall treatment is a classical wall-function approach where turbulent quantities are derived from equilibrium turbulent boundary layer theory. This approach is suitable to resolve turbulent characteristics at boundary layer which has y^+ from 30 to 50. The low y^+ wall treatment is consistent with low-Reynolds number models which assumes that the viscous sublayer is well resolved so that wall functions are unnecessary. This approach is suitable for cases where entire mesh is fine enough for y^+ to be approximately 1 or less. Setting for the analysis are summarized in Table 3.4.

Table 3.4 Settings for Simulation of COPAIN Experiments

Items			Settings
Calculation	Space	Dimension	3
		Gravity	9.81 m/s ²
	Time	Steady State	500 iteration
Multi-component gas	Common for all components	Equation of State	Ideal Gas
		Turbulent Model	Realizable k-epsilon
		Turbulent Prandtl Number	0.9
		Turbulent Schmidt Number	0.9
		Molecular Diffusivity	Set by Schmidt Number (Sc=1.0)

Turbulent Intensity		5%
Viscosity Ratio		5.0
Vapor	Dynamic Viscosity	Polynomial in Temperature
	Specific Heat	Polynomial in Temperature
	Thermal Conductivity	Polynomial in Temperature
	Molecular Weight	18.0153 kg/kmol
Air	Dynamic Viscosity	Polynomial in Temperature
	Specific Heat	Polynomial in Temperature
	Thermal Conductivity	Polynomial in Temperature
	Molecular Weight	28.9664 kg/kmol
Helium	Dynamic Viscosity	1.9891E-5 Pa-s
	Specific Heat	5197.61 J/kg-K
	Thermal Conductivity	0.154933 W/m-K
	Molecular Weight	4.0026 kg/kmol

Mixture properties are calculated by mass weighted mixture method which calculates the given mixture property by mass-weighting the component property.

$$\phi_{mix} = \sum_{i=1}^N y_i \phi_i \quad (3.23)$$

where y_i and ϕ_i are the mass fraction and property values of mixture component i-th and N is the total number of components in the mixture. Properties of the vapor, air and helium species are approximated by using following polynomials in temperature [59];

Specific Heat of Vapor:

$$-4.30484 + 5.64991 \times 10^{-2} T - 1.75247 \times 10^{-4} T^2 + 1.86832 \times 10^{-7} T^3 \quad (3.24)$$

Dynamic Viscosity of Vapor:

$$1.75670 \times 10^{-6} + 2.33785 \times 10^{-8} T + 1.29077 \times 10^{-11} T^2 \quad (3.25)$$

Thermal Conductivity of Vapor:

$$-5.18738 \times 10^{-3} + 1.52267 \times 10^{-4} T - 4.54796 \times 10^{-7} T^2 + 7.08550 \times 10^{-10} T^3 \quad (3.26)$$

Specific Heat of Air:

$$1.03437 - 2.12720 \times 10^{-4} T + 4.07314 \times 10^{-7} T^2 \quad (3.27)$$

Dynamic Viscosity of Air:

$$2.02910 \times 10^{-6} + 6.21004 \times 10^{-8} T - 2.40179 \times 10^{-11} T^2 \quad (3.28)$$

Thermal Conductivity of Air:

$$3.89745 \times 10^{-3} + 7.86562 \times 10^{-5} T - 1.67164 \times 10^{-8} T^2 \quad (3.29)$$

3.4.3 Mesh Sensitivity Analysis

In order to assess the effect of spatial discretization on diffusion layer model, test case P0444 from COPAIN experiments simulated for 3 different grid sizes as shown in Figure 3-8. In order to fully resolve the boundary layer 10 prism type mesh is used near the wall with growth factor of 1.1. Resulting grid has y^+ value for near wall cells smaller than 1 for each case. Using 3 different base size, 0.03m, 0.02m and 0.015m, grid is gradually refined so that the aspect ratio of the cells get smaller while the normal width of the cells remain constant. Grids shown in Figure 3-8 has total cell number of 52400, 153000 and 336800 from left to right. As in Table 3.5 surface average heat transfer coefficient of the face where condensation occurs is not depend on the mesh size. Condensation model with diffusion layer can be said to be grid independent. This aspect of the model is important as CFD analysis for containment applications may require large mesh size. As diffusion layer model approach has no extra effect on bulk mesh size, it is favourable for modelling wall condensation inside 1F1.

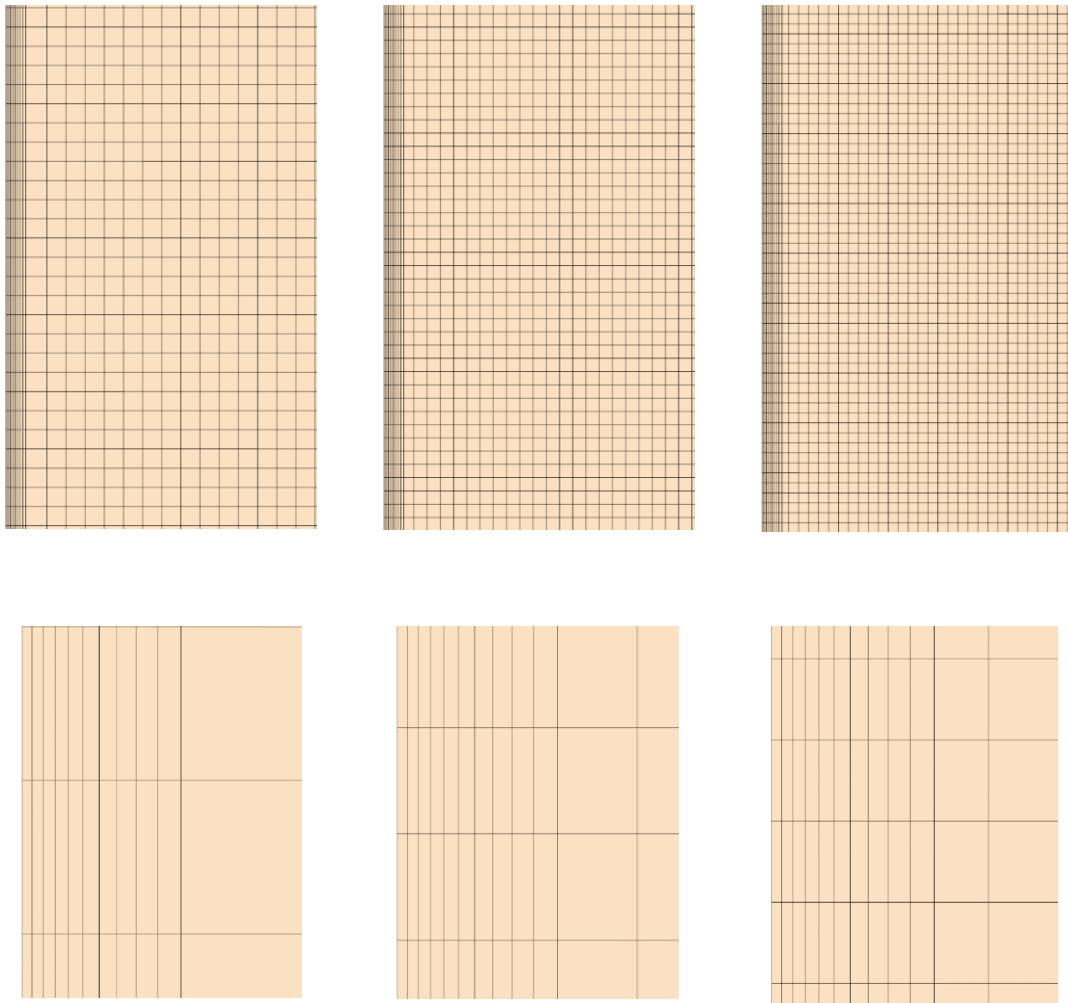


Figure 3-8 Schematic of Grids for Mesh Sensitivity Top: Outline, Bottom: Near Wall

Table 3.5 Influence of Grid Resolution on Heat Transfer Coefficient

Cell Number	Heat Transfer Coefficient (W/m ² -K)
52400	1547.5
153000	1570.3
336800	1581.8

3.4.4 Simulation Results & Discussion

In this section, results of diffusion layer model for COPAIN tests are discussion for both natural and forced convective regime including different amount of non-condensable gases. Figure 3-9 to Figure 3-13 show the simulation results of profile of condensable gas mass fraction along the z-direction for each test case and from Figure 3-14.to Figure 3-19 profile of non-condensable gas fraction is shown. As the mass fraction of the condensable gas is the driving force for the condensation in diffusion layer model estimated concentration near the wall that condensation occurs is important.

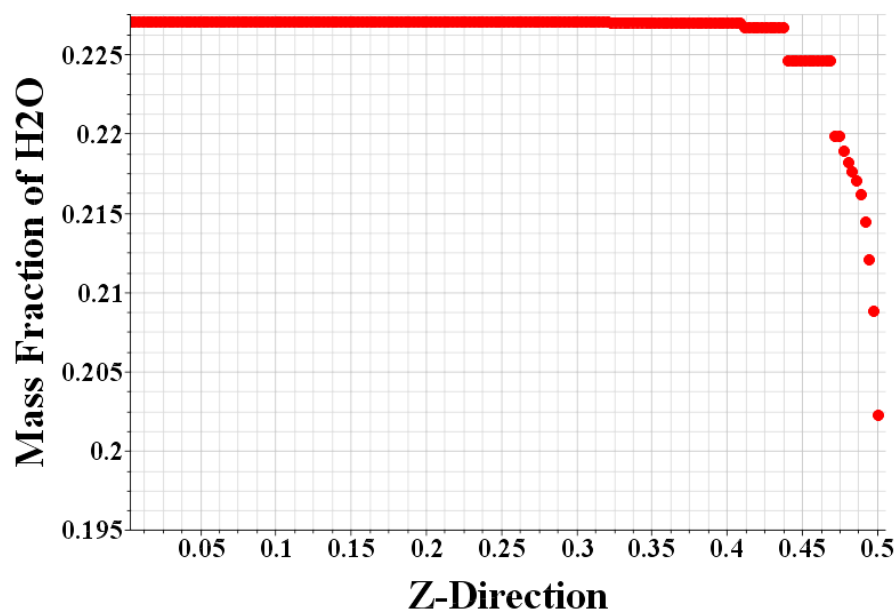


Figure 3-9 Steam Mass Fraction along Z Direction in the P0444 COPAIN Test

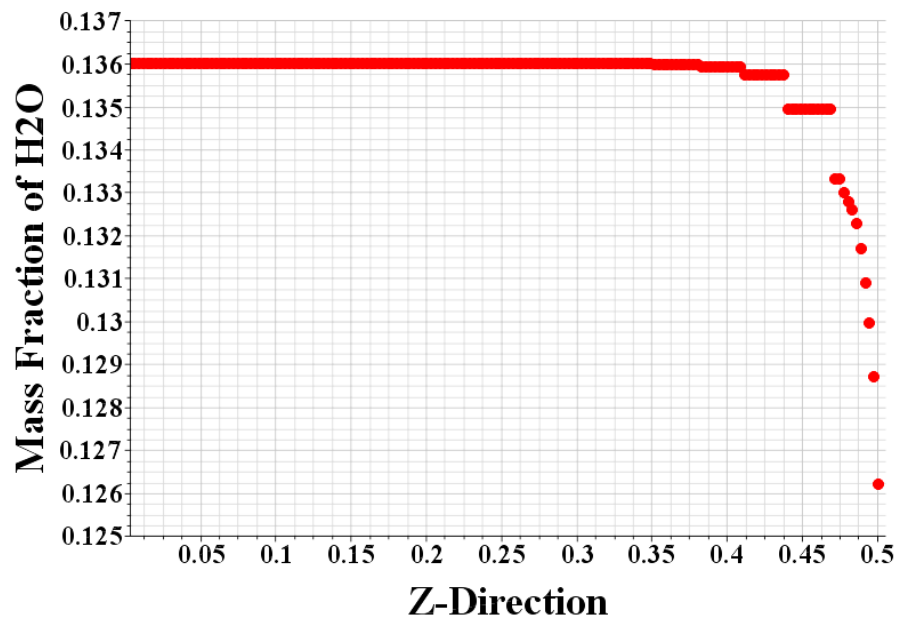


Figure 3-10 Steam Mass Fraction along Z Direction in the P0344 COPAIN Test

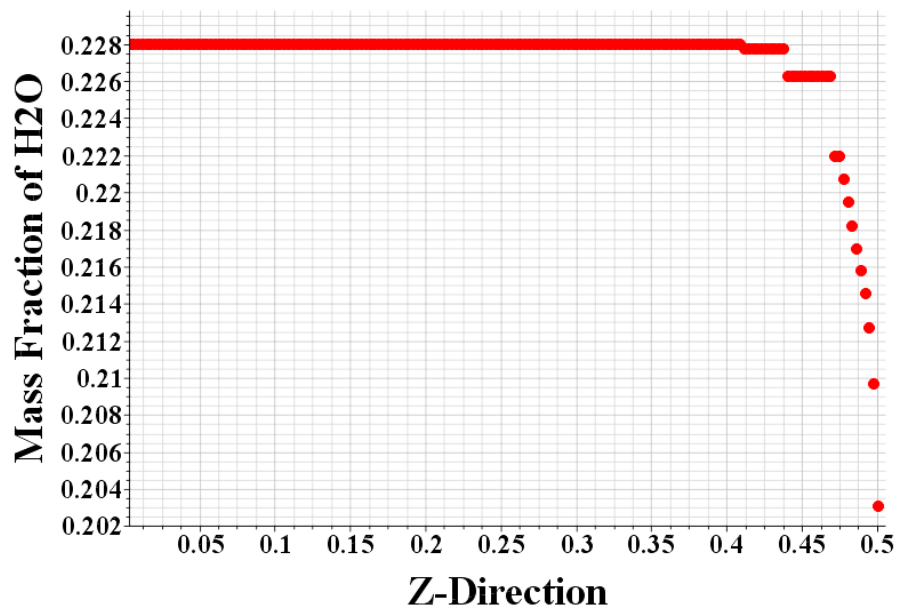


Figure 3-11 Steam Mass Fraction along Z Direction in the P0443 COPAIN Test

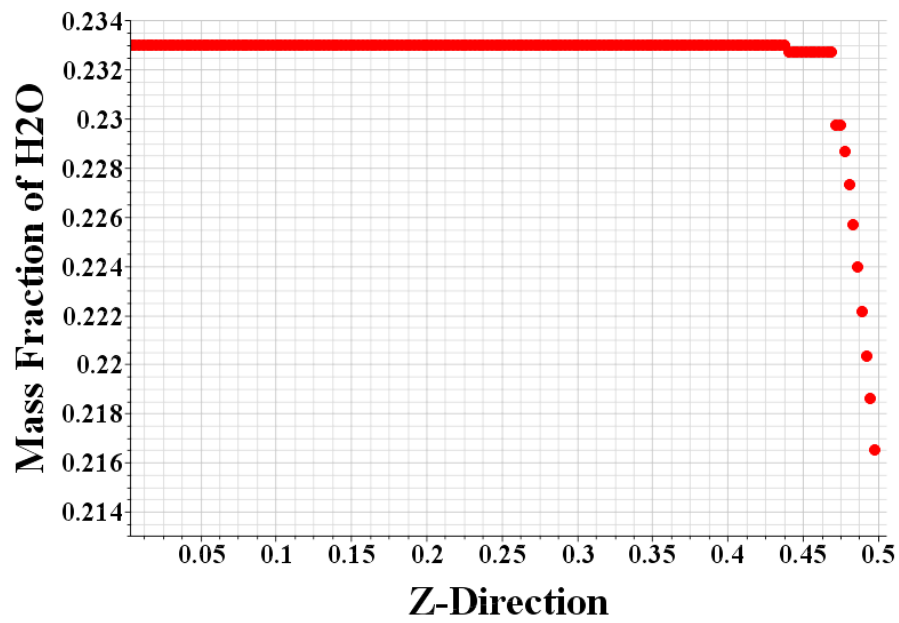


Figure 3-12 Steam Mass Fraction along Z Direction in the P0441 COPAIN Test

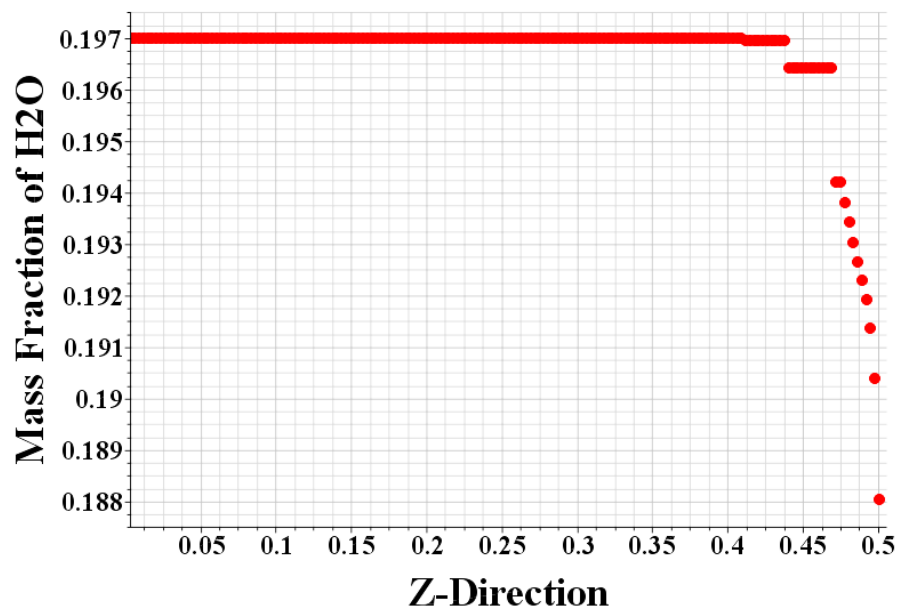


Figure 3-13 Steam Mass Fraction along Z Direction in the P0461 COPAIN Test

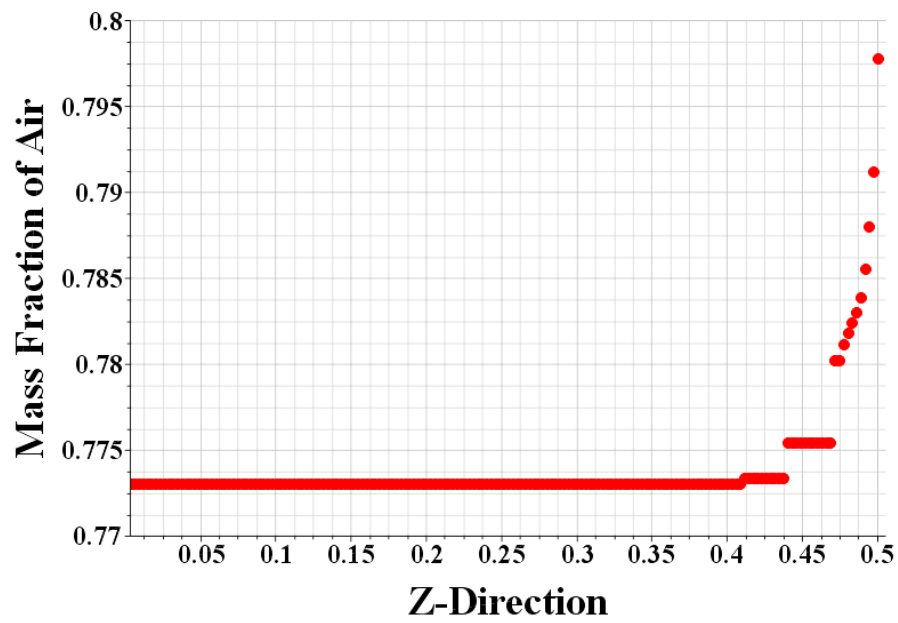


Figure 3-14 Air Mass Fraction along Z Direction in the P0444 COPAIN Test

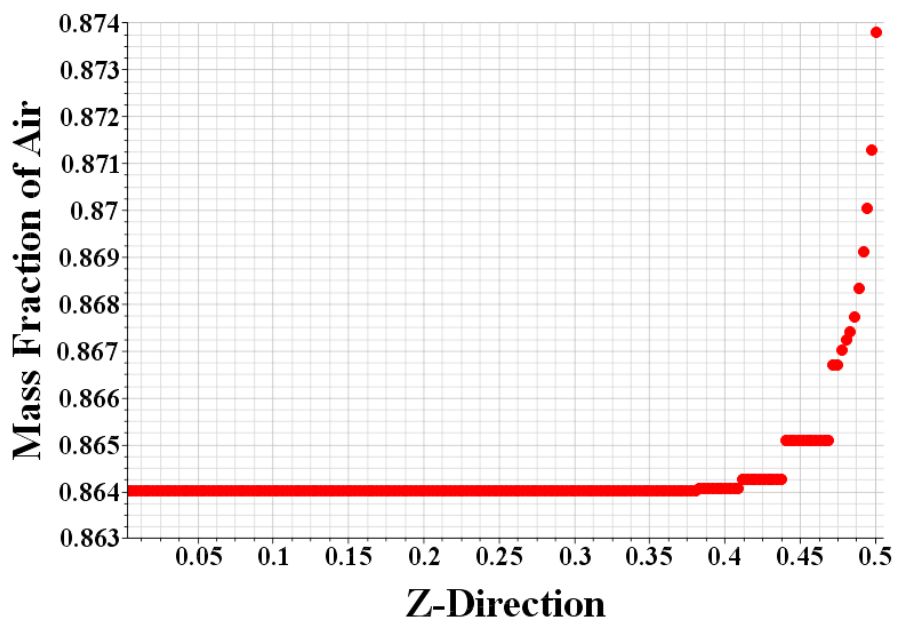


Figure 3-15 Air Mass Fraction along Z Direction in the P0344 COPAIN Test

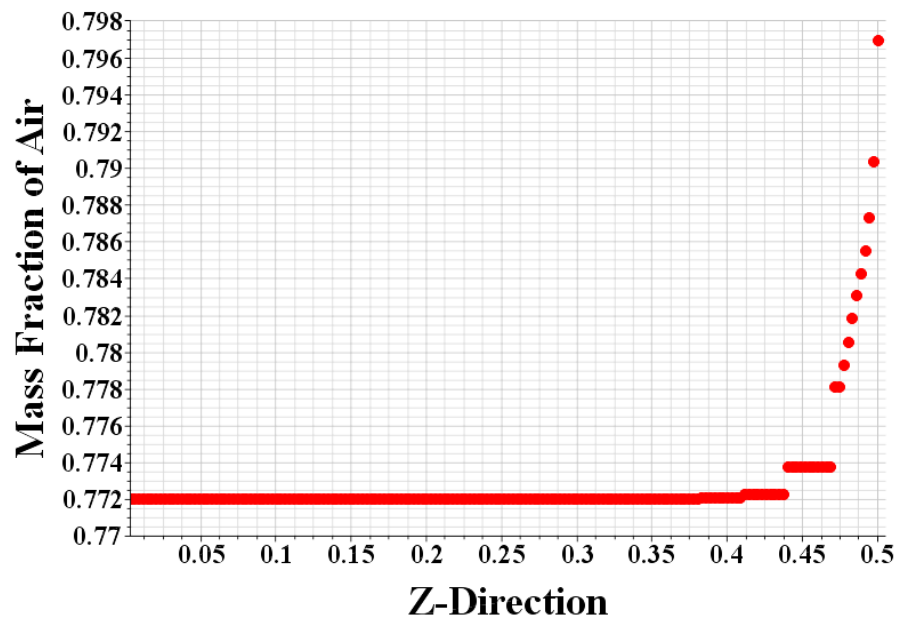


Figure 3-16 Air Mass Fraction along Z Direction in the P0443 COPAIN Test

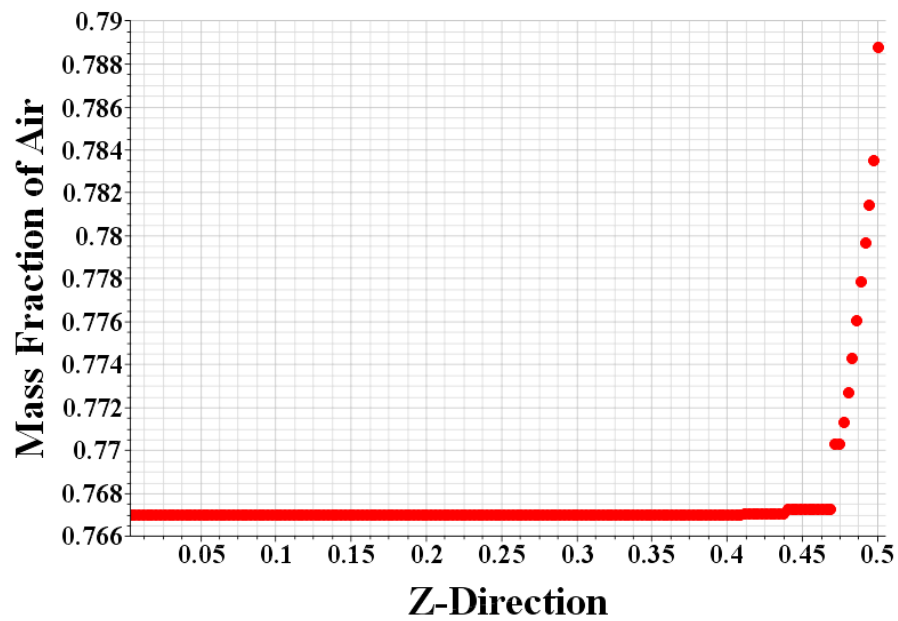


Figure 3-17 Air Mass Fraction along Z Direction in the P0441 COPAIN Test

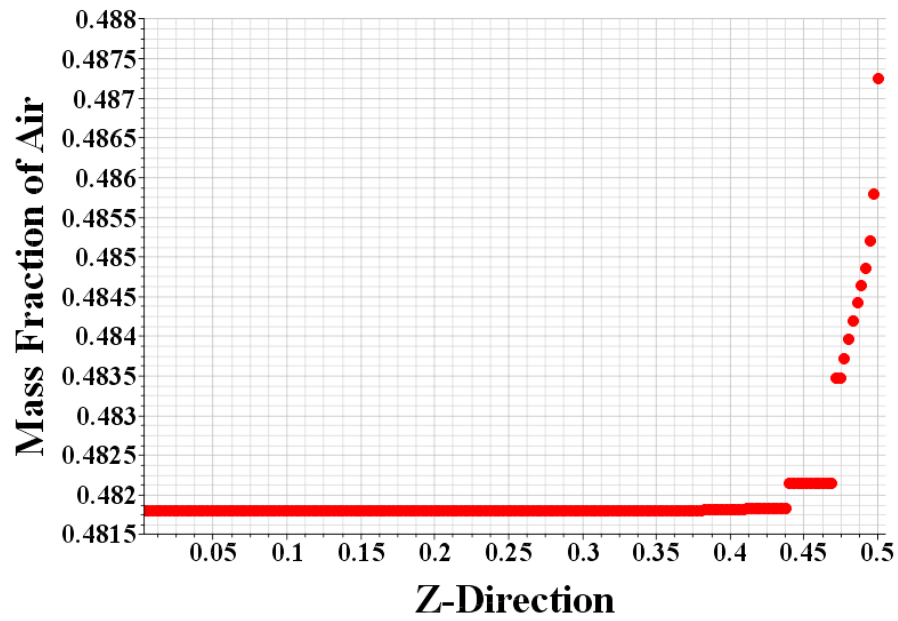


Figure 3-18 Air Mass Fraction along Z Direction in the P0461 COPAIN Test

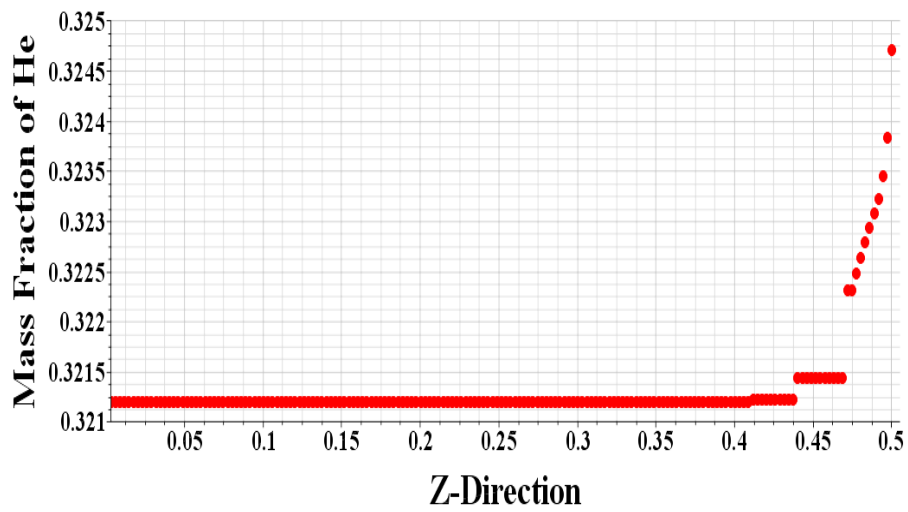


Figure 3-19 Helium Mass Fraction along Z Direction in the P0461 COPAIN Test

As an example of mass fraction of steam and air on the condensing wall along y-direction for test case P0444 is shown in Figure 3-20.

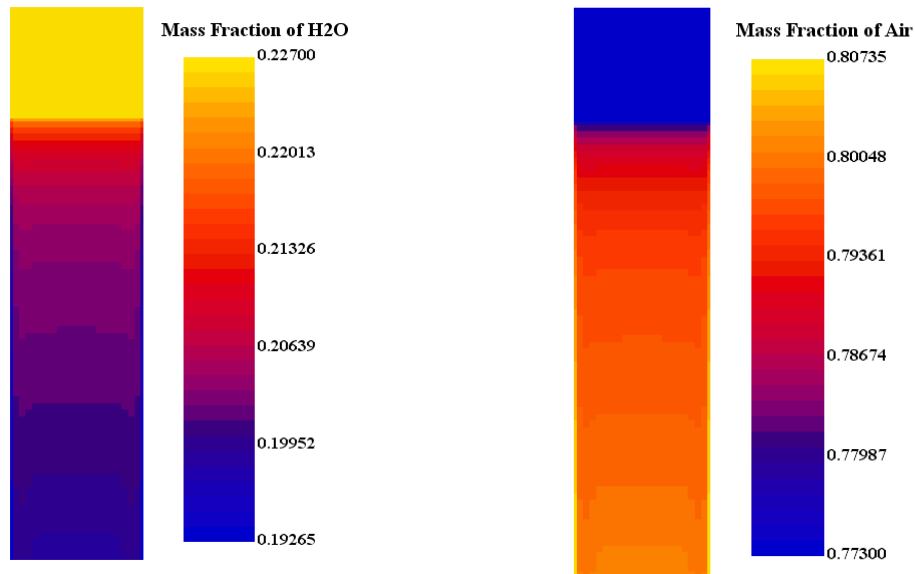


Figure 3-20 Mass fraction of steam (on left), mass fraction of air (on right) on the condensing wall in the P0444 COPAIN test

Simulation results with diffusion layer model for each cases show decrease in mass fraction of steam near wall where condensation occurs as expected. On the other hand, non-condensable gas content in this region increases. The difference between the concentration of condensable gas between the bulk and near wall region is the main driving force for the diffusion layer condensation model.

Another important parameter for the simulation of condensation in diffusion layer model is the estimated mass transfer coefficient Figure 3-21 to Figure 3-25 show the estimated mass transfer coefficient for all the fluid domain.

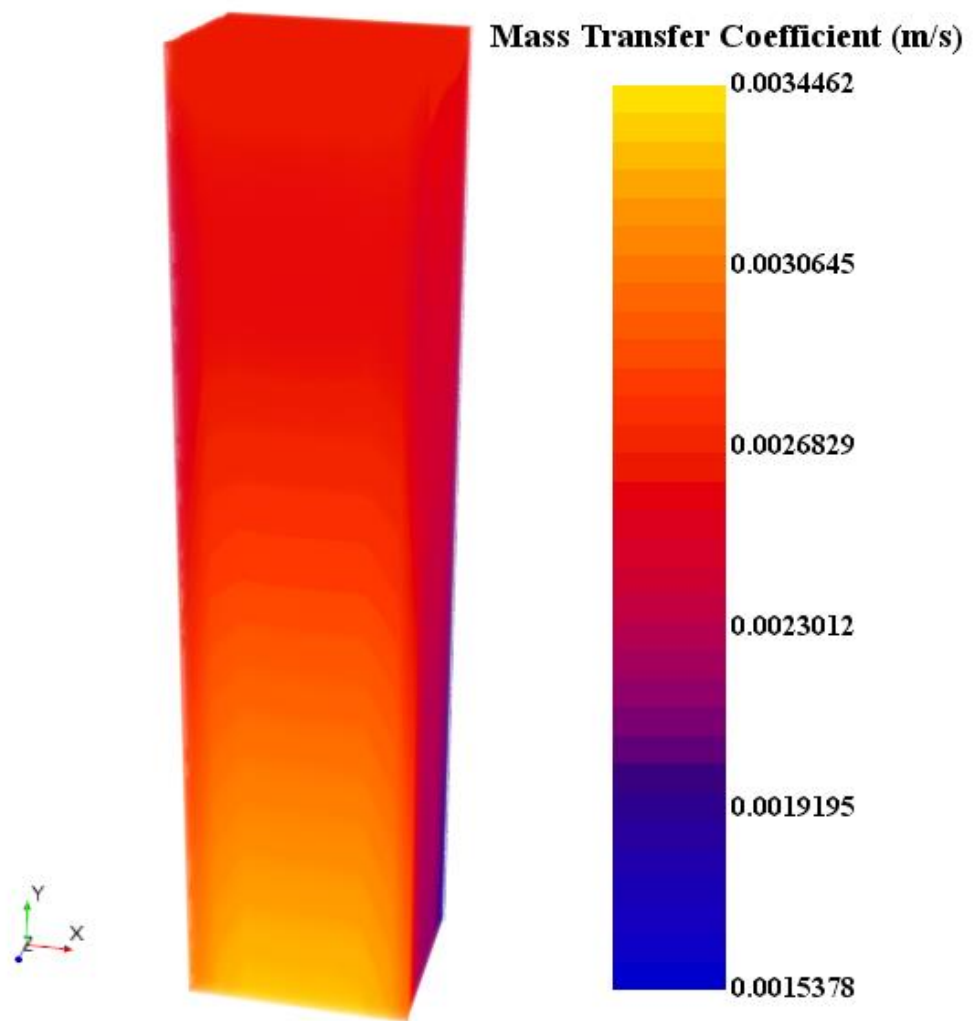


Figure 3-21 Estimated Mass Transfer Coefficient of Flow Domain in the P0444 COPAIN Test

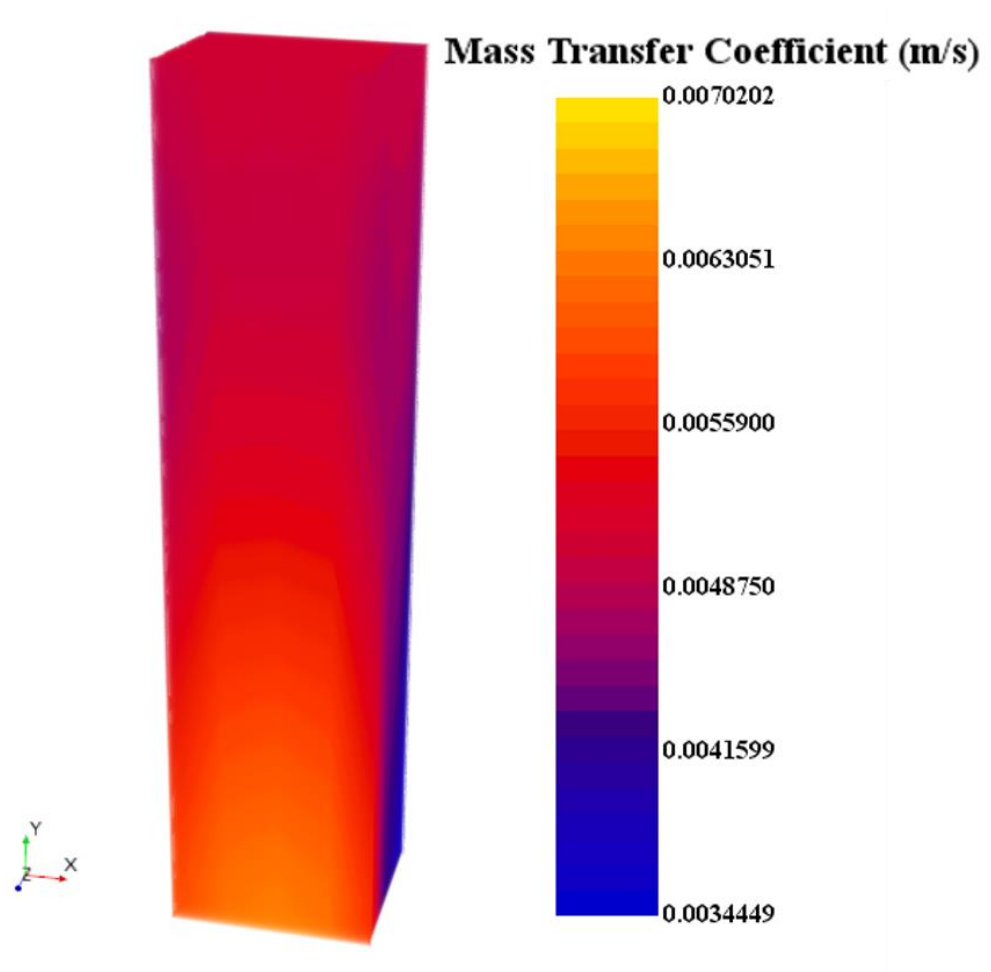


Figure 3-22 Estimated Mass Transfer Coefficient of Flow Domain in the P0344 COPAIN Test

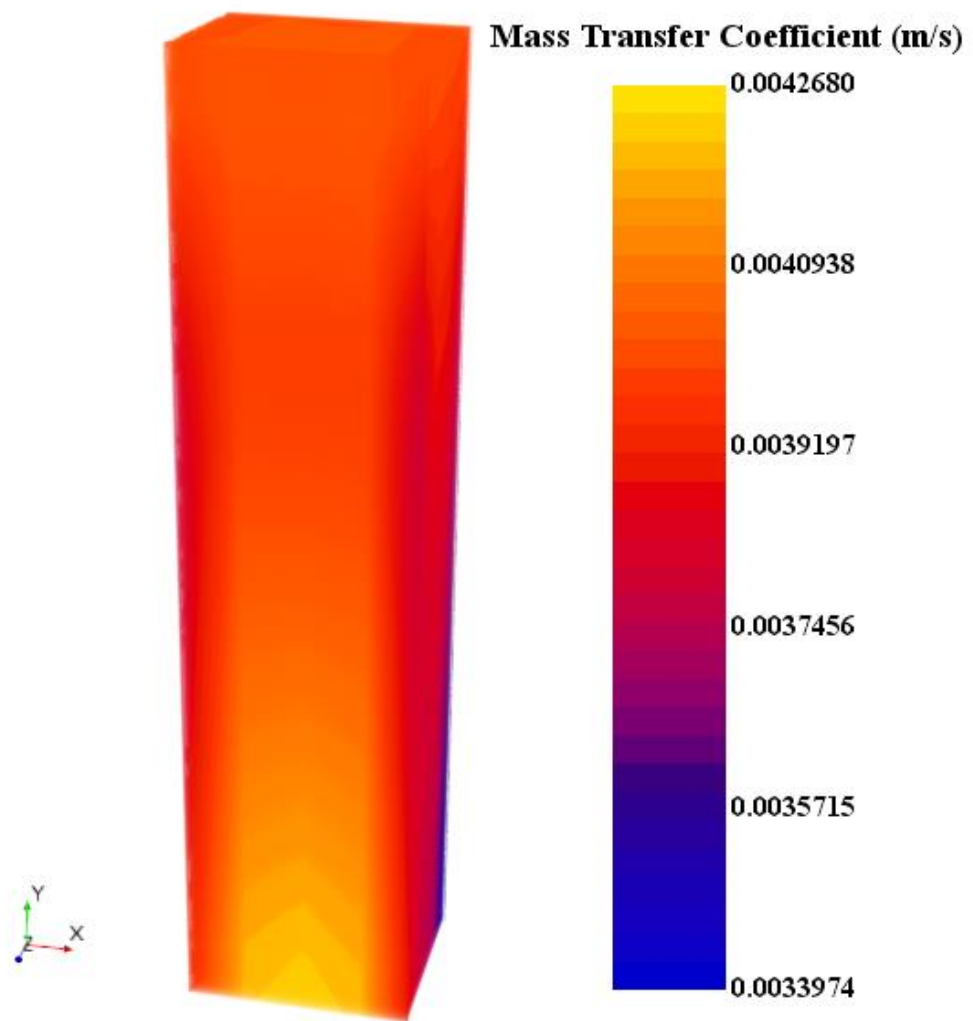


Figure 3-23 Estimated Mass Transfer Coefficient of Flow Domain in the P0443 COPAIN Test

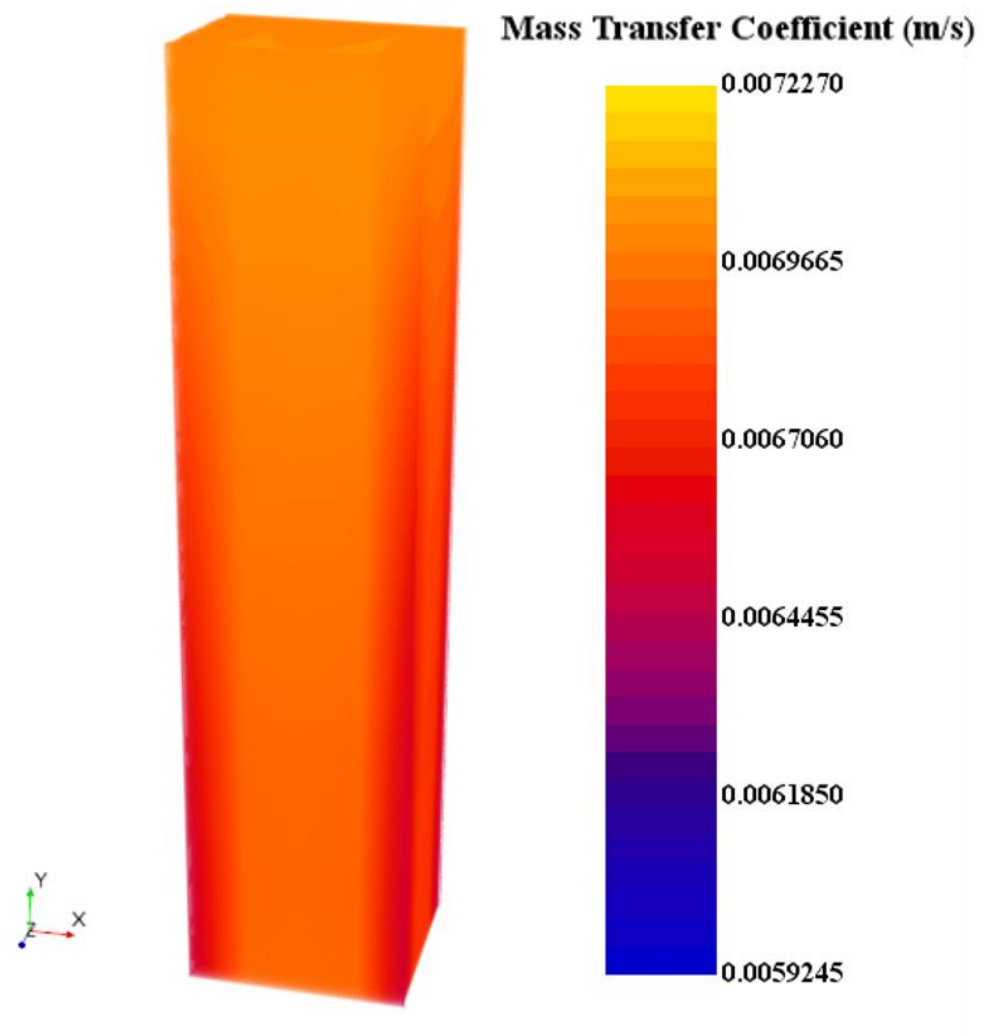


Figure 3-24 Estimated Mass Transfer Coefficient of Flow Domain in the P0441 COPAIN Test

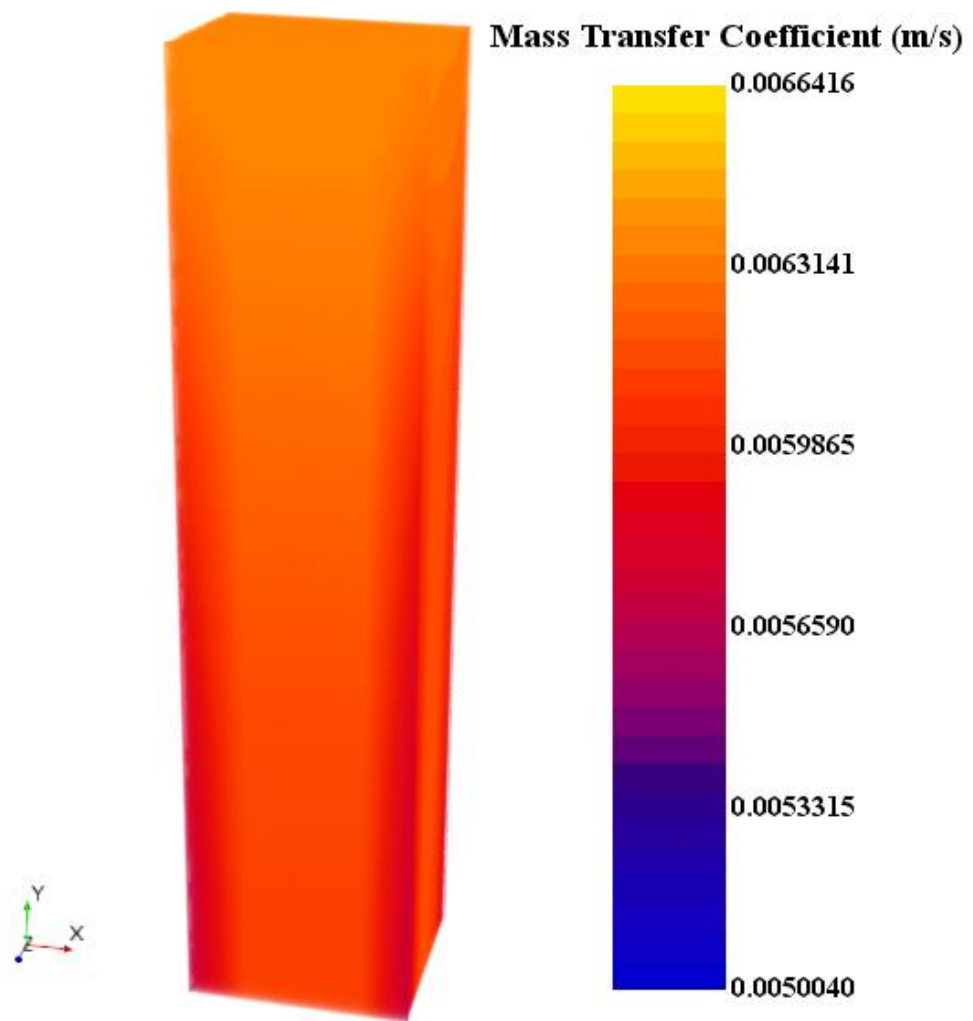


Figure 3-25 Estimated Mass Transfer Coefficient of Flow Domain in the P0461 COPAIN Test

Furthermore, estimated volume average mass transfer coefficient and calculated overall mass transfer coefficients with inlet conditions are shown in Table 3.6.

Table 3.6 Comparison between Estimated and Overall Mass Transfer Coefficients

Test No	Overall Mass Transfer Coefficient (m/s)	Estimated Volume Average Mass Transfer Coefficient (m/s)
P0441	0.00382	0.00700
P0443	0.00291	0.00401
P0444	0.00536	0.00262
P0344	0.00922	0.00503
P0461	0.00895	0.00634

Main discrepancy between the values may arise from the fact that calculation of overall mass transfer coefficient considers only bulk flow conditions with properties calculated at the inlet neglecting condensation and turbulence effects. Furthermore, in order to match the estimated heat flux from the simulations with reported values of experiments, mass transfer coefficient is adjusted with the modified Ranz-Marshall correlation for each case in order to compensate the inherent uncertainties due to flow modelling, condensation and turbulence effects. Parameterized Ranz-Marshall equation given as;

$$A + B \times Re^a \times Sc^b \quad (3.30)$$

where A is 2.0, B is 0.6, a is 1/2 and b is 1/3. Modified coefficients for Ranz-Marshall correlation is given in Table 3.7.

Table 3.7 Modified Ranz-Marshall Coefficients

Case	A	a	B	b
P0441	2.0	1/2.04	0.6	1/3.0
P0443	2.0	1/2.04	0.6	1/3.0
P0444	2.0	1/2.08	0.6	1/3.0
P0344	2.0	1/1.75	0.6	1/3.0
P0461	2.0	1/2.11	0.6	1/3.0

Wall condensation also effects the velocity field near the wall. As the walls in the simulations assumed to have no slip boundary condition, velocity at first prism layer has low velocity which increase gradually. Results shows for test cases P0443, P0444 and P0344 that are relatively having low inlet velocity values, have higher velocity near the wall region where condensation occurs compared to bulk flow. On the other hand, test cases P0441 and P0461 have higher velocity at bulk flow compared to near wall region.

Velocity field near the wall that condensation occurs can be effected by several conditions, such as no slip assumption on the wall, increase in density of the flow due to the accumulation of non-condensable species etc. Furthermore, direction of the flow is also effected by the molecular weight of non-condensable gas. In case of heavier molecules during condensation, the accumulation of such species will increase the density of the mixture therefore the force exerted by gravity also be larger. Simulation results for velocity field for each condition shown from Figure 3-26 to Figure 3-30.

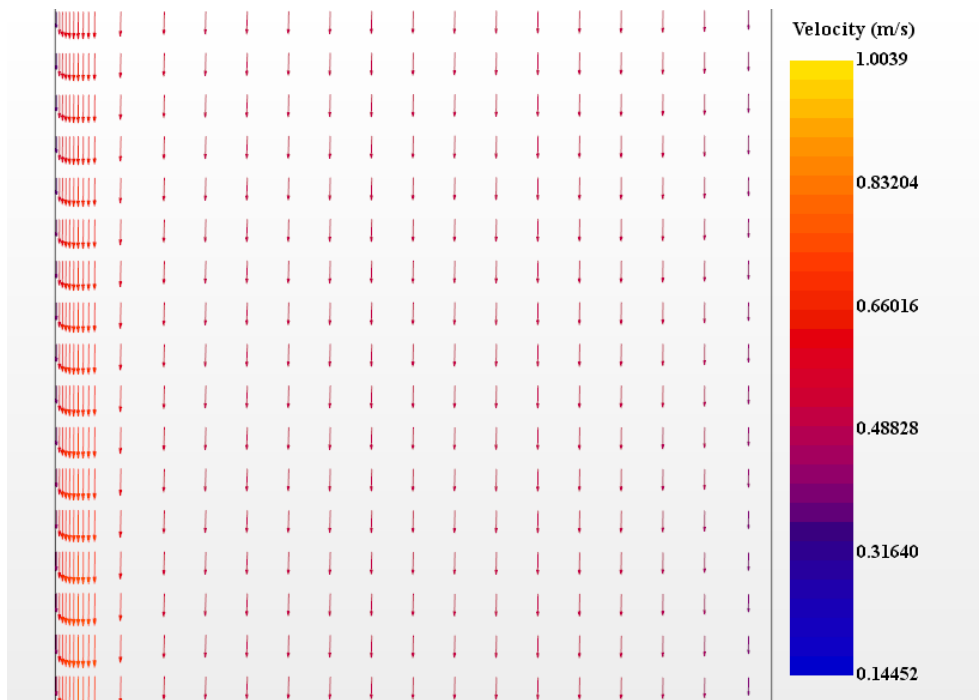


Figure 3-26 Velocity field in the P0444 COPAIN Test

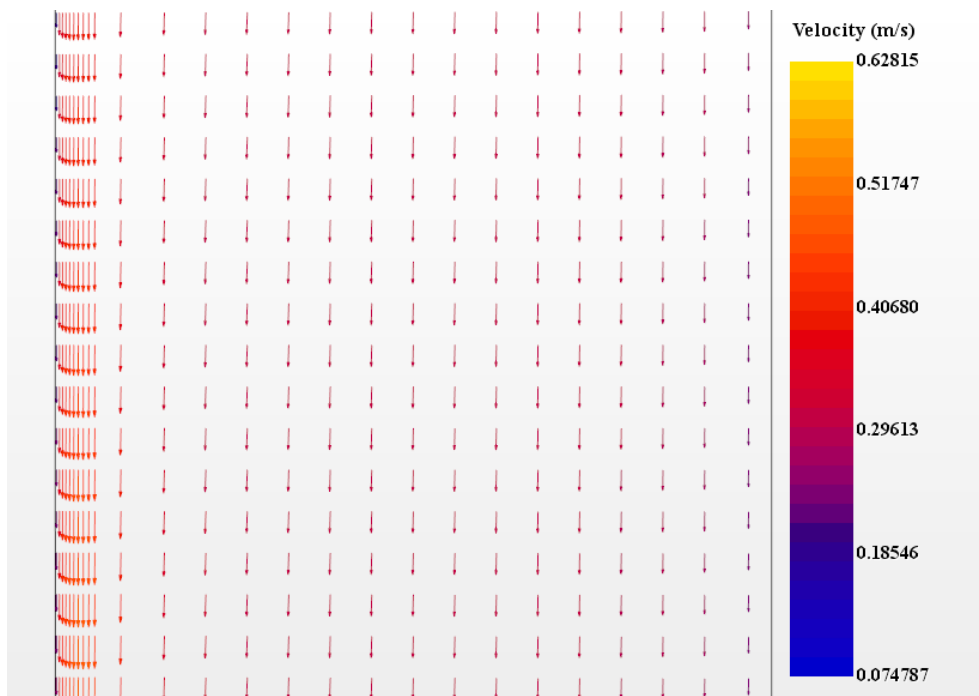


Figure 3-27 Velocity field in the P0344 COPAIN Test

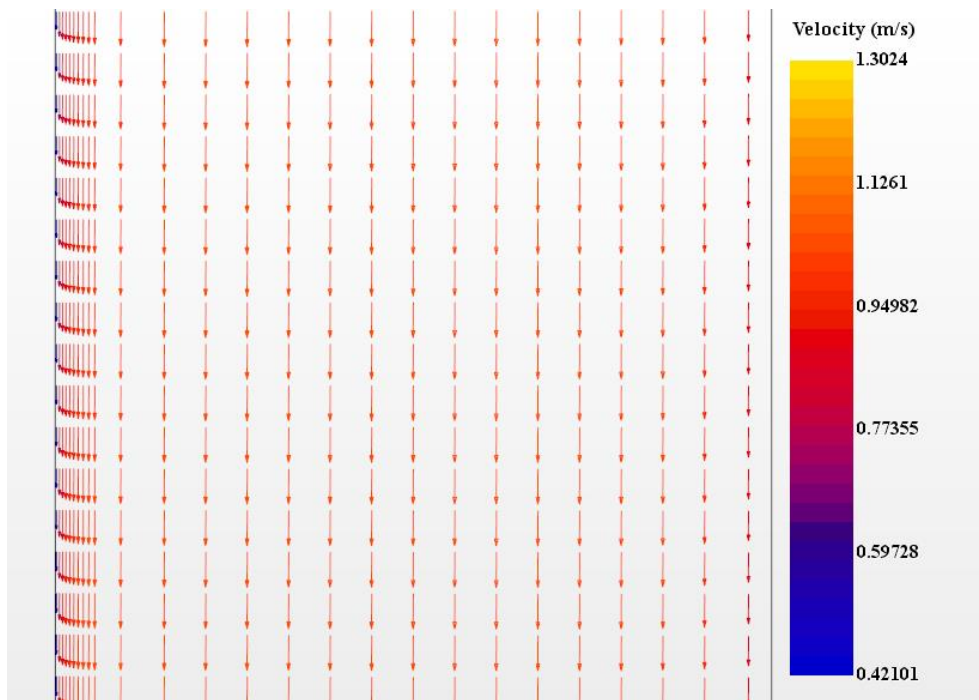


Figure 3-28 Velocity field in the P0443 COPAIN Test

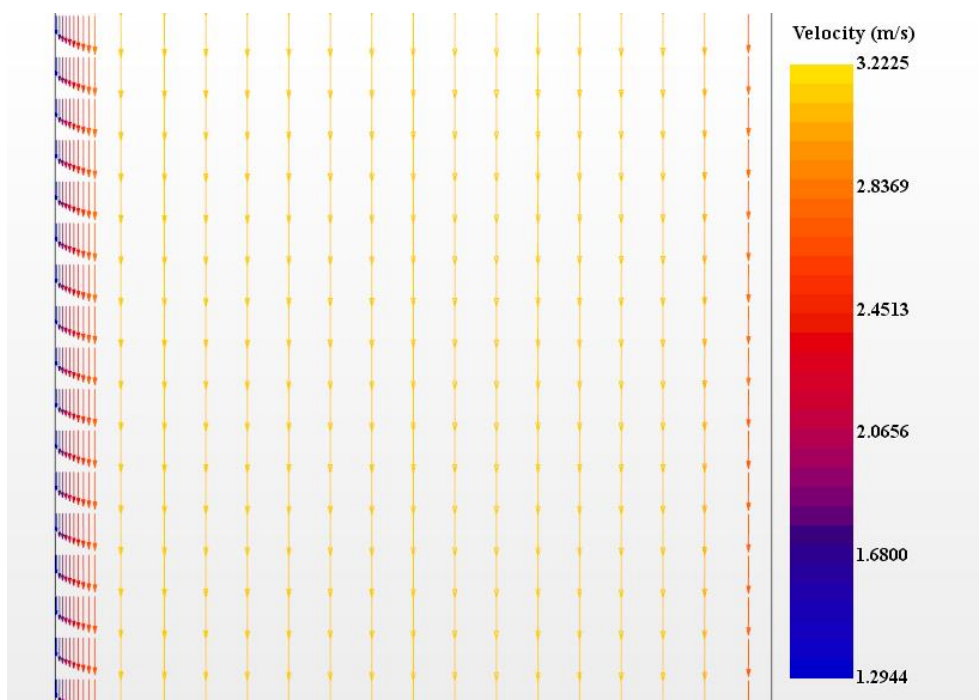


Figure 3-29 Velocity field in the P0441 COPAIN Test

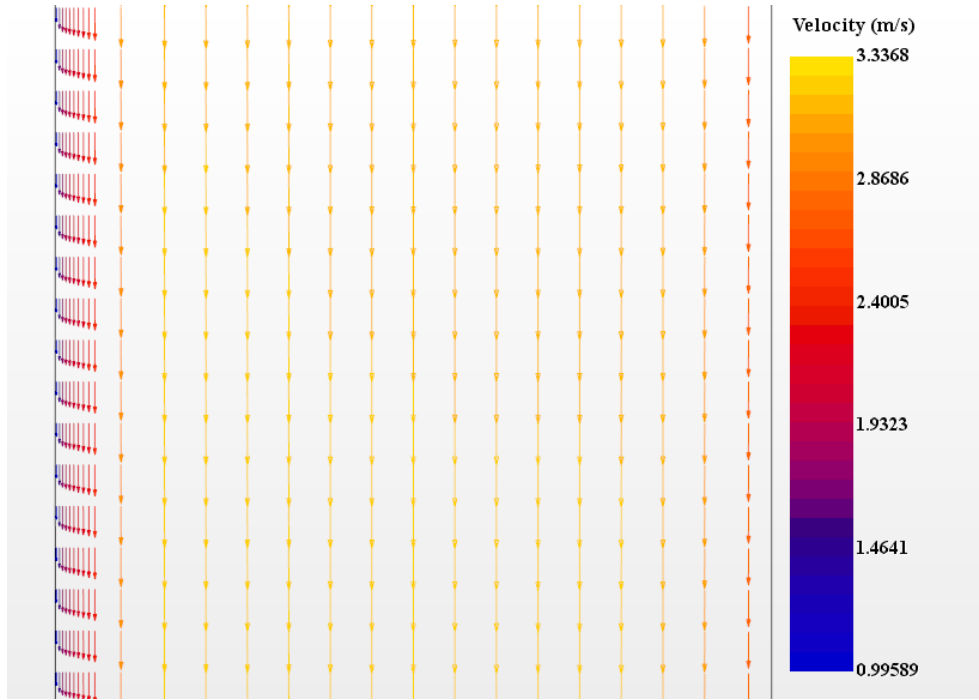


Figure 3-30 Velocity field in the P0461 COPAIN Test

In order to evaluate the accuracy of diffusion layer model to estimate the heat transfer from the wall where condensation occurs, estimated heat flux values on this surface compared with the values calculated from experimental results. Heat transfer through the wall that experience condensation has two components which are sensible heat and heat due to the condensation. Sensible component of the heat flux q_{sen}'' can be calculated by;

$$q_{sen}'' = h(T_w - T_f) \quad (3.31)$$

where h is heat transfer coefficient, T_w is the wall temperature and T_f is temperature of the surrounding fluid. On the other hand, heat flux component due to condensation estimated by using Equation (3.59).

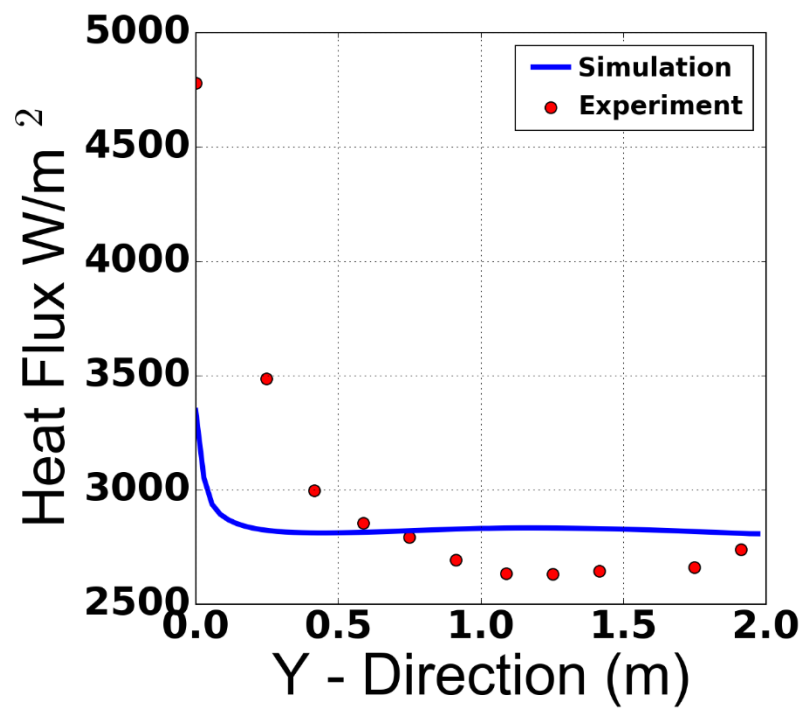


Figure 3-31 Axial Evaluation of Condensation Flux in the P0444 COPAIN Test

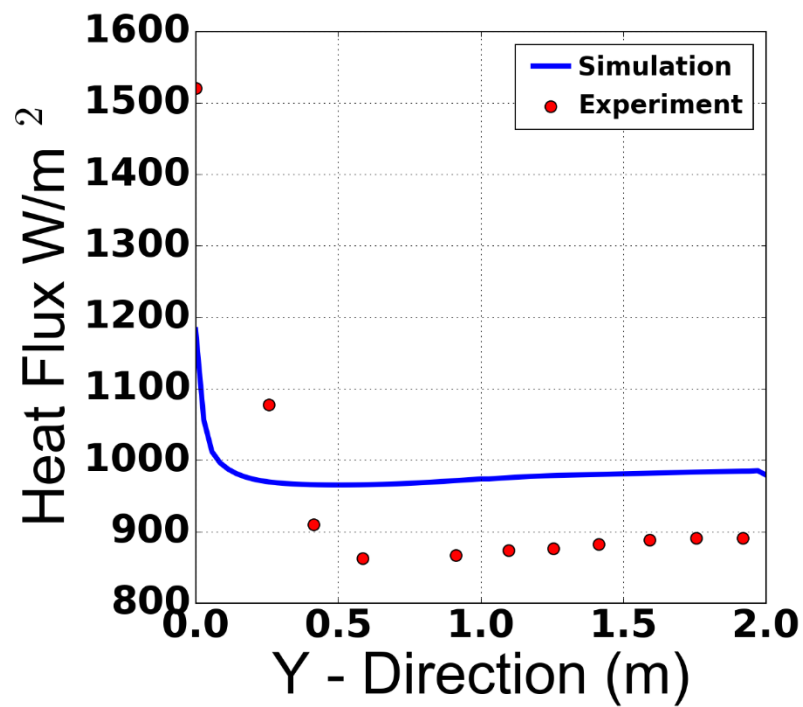


Figure 3-32 Axial Evaluation of Condensation Flux in the P0344 COPAIN Test

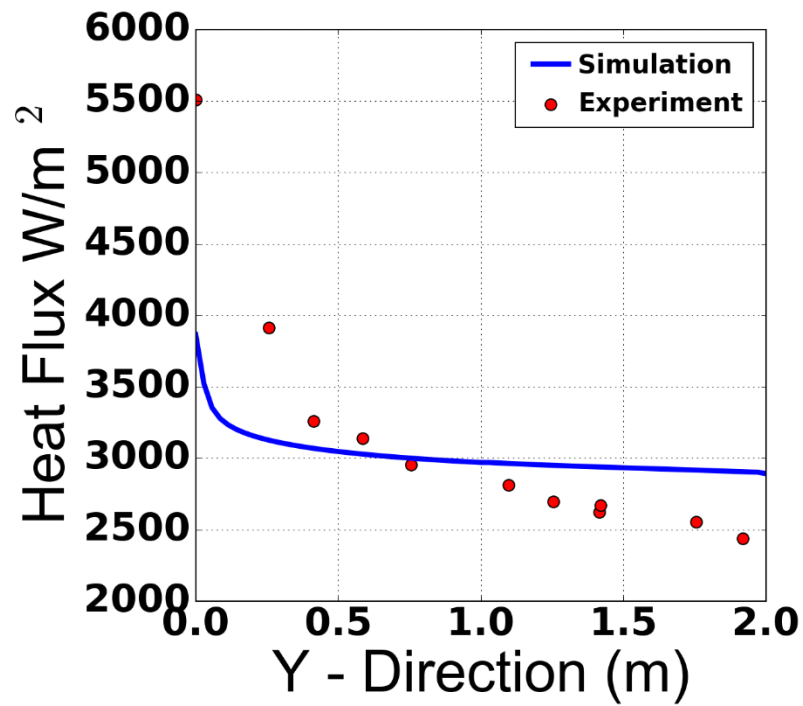


Figure 3-33 Axial Evaluation of Condensation Flux in the P0443 COPAIN Test

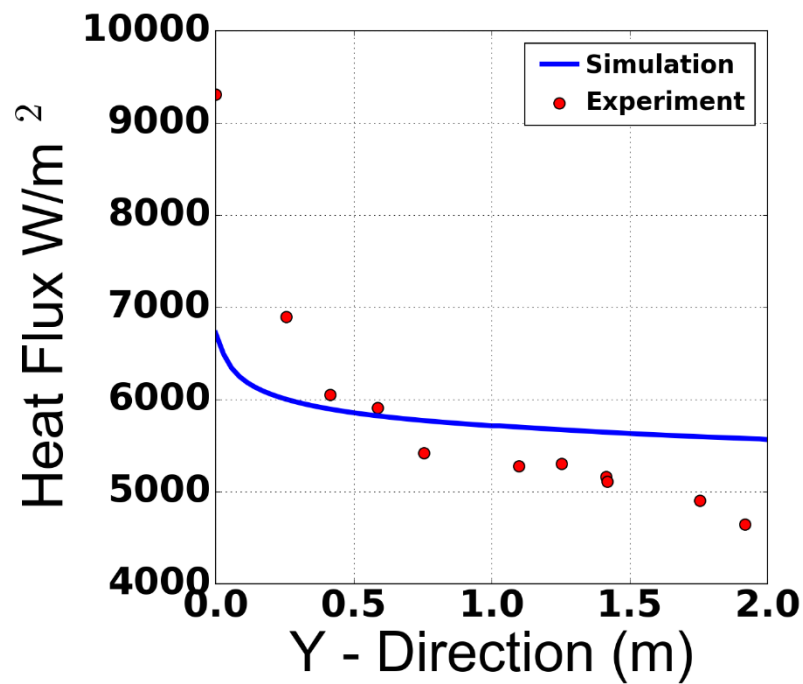


Figure 3-34 Axial Evaluation of Condensation Flux in the P0441 COPAIN Test

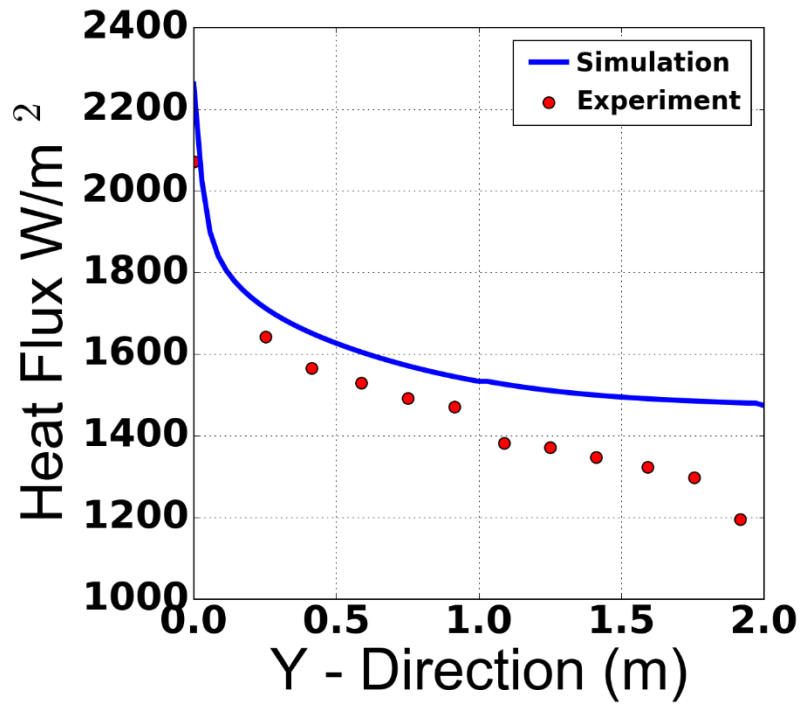


Figure 3-35 Axial Evaluation of Condensation Flux in the P0461 COPAIN Test

Simulation results estimate the heat flux from experiments within the range of 15% difference in developed region without considering uncertainties in experiments. Heat flux values for developing region is underestimated for each cases and due to simplified representation of film condensation, simulation results at developed region show no fluctuations whereas the heat flux values from experiments show some nonlinearity. Table 3.8 summarizes the estimated condensation heat flux for each case.

Table 3.8 Estimated Condensation Heat Flux for COPAIN Experiments

Test No	Condensation Heat Flux (W/m ²)
P0441	5167.9
P0443	3412.6
P0444	2603.7
P0344	884.8
P0461	1367.3

3.5 Application of Wall Condensation Model to 1F1 PCV

Following the validation of wall condensation model, simulations conducted to evaluate effect of wall condensation inside the 1F1 PCV. Heat sources are used to represent debris locations as in previous simulations and mass sources are defined to represent evaporation and condensation as shown in Figure 3-36.

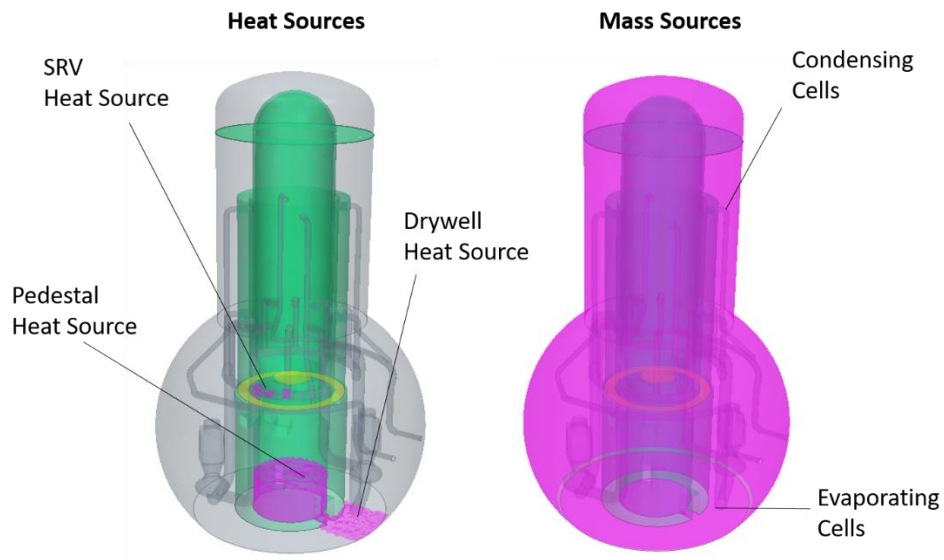


Figure 3-36 Selected Regions for Heat and Mass Sources

Condensation acts as a heat sink for the condensable content whereas it is a heat source for the cold wall. Considering this situation, boundary on the top head is modified to include heat released due to condensation which will decrease the heat loss from this boundary. Thus it will affect the convection inside the PCV and heat transfer through the top head boundary. Figure 3-37 shows the comparison of estimated temperature field on April 6th between simulations with and without wall condensation model.

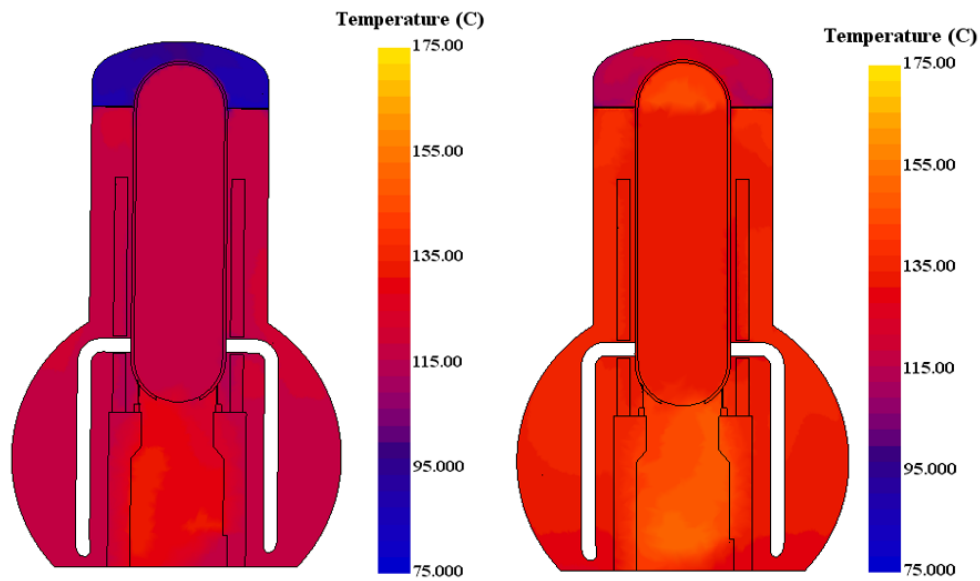


Figure 3-37 Comparison of Estimated Temperature Field without Wall Condensation Model (on left) and with Wall Condensation Model (on right)

Results by applying wall condensation model show more uniform distribution of temperature inside the PCV. Furthermore due to decrease in total heat sink on top heat boundary due to heat released during condensation, less temperature gradient observed above top plate and below top plate regions. Furthermore heightwise temperature values are compared between estimations with and without condensation model as shown in Figure 3-38. Results show that estimated temperature values in case of simulations with wall condensation model gives better agreement with measurements. Change in the convection pattern inside the PCV effect not only the top head region but also other locations inside the PCV as well.

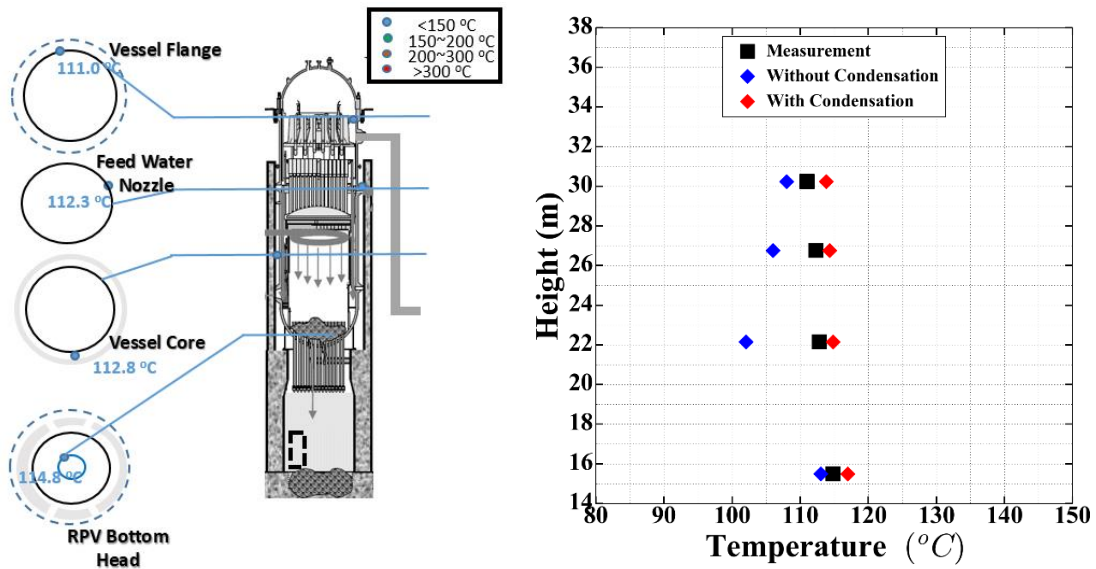


Figure 3-38 Heightwise Temperature Comparison with and without Wall Condensation Model

3.6 Summary and Conclusion

Proposed wall condensation model to evaluate condensation inside 1F1 PCV is validated with selected COPAIN tests. Main driving force in this model is the concentration of condensable gas which shows decreasing profile near the wall. Moreover, using mass and heat transfer analogy, mass transfer coefficient for each test case is estimated by modified Ranz-Marshall correlations to estimate the heat flux values reported from experiments. Estimated heat flux with diffusion layer model on the wall is within the range of 15% difference compared to results from experiments. On the other hand, heat flux for developing region is underestimated for each cases and due to simplified representation of film condensation, simulation results show steady values at developed region. As the overall heat transfer characteristics for each test case in COPAIN experiments are estimated with reasonable margin, diffusion layer model can be applied to 1F1 PCV.

Chapter 4 Nitrogen Injection Effect on Debris Cooling

4.1 Introduction

In this section effect of the nitrogen gas injection will be discussed along with its effect on the temperature distribution inside the PCV. In order to prevent possible hydrogen explosion TEPCO decided to inject nitrogen gas to 1F1 PCV on 7th of April over a period of about 6 days with approximately 28.2 m³/h flow rate [60]. Possible sources for the hydrogen inside containment are;

- Exothermic reaction between Zircaloy and steam.
- Hydrogen production from corium during core degradation when the core is reflooded.
- Molten core concrete interaction.
- Radiolysis of water.
- Oxidation of B₄C material

In case of Unit-1, oxygen could escape into PCV by in leak, makes the PCV atmosphere susceptible to reach hydrogen detonation level. Therefore, nitrogen is injected to displace the oxygen inside the PCV and reduce the risk of hydrogen explosion. During the injection time period, changes observed in temperature measurements. In this section, effect of nitrogen injection on debris cooling will be discussed by post processing measurement data.

4.2 Fukushima Unit-1 Measurement Data Post-Processing During Nitrogen Injection

Strategy to remove decay heat inside Fukushima Power Plants is to generate steam by injecting water to the power plants. Generated steam will be condensed on PCV walls which will further decrease the concentration of steam inside the PCV. Possible leakage of hydrogen from RPV to PCV raise the concern of hydrogen explosion. In order to prevent such possibility nitrogen is injected to Fukushima Power Plants to replace the void left by steam condensation. Injected nitrogen act as a non-condensable gas which

will disturb steam condensation. Even though nitrogen has no cooling capability, it will affect heat transfer by both convection and condensation which will further affect the temperatures inside the PCV. According to TEPCO press release on December 26th 2011, injection of nitrogen gas into Primary Containment Vessel started at 1:31 am on April 7th [61].

Decay heat on April 9th is estimated as 1.076 MW using a relation derived from ANS standard decay heat curve [62] and decay heat reported on April 6th which is 1.11MW.

$$P(t_s) = At_s^{-a} \quad (3.32)$$

where $P(t_s)$ is ratio of decay power to nominal power of the plant in percentage, t_s is the time after the reactor shutdown and A and a are constants which depend on t_s as in Table 4.1.

Table 4.1 Coefficients for Decay Heat Calculation

Time Range (s)	A	a
$10^{-1} \leq t_s < 10^1$	0.0603	0.0639
$10^{-1} \leq t_s < 1.5 \times 10^2$	0.0766	0.1807
$1.5 \times 10^2 \leq t_s < 4 \times 10^6$	0.1301	0.2834
$4 \times 10^6 \leq t_s < 2 \times 10^8$	0.2659	0.3350

During the nitrogen injection pressure of the PCV gradually increased whereas the pressure increase in suppression chamber was rather limited. Change in pressure values is shown as in Figure 4-1.

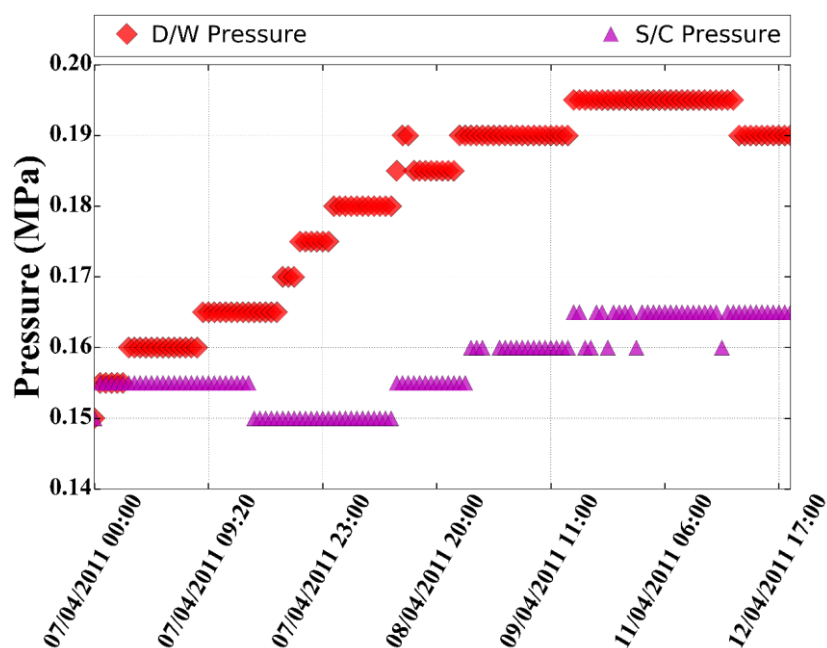


Figure 4-1 Pressure Response during Nitrogen Injection

On the other hand, during this period water injection kept steady around 1.6 kg/s. Therefore, during this period effect of nitrogen injection can readily be observed without any effect from water injection.

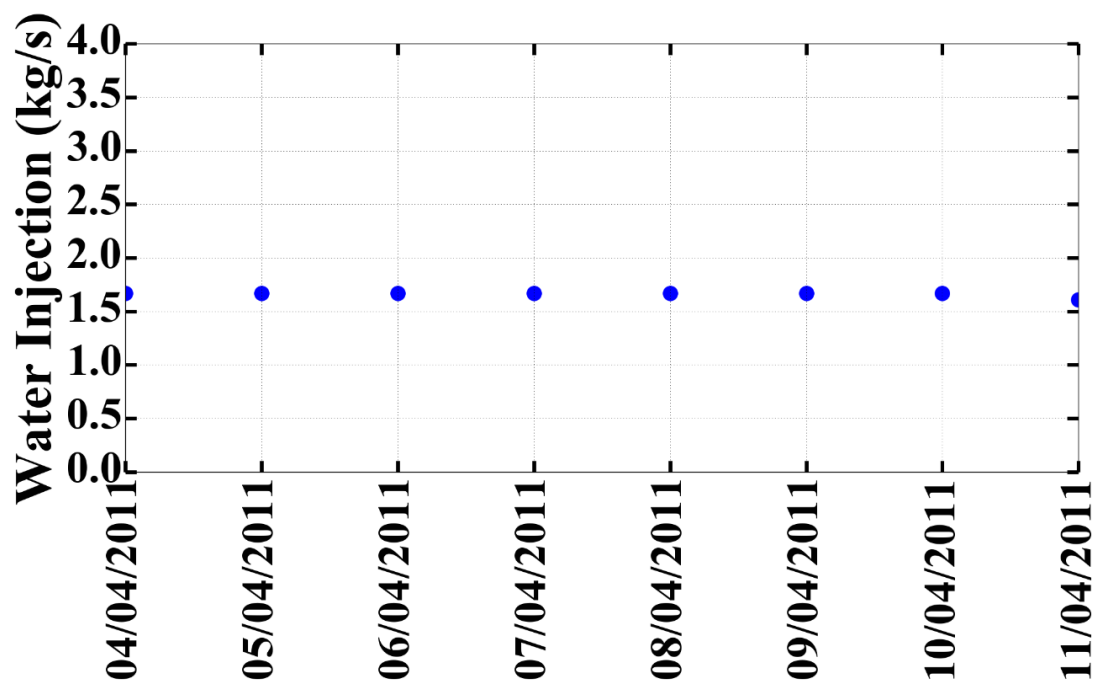


Figure 4-2 Water Injection Mass Flow Rate during Nitrogen Injection

Figure 4-3 shows the temperature measurements from April 4th to 12th. Starting from April 7th along with the nitrogen gas injection, temperature values start to increase gradually. Temperatures could be effected by the increase in saturation pressure as well as by the non-condensable gas effect on wall condensation.

Figure 4-4 shows temperature distribution inside the PCV on April 9th. Most of the thermocouples show higher temperatures compared to April 6th before nitrogen injection. Except thermocouples at safety relief valve 203-3B and safety relief valve 203-3C remaining thermocouples show less superheating. Temperature values suggests that effect of nitrogen injection on coolability of debris is ineffective.

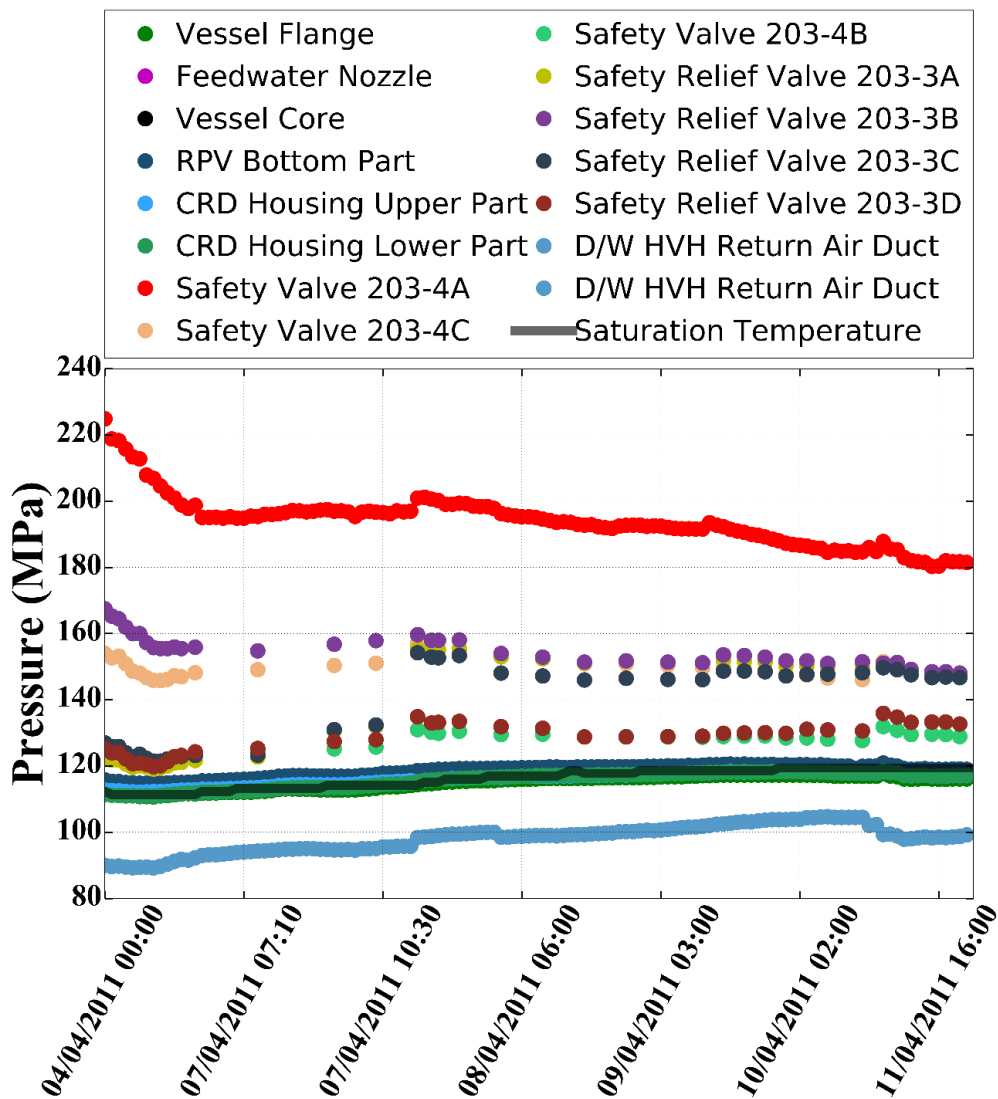


Figure 4-3 Temperature and Pressure Distribution from April 4th to April 12th@

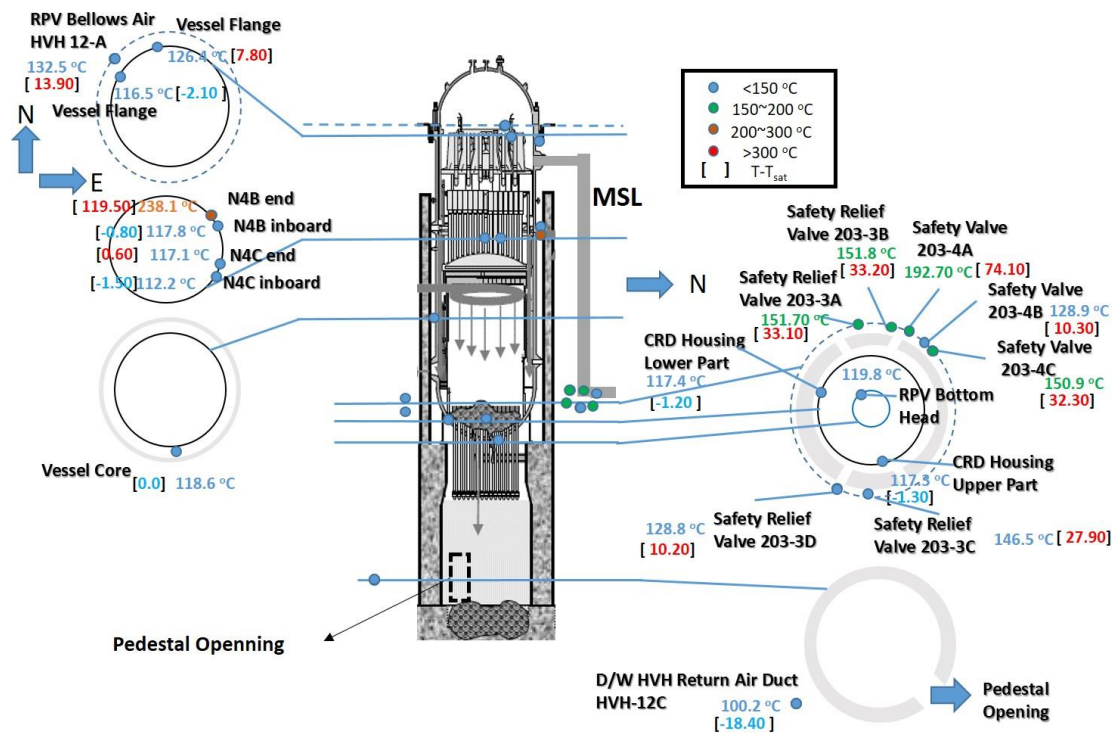


Figure 4-4 Temperature distribution inside PCV on April 9th 06:00

Pressure values inside the PCV gradually decrease after the nitrogen injection and on 26th of April shows the same values as in April 6th before the nitrogen injection.

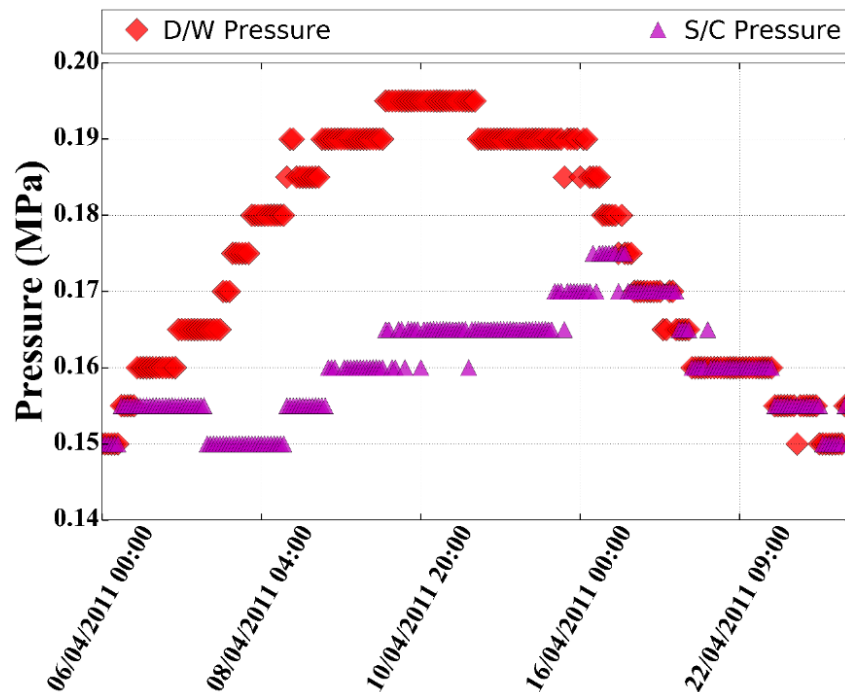


Figure 4-5 Pressure Measurement from April 6th to April 26th

At this time water injection is also increased to around 2.5 kg/s and temperatures inside the PCV decreases drastically and cooling spread to all locations.

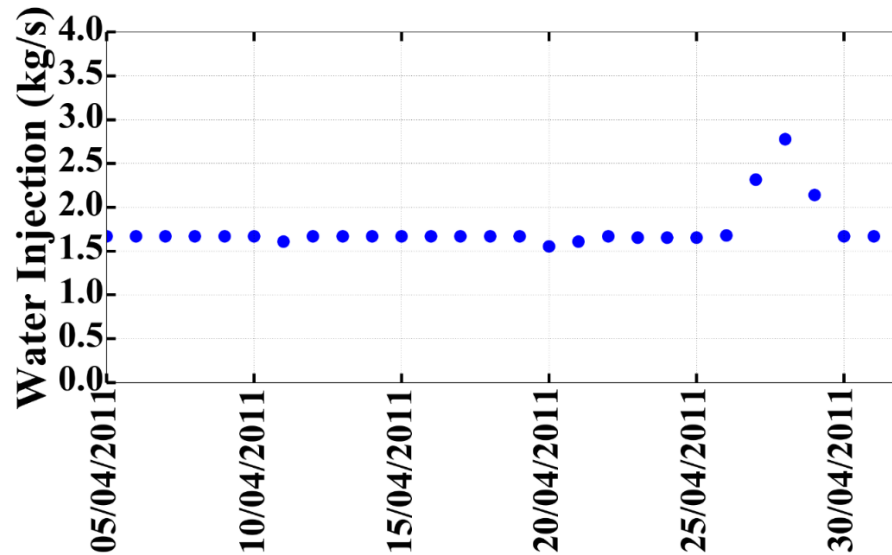


Figure 4-6 Increase in water injection on April 26th

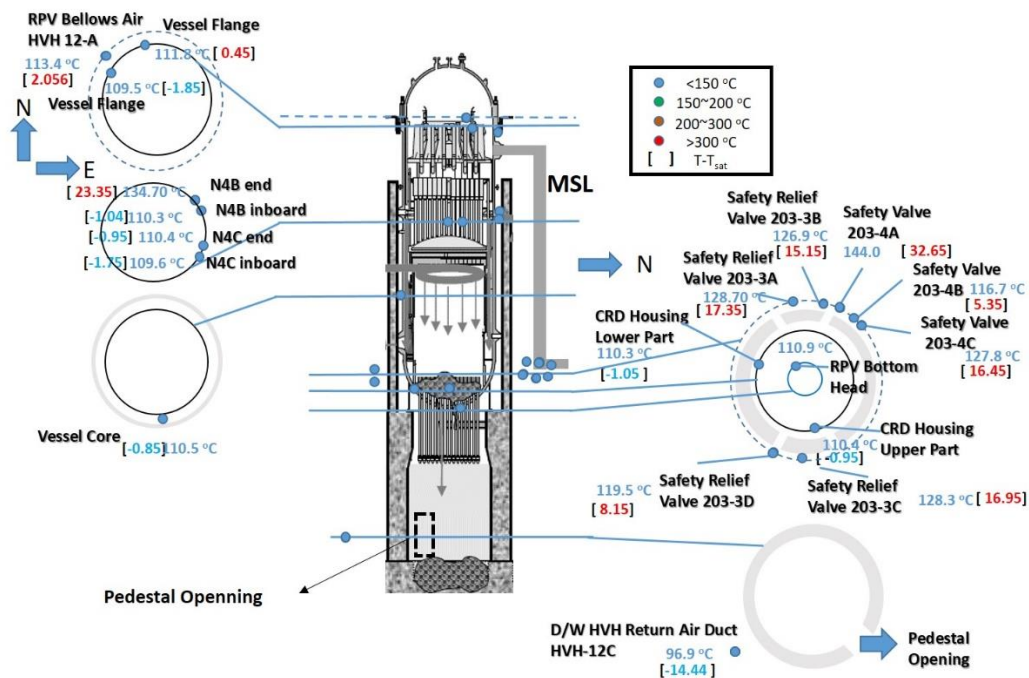


Figure 4-7 Temperature distribution inside PCV on April 26th 06:00

Despite the fact that decay heat decreases on April 9th thermocouples show temperature increase compared to April 6th. This could be due to increased pressure in the drywell which further increase the saturation temperature. On the other hand, due to the nitrogen injection, ongoing condensation might be hindered so that the heat transfer though the PCV walls decreased and effect of dispersed debris or radionuclides attached to structural surfaces become more effective on temperature distribution inside the PCV. After the nitrogen injection, even though the superheating level of the circulating gas is decreased which indicates that the cooling still continues inside the PCV, due to increase in saturation pressure, temperature values are increased. Thus nitrogen injection is said to be ineffective in case of debris cooling.

4.3 Simulation of Wall Condensation with Consideration of Nitrogen Injection

In this section, effect of nitrogen injection will be analyzed with simulations conducted including wall condensation model developed at previous chapter. Simulations conducted for the same geometry and meshing used in Chapter 2 analysis. Analysis conducted for 2 days after the nitrogen injection on April 9th and decay heat estimated using Equation (4.1) for the analysis date. As the total amount of nitrogen and its concentration inside the vessel is unknown 3 different cases conducted to estimate the effect of nitrogen injection on estimated temperature values.

4.3.1 Simulation Results and Discussion

Simulations conducted for 3 cases with different nitrogen mass fraction 10wt.%, 15wt.% and 20wt.% are conducted to see the effect of nitrogen injection on estimated temperature values. Results suggest that condensation occurs only at top head region whereas below top head region wall temperature still higher than the saturation temperature. Location of condensation tracked in STAR-CCM+ by defining a flag where it raises as condensation occurs as shown in Figure 4-8.

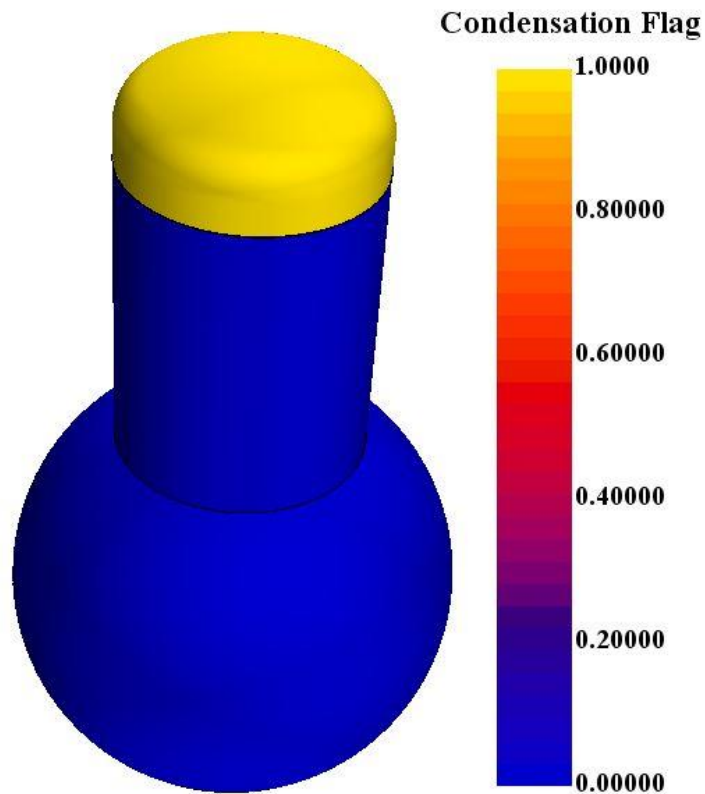


Figure 4-8 Location of Condensation

Amount of condensate is estimated for each case as shown in Table 4.2. With increase in non-condensable gas amount of condensate decreased. This could be due to the additional resistance created by the accumulation of non-condensable gas near condensing wall.

Table 4.2 Estimated Condensate Amount for Different Non-condensable Amount

Case	Nitrogen Mass Fraction	Condensate Amount (gr)
Case-1	10%	171.53
Case-2	15%	166.87
Case-3	20%	159.95

Figure 4-9 Partial Pressure of Steam for Case-3

Decay heat dissipated for condensation also estimated for each case as summarized in Table 4.3.

Table 4.3 Estimated Decay Heat Dissipation as Condensation

Case	Nitrogen Mass Fraction	Dissipated Decay Heat
Case-1	10wt. %	2.9 %
Case-2	15wt. %	2.3 %
Case-3	20wt. %	2.0 %

As seen on Table 4.2 condensation characteristics varies slightly with different non-condensable amount. On the other hand, effect of condensation on estimated temperatures are rather limited. From Figure 4-10, temperature values close the top head region seem to be effected by different nitrogen concentration however effect on the lower elevation is insignificant. Thus, increase in temperature values observed on April 9th during nitrogen injection can be said to be due to the increase in pressure which in turn increases the saturation pressure. On the other hand, nitrogen acts as a non-condensable gas which deteriorates the condensation. In this study, condensation modelled as a heat source on the condensing wall which decreases the effect of heat sink which increasing nitrogen content heat sink on the wall become more effective thus the temperatures on the higher elevation decreases as seen on Figure 4-10. Case with 15wt.% nitrogen content agrees well with the measurement results.

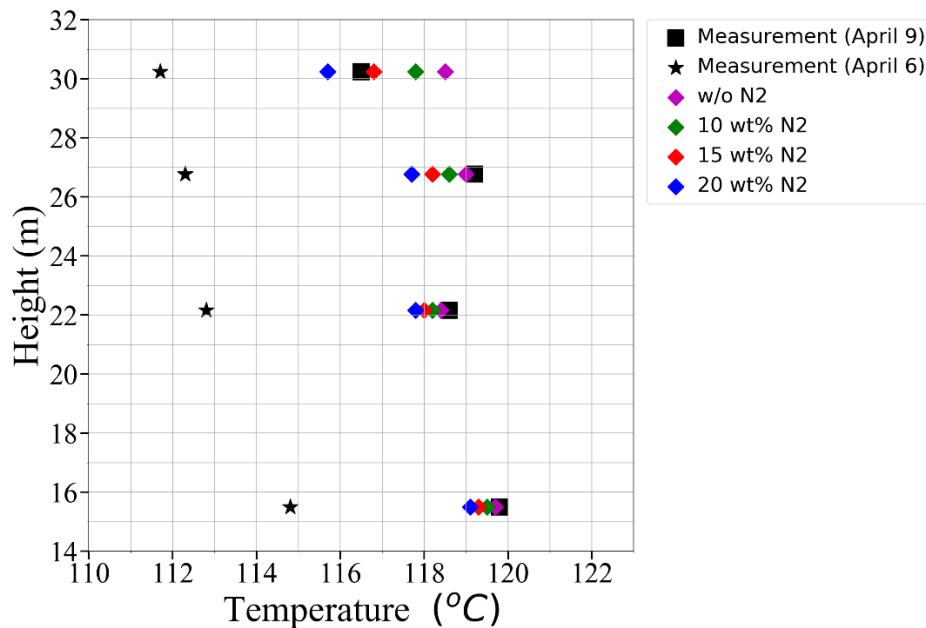


Figure 4-10 Heightwise Temperature Comparison for Cases with Different Nitrogen Amount

Figure 4-11 shows the mass fraction of nitrogen and partial pressure of steam for the middle cut section of 1F1 PCV. Results show that nitrogen gas is accumulation on the top head region where condensation occurs whereas the partial pressure of steam decreases. Thus with those results obtained, wall condensation model applied to 1F1 PCV is representing condensation phenomena as intended.

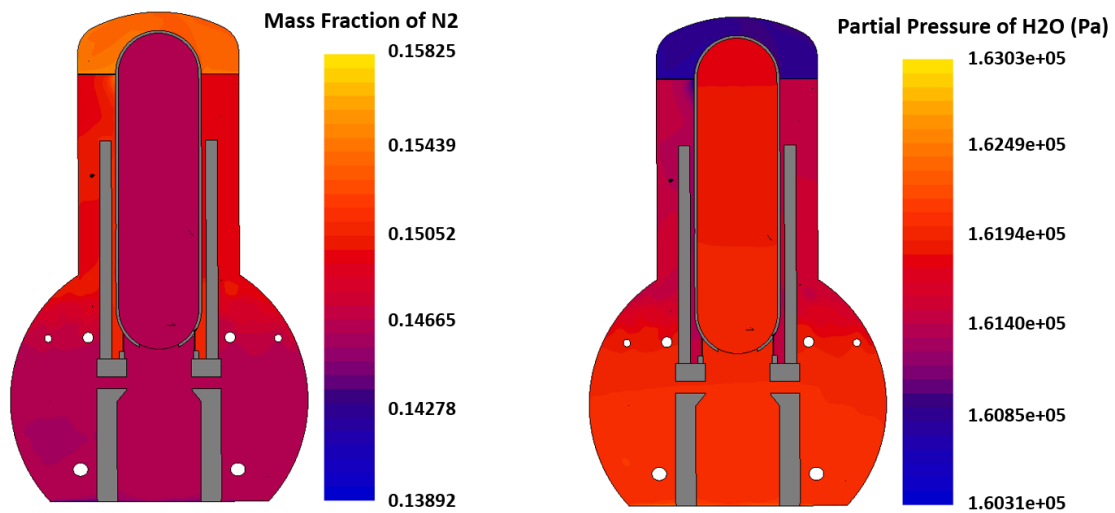


Figure 4-11 Estimated Mass Fraction of Nitrogen and Partial Pressure of Steam for case with 15wt.% Nitrogen Content

Chapter 5 Conclusion and Future Work

5.1 Conclusion

In this study an alternative approach to investigate debris location in 1F1 using computer simulations and measurements taken after the accident is introduced. Simulations conducted for the selected date after the post-processing of measurement data considering availability and stability of the measurements. By defining heat sources to represent possible debris locations and heat sink on PCV walls, simulations conducted to estimate gas flow and related heat transfer inside the containment. Simulations considering debris only on pedestal floor and spread to drywell floor could not address the temperature asymmetry on the safety valves. Therefore, another set of simulations conducted with additional heat sources on safety valve locations in order to address the temperature asymmetry.

Results suggests that approximately 7% to 11% of the decay heat is dissipated to heat up the gas inside the containment on April 6th. Amount of heat source to represent temperature asymmetry is estimated to be around 2% which gives good agreement for the temperature values measured at safety relief valve locations. Another parameter analysis conducted to check whether it is possible to assess debris spreading through the opening of the pedestal. Nonetheless, due to mixing and lack of available measurement data, simulations could not reflect the effect of debris spreading with current modelling.

In order to address effect of nitrogen injection along with steam condensation, a wall condensation model is developed which can be applicable to 1F1 PCV. The suggested wall condensation model so called diffusion layer model is originated from the diffusion theory where the driving force is the concentration difference of steam fraction at saturation pressure and bulk pressure. Model is applied to simulate COPAIN experiments which is a simple duct geometry where the 2D flow characteristics are dominant so that uncertainties for the evaluation can be attributed to the modelling and turbulence characteristics rather than numerical errors. Selected 5 COPAIN test cases simulated with diffusion layer model and wall heat flux values from experiments compared with calculation results. Calculated heat flux values show good agreement within the range of 20% difference from the experiment results in the developed region. Thereafter, validated condensation model applied to the 1F1 PCV and estimated

temperature values give better estimation of temperature measurements. In chapter 4, effect of nitrogen injection is discussed through the analysis of measured data and simulation. Temperature values during nitrogen injection show higher values compared to few days before the injection however the superheating level remained similar. This condition suggests that while condensation still continues inside the PCV due to increase in pressure, saturation temperature of the steam is increased so that measurements indicates higher values. Simulation results show that 15 wt.% nitrogen in gas mixture gives better temperature estimation of temperature measurements.

5.2 Future Work

In order to assess the validity of the approach to simulate conditions inside the 1F1 PCV, more simulations considering different time intervals are needed. Furthermore, current modelling can be applied to a time interval where the transient phenomena is important. Moreover, recent study only considers steam and nitrogen as a gas mixture, however in real case more non-condensable gases may remain inside PCV such as hydrogen or air. In order to assess their effect more parameter analysis can be conducted.

References

- [1] TEPCO, Tokyo Electric Power Company, Inc., 2015, Reactor imaging technology for fuel debris detection by cosmic ray muon Measurement status report in Unit-1 March 2015. Available at:
http://www.tepco.co.jp/en/nu/fukushima-np/handouts/2015/images/handouts_150319_.
- [2] TEPCO, Tokyo Electric Power Company, Inc., 2015., Development of a technology to investigate inside the Reactor Primary Containment Vessel (PCV) Site test Investigation B1 on grating around the pedestal inside Unit 1 PCV. Available at: http://www.tepco.co.jp/en/nu/fukushima-np/handouts/2015/images/handouts_150406_01-e.pdf.
- [3] M. Pellegrini *et al.*, “Benchmark Study of the Accident at the Fukushima Daiichi NPS: Best-Estimate Case Comparison,” *Nucl. Technol.*, vol. 196, no. 2, pp. 198–210, Nov. 2016.
- [4] M. Pellegrini, H. Suzuki, H. Mizouchi, and M. Naitoh, “Early Phase Accident Progression Analysis of Fukushima Daiichi Unit 3 by the SAMPSON Code,” *Nucl. Technol.*, vol. 186, no. 2, pp. 241–254, 2014.
- [5] F. Nagase, R. O. Gauntt, and M. Naito, “Overview and Outcomes of the OECD/NEA Benchmark Study of the Accident at the Fukushima Daiichi Nuclear Power Station,” *Nucl. Technol.*, vol. 196, no. 3, pp. 499–510, 2016.
- [6] H. Zhang, F. Niu, Y. Yu, S. Zhang, H. Wang, and Z. Gang, “Modeling and experimental studies on mixing and stratification during natural convection in containments,” *Ann. Nucl. Energy*, vol. 85, pp. 317–325, Nov. 2015.
- [7] M. Houkema, N. B. Siccama, J. A. Lycklama à Nijeholt, and E. M. J. Komen, “Validation of the CFX4 CFD code for containment thermal-hydraulics,” *Nucl. Eng. Des.*, vol. 238, no. 3, pp. 590–599, 2008.
- [8] M. Babić, I. Kljenak, and B. Mavko, “Prediction of light gas distribution in experimental containment facilities using the CFX4 code,” *Nucl. Eng. Des.*, vol.

238, no. 3, pp. 538–550, Mar. 2008.

- [9] Atomic Energy Society of Japan, *The Fukushima Daiichi Nuclear Accident*. 2015.
- [10] “Strategic plan for fuel debris retrieval, Available at: https://fdada.info/en/home2/decommissioning2/obj_00-en/,” 2016.
- [11] T. Bergman, A. Lavine, F. Incropera, and D. Dewitt, *Fundamentals of Heat and Mass Transfer, 7th Edition*. JOHN WILEY & SONS, INC, 2011.
- [12] STAR-CCM+, “STAR-CCM+ Version 12.02, User Guide, CD-Adapco, 2017,” 2017.
- [13] W. Ambrosini, N. Forgione, and F. Oriolo, “Experimental and CFD analysis on condensation heat transfer in a square cross section channel,” in *In Proceeding of the NURETH 11 conference, Pope’s Palace Conference Center, Avignon, France,*.
- [14] W. Bazin and P. Castelli, “COPAIN: Rapport d’essai. Technical Report 85, CEA/DEN/DTP/SETEX/LETS,” 1999.
- [15] K. Fischer, A. K. Rastogi, T. Braun, T. Drath, A. Lyubar, and S. Schwarz, “Containment code comparison exercise on experiment ThAI TH7,” in *In Proceeding of the NURETH 10 conference, Seoul, South Korea*.
- [16] J. Malet, E. Porcheron, and J. Vendel, “OECD International Standard Problem ISP-47 on containment thermal-hydraulics—Conclusions of the TOSQAN part,” *Nucl. Eng. Des.*, vol. 240, no. 10, pp. 3209–3220, 2010.
- [17] J. Malet, E. Porcheron, and J. Vendel, “OECD International Standard Problem ISP-47 on containment thermal-hydraulics—Conclusions of the TOSQAN part,” *Nucl. Eng. Des.*, vol. 240, no. 10, pp. 3209–3220, Oct. 2010.
- [18] N. Erkan, R. Kapulla, G. Mignot, R. Zboray, and D. Paladino, “Experimental investigation of spray induced gas stratification break-up and mixing in two interconnected vessels,” *Nucl. Eng. Des.*, vol. 241, no. 9, pp. 3935–3944, Sep. 2011.

- [19] TEPCO, Tokyo Electric Power Company, Inc., 2017, Reliability Evaluation of the Thermometers Used in Units 1-3 Reactors and PCV at Fukushima Daiichi Nuclear Power Station Available at?: http://www.tepco.co.jp/en/press/corp-com/release/2013/1228656_5130.html.
- [20] K. OKUMURA, “Decay Heat Evaluation of the Fukushima Daiichi Nuclear Power Station (Units 1,2,3) after the Accident,” 2016.
- [21] T. Fukuda, “Fuel debris retrieval strategy for Fukushima Daiichi Nuclear Power Station.”
- [22] J. Mahaffy *et al.*, “Best Practice Guidelines for the use of CFD in Nuclear Reactor Safety Applications,” Nuclear Energy Agency of the OECD (NEA).
- [23] J. C. de la Rosa, A. Escrivá, L. E. Herranz, T. Cicero, and J. L. Muñoz-Cobo, “Review on condensation on the containment structures,” *Prog. Nucl. Energy*, vol. 51, no. 1, pp. 32–66, 2009.
- [24] A. A. Dehbi, W. M. Golay, and S. M. Kazimi, “The effects of noncondensable gases on steam condensation under turbulent natural conditions,” 1999.
- [25] M. Siddique, M. W. Golay, and M. S. Kazimi, “Local Heat Transfer Coefficients for Forced-Convection Condensation of Steam in a Vertical Tube in the Presence of a Noncondensable Gas,” *Nucl. Technol.*, vol. 102, no. 3, pp. 386–402, 1993.
- [26] M. H. Anderson, L. E. Herranz, and M. L. Corradini, “Experimental analysis of heat transfer within the AP600 containment under postulated accident conditions,” *Nucl. Eng. Des.*, vol. 185, no. 2, pp. 153–172, 1998.
- [27] A. Manthey and K. Schaber, “The formation and behavior of fog in a tube bundle condenser,” *Int. J. Therm. Sci.*, vol. 39, no. 9, pp. 1004–1014, 2000.
- [28] J. M. Martín-Valdepeñas, M. A. Jiménez, F. Martín-Fuertes, and J. A. F. Benítez, “Comparison of film condensation models in presence of non-condensable gases implemented in a CFD Code,” *Heat Mass Transf.*, vol. 41, no. 11, pp. 961–976, Sep. 2005.
- [29] E. C. Siow, S. J. Ormiston, and H. M. Soliman, “Two-phase modelling of

- laminar film condensation from vapour–gas mixtures in declining parallel-plate channels,” *Int. J. Therm. Sci.*, vol. 46, no. 5, pp. 458–466, 2007.
- [30] “International standard problem ISP-47 on containment thermal hydraulics.Final Report, NEA/CSNI/ R(2007)10, OECD/NEA;”
- [31] M. Kondo, K. Yoneda, M. Furuya, and Y. Nishi, “An evaluation model to predict steam concentration in a BWR reactor building,” *J. Nucl. Sci. Technol.*, vol. 52, no. 11, pp. 1369–1382, Nov. 2015.
- [32] S. Mimouni, A. Foissac, and J. Lavieville, “CFD modelling of wall steam condensation by a two-phase flow approach,” *Nucl. Eng. Des.*, vol. 241, no. 11, pp. 4445–4455, 2011.
- [33] E. Porcheron, P. Lemaitre, A. Nuboer, V. Rochas, and J. Vendel, “Experimental investigation in the TOSQAN facility of heat and mass transfers in a spray for containment application,” *Nucl. Eng. Des.*, vol. 237, no. 15–17, pp. 1862–1871, Sep. 2007.
- [34] J. Malet, E. Porcheron, F. Dumay, and J. Vendel, “Code-experiment comparison on wall condensation tests in the presence of non-condensable gases—Numerical calculations for containment studies,” *Nucl. Eng. Des.*, vol. 253, pp. 98–113, 2012.
- [35] L. M. Tobias Zitzman, Malcolm Cook, Peter Pfrommer, Simon Rees, “Simulation of Steady-State Natural Convection Using CFD,” 2005.
- [36] D. J. A., “Modelling liquid–solid phase changes with melt convection,” *Int. J. Numer. Methods Eng.*, vol. 28, no. 8, pp. 1769–1785, May 2018.
- [37] H. Hu and S. A. Argyropoulos, “Mathematical modelling of solidification and melting: a review,” *Model. Simul. Mater. Sci. Eng.*, vol. 4, pp. 371–396, 1996.
- [38] V. R. Voller and C. Prakash, “A fixed grid numerical modelling methodology for convection-diffusion mushy region phase-change problems,” *Int. J. Heat Mass Transf.*, vol. 30, no. 8, pp. 1709–1719, Aug. 1987.
- [39] M. Yao and A. Chait, “An Alternative Formulation of the Apparent Heat

- Capacity Method for Phase-Change Problems,” *Numer. Heat Transf. Part B Fundam.*, vol. 24, no. 3, pp. 279–300, Oct. 1993.
- [40] B. D. Nichols and C. W. Hirt, “Methods for calculating multi-dimensional, transient free surface flows past bodies,” 1975.
- [41] C. . Hirt and B. . Nichols, “Volume of fluid (VOF) method for the dynamics of free boundaries,” *J. Comput. Phys.*, vol. 39, no. 1, pp. 201–225, Jan. 1981.
- [42] N. W., “Z. Ver. Deut. Ing.,” vol. 541, p. 60, 1916.
- [43] R. B. Bird, W. E. Stewart, and E. N. Lightfoot, *Transport Phenomena*. Wiley, 2007.
- [44] S. W. E., “Multicomponent mass transfer. By Ross Taylor and R. Krishna, Wiley, New York, 1993, 579 pp,” *AIChE J.*, vol. 41, no. 1, pp. 202–203, May 2018.
- [45] FROSSLING and N., “Über die Verdunstung Fallender tropfen,” *Gerlands Beitr. Geophys.*, vol. 52, pp. 170–216, 1938.
- [46] W. E. Ranz and W. R. Marshall, “Evaporation from drops: Part 2,” *Chem. Eng. Prog.*, vol. 48, no. 4, pp. 173–180, 1952.
- [47] R. Clift, J. R. Grace, and M. E. Weber, *Bubbles, Drops, and Particles*. Academic Press, 1978.
- [48] P. CHUCHOTTAWORN, A. FUJINAMI, and K. ASANO, “Numerical Analysis of the Effect of Mass Injection or Suction on Drag Coefficients of a Sphere,” *J. Chem. Eng. Japan*, vol. 16, no. 1, pp. 18–24, 1983.
- [49] Maruzen, *JSME Data Book : Heat Transfer, 5th Edition*. 2009.
- [50] A. Dehbi, F. Janasz, and B. Bell, “Prediction of steam condensation in the presence of noncondensable gases using a CFD-based approach,” *Nucl. Eng. Des.*, vol. 258, pp. 199–210, 2013.
- [51] M. Bucci, M. Sharabi, W. Ambrosini, N. Forgione, F. Oriolo, and S. He, “Prediction of transpiration effects on heat and mass transfer by different

- turbulence models,” *Nucl. Eng. Des.*, vol. 238, no. 4, pp. 958–974, Apr. 2008.
- [52] J. C. de la Rosa, L. E. Herranz, and J. L. Muñoz-Cobo, “Analysis of the suction effect on the mass transfer when using the heat and mass transfer analogy,” *Nucl. Eng. Des.*, vol. 239, no. 10, pp. 2042–2055, Oct. 2009.
- [53] O. TETENS, “Uber einige meteorologische begriffe,” *Z. Geophys.*, vol. 6, pp. 297–309, 1930.
- [54] X. Cheng *et al.*, “Experimental data base for containment thermohydraulic analysis,” *Nucl. Eng. Des.*, vol. 204, no. 1–3, pp. 267–284, Feb. 2001.
- [55] J. M. Yoo, J. H. Kang, B. J. Yun, S. W. Hong, and J. J. Jeong, “Improvement of the MELCOR condensation heat transfer model for the thermal-hydraulic analysis of a PWR containment,” *Prog. Nucl. Energy*, vol. 104, pp. 172–182, Apr. 2018.
- [56] X. W. Jiang, E. Studer, and S. Kudriakov, “A simplified model of Passive Containment Cooling System in a CFD code,” *Nucl. Eng. Des.*, vol. 262, pp. 579–588, Sep. 2013.
- [57] H. Bian, Z. Sun, M. Ding, and N. Zhang, “Local phenomena analysis of steam condensation in the presence of air,” *Prog. Nucl. Energy*, vol. 101, pp. 188–198, Nov. 2017.
- [58] S. Mimouni, A. Foissac, and J. Lavieville, “CFD modelling of wall steam condensation by a two-phase flow approach,” *Nucl. Eng. Des.*, vol. 241, no. 11, pp. 4445–4455, Nov. 2011.
- [59] M. Bucci, “Experimental and Computational Analysis of Condensation Phenomena for the Thermal-hydraulic Analysis of LWRs Containments,” 2009.
- [60] TEPCO, Tokyo Electric Power Company Inc., 2011, “TEPCO, Tokyo Electric Power Company Inc. Status of Fukushima Daiichi Nuclear Power Station. Available at: <http://irid.or.jp/debris/S1-1E.pdf>.”
- [61] TEPCO, Tokyo Electric Power Company, Inc., 2011, “Press Release, Plant Status of Fukushima Daiichi Nuclear Power Station (as of 3:00 pm, December 26)

Available at: <http://www.tepco.co.jp/en/press/corp-com/release/11122606-e.html>,”

- [62] “ANS-5.1 Decay Energy Release Rates Following Shutdown of Uranium-Fueled Thermal Reactors, Draft ANS-5.1/N18.6.”